

The Effect of Weld Design on the Formability of Laser Tailor Welded Blanks

by

Jennifer Li

A thesis
presented to the University of Waterloo
in fulfillment of the
thesis requirement for the degree of
Master of Applied Science
in
Mechanical Engineering

Waterloo, Ontario, Canada, 2010

© Jennifer Li 2010

AUTHOR'S DECLARATION

I hereby declare that I am the sole author of this thesis. This is a true copy of the thesis, including any required final revisions, as accepted by my examiners.

Jennifer Li

I understand that my thesis may be made electronically available to the public.

Jennifer Li

ABSTRACT

Tailor welded blanks (TWBs) are used in the automotive industries as a method to meet economic, environmental and governmental demands. TWBs are welded blanks that consist of dissimilar material, thicknesses, shapes and/or coating prior to stamping it into the desired three dimensional shapes. The advantages of using TWBs include weight reduction, cost reduction, parts reductions while maintaining structural integrity and crash performance. The disadvantage of employing TWBs is the inhomogeneity of the blanks due to the material and weldment, which can affect the formability of the TWBs. Conventionally, TWBs incorporated mild and low strength steels such as interstitial free and draw quality steels because of their excellent formability traits. However, due to their low strength they are unsuitable for energy absorption applications; thus, the interest of incorporating advanced high strength steels (AHSS) into the TWBs. Dual phase (DP) steel is a type of AHSS that is of interest because of its combination of high strength and good formability that is comparable to high strength low alloy (HSLA) steels. However, welding DP steel causes softening in the heat affected zone (HAZ), which leads to premature failure and reduces formability.

The aim of this thesis was to study the effect of weld design on the formability of TWBs with DP steels (DP600 and DP980 steels) and with HSLA steel. This thesis is divided into three parts; the first part examines TWBs with different weld line positions, weld line orientations and strain paths. The second part investigates bead-on plate curvilinear blanks and its effect on formability of the blanks. The last part examines the effects of multiple welds on the formability of TWBs. Weld positions, orientations and strain path were studied. The formability could be optimized by placing the weld line away from major strain concentration regions and orientated normal to the major strain direction. The formability of curvilinear weld blanks were not studied extensively as the applications are limited at present; however, with better understanding the incorporation of curvilinear welds in TWBs would increase. The formability of multiple-weld TWBs are of interest because the demand for multiple welds applications is increasing.

In the first part of this thesis, it was found that formability was affected by the difference in material properties and weld positions. In the similar material properties combination, formability increased when the weld was placed furthest from the pole. In contrast, with a large material properties difference the formability did not improve. In addition, weld orientation played a dominant role when the material properties difference was large.

In the second part of this thesis, the formabilities of curvilinear welded HSLA and DP980 steels were similar to that of the linear welded blank. DP600 steel was the only steel where weld

geometry had an effect on formability. Moreover, weld position changed the formability of the welded blanks which was reflected in the limiting dome heights and the strain distribution profiles.

In the last part of this thesis, the formability of multiple-weld TWBs was better (if not comparable) to that the single weld TWBs. The large difference in material properties resulted in similar formability of the multiple welds TWBs; whereas, in TWBs with similar material properties a change in the formability was noted.

ACKNOWLEDGEMENTS

I am grateful for the guidance and support of my academic supervisor, Professor Y. Norman Zhou. His dedication to excellence and getting the problem solved was and is a source of motivation. Special thanks to Dr. Panda and Victor Baltazar for providing me with directions and their expertise; and for their patience with helping me understand the problem.

This thesis would not have been possible without the financial supports of Zinc, Arcelor Mittal, Auto21 and IamI.

The progression of this thesis would not be smooth without the support of the forming experts at Arcelor Mittal, and the CAMJ members for their time, advice, and assistance.

DEDICATION

To my parents for believing that I could.

TABLE OF CONTENTS

AUTHOR'S DECLARATION	ii
ABSTRACT.....	iii
ACKNOWLEDGEMENTS.....	v
DEDICATION	vi
TABLE OF CONTENTS	vii
LIST OF FIGURES	x
LIST OF TABLES	xiv
LIST OF EQUATIONS.....	xv
CHAPTER 1	1
1 INTRODUCTION	1
1.1 Tailor-Welded Blanks	1
1.1.1 Welding.....	4
1.2 Advanced High Strength Steels.....	7
1.3 Formability.....	10
1.3.1 Analytical Methods Of Quantifying Formability.....	11
1.4 The Problem.....	16
1.4.1 Objectives	17
CHAPTER 2	19
2 LITERATURE REVIEW	19
2.1 Factors Affecting Formability And Fracture Modes	19
2.1.1 Fracture Modes	20
2.2 The Effect Of Strain Hardening And Plastic Anisotropy.....	21
2.3 The Effect Of Thickness And Strength Ratios.....	22
2.4 The Effect Of Welding	27
2.4.1 Welding AHSS.....	29
2.5 The Effect Of Weld Positions	34
2.6 The Effect Of Weld Orientation	34
2.7 The Effect Of Curvilinear Welds	35

CHAPTER 3	37
3 EXPERIMENTAL	37
3.1 Metallurgical Examination	37
3.1.1 Base Metal	37
3.1.2 Sample Preparation	38
3.1.3 Optical Microscopy and SEM Analysis	38
3.2 Hardness Examination	38
3.3 Mechanical Testing	39
3.3.1 Uniaxial Tensile Testing	39
3.4 Laser Welded Blank Fabrication	42
3.4.1 Diode Laser	43
3.4.2 Clamping Fixture and Shielding Gas	45
3.5 Formability Testing And Analysis	47
3.5.1 Gridding	47
3.5.2 Limiting Dome Height Test Equipment: Hecker’s Hemispherical Punch	48
3.5.3 Strain Measurement	50
 CHAPTER 4	 52
4 EFFECT OF WELD LOCATION, ORIENTATION AND STRAIN PATH	52
4.1 Limiting Dome Height Testing	52
4.1.1 Weld Line Positions: Biaxial Stretch Forming	52
4.1.2 Weld Orientation: Plane Strain Stretch Forming	54
4.2 Hardness Measurements	55
4.2.1 Uniaxial Tensile Test	57
4.3 Fracture Observations	61
4.3.1 Failure Locations	61
4.3.2 Fracture Modes	64
4.4 Limiting Dome Height	68
4.4.1 Effect Of Material Properties On Weld Location	68
4.4.2 Effect Of Weld Orientation And Strain Path (Strain Ratio)	71
4.5 Strain Distribution	74
4.5.1 Biaxial Stretch Forming	74
4.5.2 Plane Strain Stretch Forming	77
4.6 Summary	79

CHAPTER 5	80
5 EFFECT OF CURVILINEAR SEAMS WITH DIFFERENT WELD POSITIONS ON FORMABILITY	80
5.1 Limiting Dome Height Testing.....	80
5.2 Hardness Measurements And Microstructures	81
5.3 Strain Distribution Profiles.....	84
5.4 Fracture Locations.....	89
5.5 Limiting Dome Height.....	91
5.6 Summary.....	94
CHAPTER 6	95
6 EFFECT OF TWBS WITH MULTIPLE WELDS ON FORMABILITY	95
6.1 Limiting Dome Height Testing.....	95
6.2 Strain Distribution Profiles.....	97
6.3 Fracture Locations.....	99
6.4 Limiting Dome Height.....	100
6.5 Summary.....	102
CHAPTER 7	103
7 CONCLUSIONS AND RECOMMENDATIONS	103
7.1 Conclusions	103
7.1.1 The Effect Of Weld Location, Orientation And Strain Path.....	103
7.1.2 The Effect Of Curvilinear Welds	104
7.1.3 The Effect Of TWBs With Multiple Welds	105
7.2 Recommendations	105
REFERENCES	106
APPENDICES	115
A LASER	115
A.1 Laser Welding	115
A.2 Laser Systems.....	116
B STRAIN PATHS WITH RESPECT TO EXPERIMENTAL FLD	117
B.1 Uniaxial Tensile Strain Paths For Different Weld Position.....	118
B.2 Biaxial Stretching Strain Paths For Different Weld Positions.....	120
B.3 Near Plane-Strain Stretching Strain Paths For Different Weld Orientations	122

LIST OF FIGURES

CHAPTER 1

Figure 1.1 Examples of tailored blanks in an automobile [3]	2
Figure 1.2 Types of materials and the strength required for body-in-white parts [7].....	3
Figure 1.3 Continuous-cooling transformation diagram for weld metal of low-carbon steel [10].....	4
Figure 1.4 Effect of alloying element, grain size an, and oxygen on the CCT diagrams for weld metal of low-carbon steel [10]	5
Figure 1.5 Grain growth in HAZ: a) phase diagram, b) thermal cycles, and c) grain size variations [10]6	
Figure 1.6 HAZ microstructure of a gas-tungsten arc weld of 1018 steel (magnification 200x) [10].....	7
Figure 1.7 Tensile strength-total elongation relationship for low strength, conventional HSS, and Advanced HSS steels [20].....	8
Figure 1.8 Materials breakdown in TWBs for a vehicle [23]	9
Figure 1.9 Deformed welded steel specimen under the limiting dome height test.....	12
Figure 1.10 Strain distribution profile [33].....	13
Figure 1.11 A forming limit diagram generated in laboratory tests by changing the width of the blanks [33].....	15
Figure 1.12 Major and minor strains (strain paths) of various automotive parts	16

CHAPTER 2

Figure 2.1 Failure modes: I) fracture across the weld, and II) fracture in the base metal [41]	21
Figure 2.2 Numerical effect of a) n -value, and b) R -value on the limiting dome height [29]	22
Figure 2.3 The relationship between the strength ratio and forming height for steel TWB [49]	24
Figure 2.4 Comparison of the FLCs of the TWB with 1 mm base metals [45]	25
Figure 2.5 The relationship of thickness ratio to minimum major strain [45]	26
Figure 2.6 Comparison of equiaxial stretch formability between laser-welded blanks and the parent materials [53].....	28
Figure 2.7 Strain distributions along the centreline perpendicular to the weld of the TWB with 32 mm width [54]	29
Figure 2.8 Hardness profiles of a) DP980 and HSLA at welding speed of 1.0m/min, and b) DP980 and HSLA welds at different welding speeds [38].....	30
Figure 2.9 Hardness profile of diode laser welded DP steel [39].....	31
Figure 2.10 Top view of LDH of bead-on plate a) DP980, and b) HSLA fracture locations [61]	31
Figure 2.11 Comparison of LDH of parent metals and dissimilar TWB combinations [27]	33
Figure 2.12 Relationship between formability, thickness ratio and curved weld radius [72].....	36

CHAPTER 3

Figure 3.1 Microstructure of base metal a) HSLA, b) DP600, and c) DP980.....	37
Figure 3.2 ASTM E8 schematic of tensile specimen.....	39
Figure 3.3 Tensile specimens of unwelded metal with different orientations relative to the rolling direction.....	40
Figure 3.4 Tensile specimens with the weld placed a) -30 mm, b) -15 mm, c) 0 mm, d) +15 mm, and e) +30 mm offset from the centre	41
Figure 3.5 Sub-size tensile specimens used to evaluate the fusion zone of the TWB	42
Figure 3.6 Nuvonyx diode laser head mounted on a Panasonic robotic arm	43
Figure 3.7 Schematic of a diode laser [78]	44
Figure 3.8 Clamping fixture for laser welding of TWBs [11].....	45
Figure 3.9 Clamping fixture for laser welding of curvilinear seam blank	45
Figure 3.10 A schematic of the laser head configuration	46
Figure 3.11 Grid etching system A) Power supply, B) conductive roller, C) specimen, D) wicking pad, E) stencil, and F) ground electrode [79].....	48
Figure 3.12 MTS 866.02 formability press [79]	49
Figure 3.13 Hecker's hemispherical punch [41,79]	50
Figure 3.14 Grid measuring system [79]	51

CHAPTER 4

Figure 4.1 Biaxial TWBs with the weld placed a) -30 mm, b) -15 mm, c) 0 mm, d) +15 mm, and e) +30 mm offset from the centre	53
Figure 4.2 Strain distribution of the base unwelded metal in biaxial stretch forming a) DP980, b) DP600, and c) HSLA	53
Figure 4.3 Strain distribution of the plane strain TWBs the base unwelded material a) DP980, b) DP600, and c) HSLA	54
Figure 4.4 Plane strain TWBs with different weld orientations a) longitudinal TWB, and b) transverse TWB.....	55
Figure 4.5 Vickers hardness profiles of dissimilar materials TWB: a) DP600-HSLA, and b) DP980-HSLA	56
Figure 4.6 Deformed tensile specimens with different weld locations.....	58
Figure 4.7 Engineering stress-strain graph of TWB (weld position at the middle) and parent materials	58
Figure 4.8 %elongation of tensile specimens with different weld position for DP600-HSLA, and DP980-HSLA	59
Figure 4.9 Major-strain distribution profiles of uniaxial tensile specimens with different weld locations: a) DP600-HSLA, and b) DP980-HSLA.....	60

Figure 4.10 Deformed DP600-HSLA biaxial specimens with different weld positions a) -30 mm, b) -15 mm, c) 0 mm, d) +15 mm, and e) +30 mm offset from centre	62
Figure 4.11 Deformed DP980-HSLA biaxial specimens with different weld positions a) -30 mm, b) -15 mm, c) 0 mm, d) +15 mm, and e) +30 mm offset from centre	62
Figure 4.12 Deformed plane strain TWBs a) DP600-HSLA longitudinal TWB, b) DP600-HSLA transverse TWB, c) DP980-HSLA longitudinal TWB, and d) DP980-HSLA transverse TWB.....	63
Figure 4.13 Representative images of the biaxial stress forming specimen showing a) cross section macrostructure at the failure location, b) microstructure at the tip of failure, and c) fracture surface	64
Figure 4.14 Representative images of the transverse plane strain forming specimen showing a) cross section macrostructure at the failure location, b) microstructure at the tip of failure, and c) fracture surface	66
Figure 4.15 Representative images of the longitudinal plane strain forming specimen showing a) cross section macrostructure at the failure location, b) microstructure at the tip of failure, and c) fracture surface	67
Figure 4.16 LDH of the biaxial TWBs with different weld positions for DP600-HSLA, and DP980-HSLA	68
Figure 4.17 Load progression curves of TWBs with different weld line positions: a) DP600-HSLA, and b) DP980-HSLA.....	70
Figure 4.18 LDH of the plane strain TWB with different weld orientations for DP600-HSLA, and DP980-HSLA	71
Figure 4.19 Load progression curves of plane strain TWB specimens: a) DP600-HSLA, and b) DP980-HSLA.....	73
Figure 4.20 Strain distribution patterns of DP600-HSLA TWBs with different weld locations	75
Figure 4.21 Strain distribution patterns of DP980-HSLA TWBs with different weld locations	76
Figure 4.22 Strain distribution patterns of TWBs with different weld orientations for DP600-HSLA, and DP980-HSLA.....	78

CHAPTER 5

Figure 5.1 Curvilinear welded TWB	81
Figure 5.2 Vickers hardness profiles of curvilinear welds: a) HSLA steel, b) DP600 steel, c) DP980 steel, and d) macrograph of cross-section (DP980).....	83
Figure 5.3 Strain distribution profiles of HSLA linear and curvilinear welded blanks with different weld placements.....	86
Figure 5.4 Strain distribution profiles of DP600 linear and curvilinear welded blanks with different weld placements.....	87
Figure 5.5 Strain distribution profiles of DP980 linear and curvilinear welded blanks with different weld placements.....	88
Figure 5.6 HSLA linear welded blanks a) to c); and curvilinear welded blanks d) to f) with weld locations at 0, 15, and 30 mm.....	90

Figure 5.7 DP600 linear welded blanks a) to c); and curvilinear welded blanks d) to f) with weld locations at 0, 15, and 30 mm.....	90
Figure 5.8 DP980 linear-welded blanks a) to c); and curvilinear welded blanks d) to f) with weld locations at 0, 15, and 30 mm.....	91
Figure 5.9 Comparison of limiting dome height of laser welded bead-on plate straight weld blanks and bead-on plate curvilinear blanks with different weld locations from the centre during biaxial stretch forming.....	93

CHAPTER 6

Figure 6.1 Multiple-weld TWBs with different weld slopes a) parallel welds, b) low angle welds, and c) high angle welds	96
Figure 6.2 Strain distribution of the multiple welded TWBs.....	98
Figure 6.3 Multi weld TWB DP600-HSLA-DP600 a) parallel welds, b) low angle welds, and c) high angle welds; DP980-HSLA-DP980 d) parallel welds, e) low angle welds, and f) high angle welds	100
Figure 6.4 LDH graph of multiple weld TWBs	101

APPENDICES

Figure A.1 Modes of welding, conduction mode (left) and keyhole mode (right).....	116
Figure B.1 Strain paths of the DP600-HSLA uniaxial tensile specimens with different weld positions	118
Figure B.2 Strain paths of the DP980-HSLA uniaxial tensile specimens with different weld positions	119
Figure B.3 Strain paths for DP600-HSLA biaxial stretched TWBs with different weld positions	120
Figure B.4 Strain paths for DP980-HSLA biaxial stretched TWBs with different weld positions	121
Figure B.5 Strain paths for DP600-HSLA plane strain TWBs with different weld orientations	122
Figure B.6 Strain paths for DP980-HSLA plane strain TWBs with different weld orientations	122

LIST OF TABLES

CHAPTER 1

Table 1-1 Modes of stretch forming determined by the strain distribution profile	13
----------------------------------------------------------------------------------------	----

CHAPTER 2

Table 2-1 Factors that affect formability	19
Table 2-2 Summary of the effect of the three material properties on formability	20
Table 2-3 Summary of the types of fracture modes	20
Table 2-4 LSR and strength ratio of different laser welded blanks [53].....	27
Table 2-5 LDH comparison bead-on plate DP980 and HSLA to parent base metal DP980 and HSLA [61].....	32

CHAPTER 3

Table 3-1 Tensile properties of various AHSS sheets present in this study	40
Table 3-2 Flow properties of the weld bead.....	42
Table 3-3 Beam characteristics of the diode laser	45

APPENDICES

Table A-1 Summary of laser system characteristics.....	117
--------------------------------------------------------	-----

LIST OF EQUATIONS

CHAPTER 1

Equation 1.1 Keeler-Brazier relationship for FLD_0	15
------------------------------------------------------------	----

CHAPTER 2

Equation 2.1 Strength ratio [46].....	23
Equation 2.2 Limiting strength ratio [46].....	23
Equation 2.3 Limiting thickness ratio [46].....	23

CHAPTER 3

Equation 3.1 Major engineering strain	51
Equation 3.2 Minor engineering strain	51

CHAPTER 1

1 INTRODUCTION

Economic concerns and government regulations are forcing the automotive industries to push the limits in the design of their vehicles for weight reduction and cost reduction; while maintaining/improving structural integrity and crash performance. Now with raising environmental concerns on automotive emissions and the scarcity of natural resources (gas, oil and fossil fuels), the need to reduce vehicle weight to improve fuel economy is greater than ever. As a result, the automotive industries are employing tailor welded blanks (TWBs). In addition, steel makers are developing lighter and stronger steels, such as dual phase (DP) steel that have the same formability potential as conventional automotive steels such as interstitial-free (IF), drawing quality (DQ) and high-strength low-alloy (HSLA) steel for incorporation into the TWB designs. DP steel is a type of steel being investigated in TWB applications to reduce vehicle weight while maintaining structural integrity and crash performance.

1.1 *Tailor-Welded Blanks*

TWBs are blanks that consist of two or more sheet pieces differing in materials, thickness, coating, and/or material properties that are welded together before forming into the required part. Adjusting or tailoring the blank allows for the use of different materials and composites for various parts of the same component thereby reducing body-in-white weight while providing extra reinforcements where locally required. Moreover, the structural integrity is maintained without changing the forming dies. The advantages of using TWBs are numerous, they ensure that the components are light, stronger, and provide required functionality at lower cost than parts made from monolithic pressed sheets [1], as well as improving structural integrity, safety and corrosion resistance in specific areas; and they allow greater flexibility in materials selection. The part integration possible with TWB reduces the number of parts and assembly time required per vehicle. However, the disadvantages of TWB are related to the heterogeneous nature of the blank (due to the weld and dissimilar materials used), where the thinner/weaker material may deform preferentially and tear prematurely in stamping, which also results in weld line movement [2].

In terms of applications, TWBs were first used to overcome design challenges with the available material, such as the floor plate of the Audi 100 [1]. The floor plate of the Audi design specification was greater than the width of the steel supplied and thus, two sheets of steels were welded

together to create the TWB. Other applications of TWBs have been in structural members where different thicknesses of steels were welded together such as for centre pillars as commonly used in North America [3]. Currently most chassis/body structural members are being made as TWBs.

Figure 1.1 shows examples where TWBs can be found in a vehicle [3]. These TWBs consist of different grades and/or thicknesses of steel welded together to form optimized blanks that take advantage of the localized materials properties. For example, a) using thicker material near the engine fire wall and hinge area improves the crash performance, and b) using thinner material near the rear to reduce weight [4]; thereby, reducing the overall weight of the vehicle. Therefore, it is expected that the number of TWBs in automotive parts manufacturing will increase with the improvement in welding technology and development of newer light materials available.

From 1998 to 2009, roughly 552 million passenger cars were produced worldwide [5]. It was estimated in 1997 that each vehicle contained on average three to five TWBs [6] that would result in approximately 2-3 billion TWBs used. It is expected that more TWBs will be in use with the increasing and pressing demand for better fuel economy and environmental performance.

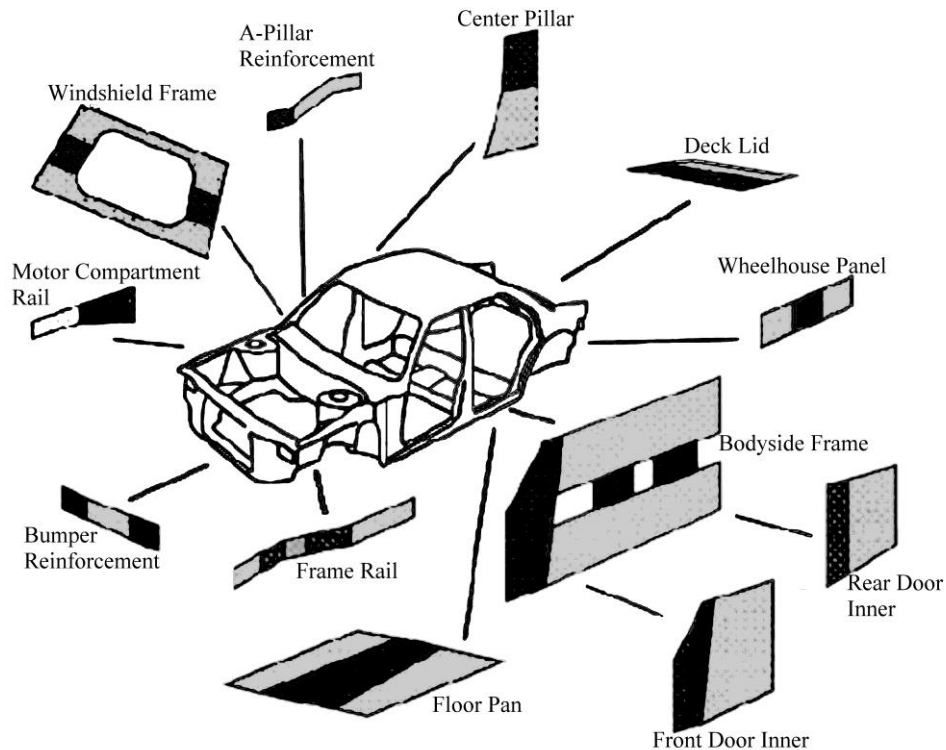


Figure 1.1 Examples of tailored blanks in an automobile [3]

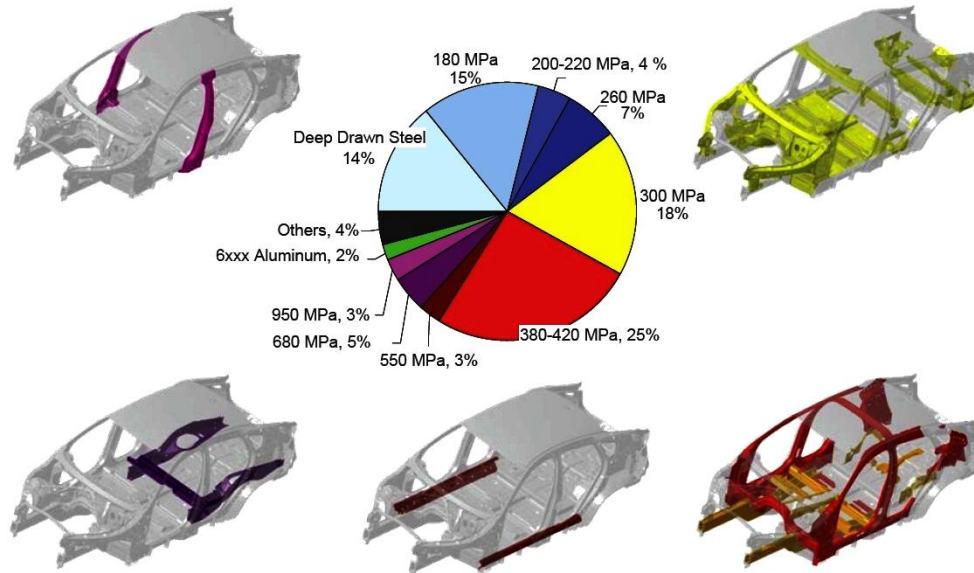


Figure 1.2 Types of materials and the strength required for body-in-white parts [7]

Figure 1.2 shows a pie chart of the materials used in the body-in-white (BIW). As can be seen in this chart 94% of the BIW is composed of steels and the other 6% is made up of aluminum and others such as thermoplastics and magnesium. Although, the application of aluminum and magnesium offer additional weight reduction in TWBs for the BIW, there are many obstacles that make these materials difficult to incorporate. The main issues are welding aluminum and magnesium to themselves and other materials. The high reflectivity of aluminum makes laser welding difficult and the weld in an aluminum TWB is not significantly stronger than the base metal as it can be with steel TWBs [8]; besides, the heat generated from welding tends to anneal the material of the weld and the heat affected zone (HAZ), which affects the performance of the TWB [9,10]. Consequently, the formability of aluminum TWBs may be limited by the inherent weld ductility. Further heat-treatment to manipulate local properties is possible; however, this method is not economically feasible for automotive applications [2,8]. In comparison, magnesium alloys are very light in weight, but pose different challenges. The challenges of magnesium include, low strength and generally poor ductility, low melting point compared to steel which makes them unsuitable for high temperature applications. Welding magnesium alloys is problematic because molten magnesium is highly reactive in air if not properly shielded [11]. Finally, applying magnesium may not be economically feasible in some cases because the cost of magnesium can reach up to six times that of steel [12]. Thus, steel is still predominating in the automotive industries.

1.1.1 Welding

Some welding methods used to create TWBs include laser, electron beam, mash seam welding (resistance welding) and friction stir welding. The most popular welding methods for TWBs are laser welding and mash seam welding because the low heat input applied by these methods does not cause too much thermal distortion. Laser welding is favourable in North America for TWB manufacturing because it can meet the increasingly “[tight] standards for weld quality, manufacturing flexibility and [offer] higher productivity [6].” Conversely, mash welding is favourable to European automakers and about 60% of the tailored blanks in Europe are created with this welding method. The differences between laser welding and mash welding are as follows:

1. Laser welding is a fusion-welding process, which joins the materials by localized melting by using a laser beam. The fusion zone (FZ) and heat-affected zone (HAZ) are narrow due to low heat input; and
2. Mash welding is a fusion-welding process that bonds two pieces of overlapping materials together through diffusion when passing through rollers under a high load.

In the laser welding process, a molten pool is created through the absorption of the incident radiation as the laser beam travels along the interface of the components. Upon cooling, the liquid melt pool solidifies and the components are joined leaving behind a FZ and a HAZ. The resultant FZ and HAZ have different microstructure from the base metal and material properties. For example, the final microstructures in the FZ depend on the heat input and cooling rate. Figure 1.3 shows a continuous-cooling transformation diagram for weld metal of low carbon steel [10].

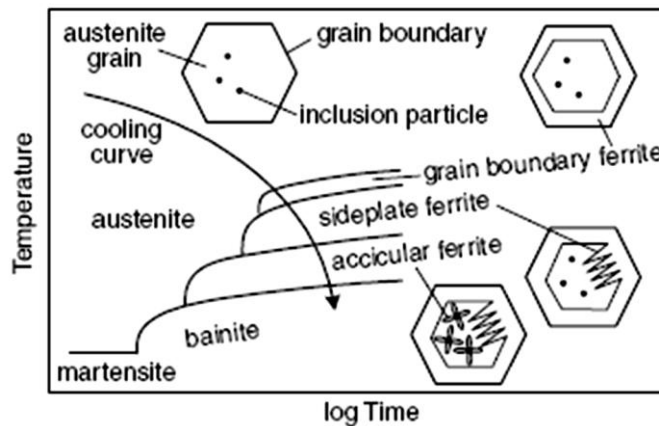


Figure 1.3 Continuous-cooling transformation diagram for weld metal of low-carbon steel [10]

From this figure, it can be seen that as the FZ cools the microstructure can contain a combination of grain boundary ferrite, side-plate ferrite, acicular ferrite, bainite and martensite. In addition, the microstructure changes depending on factors such as the alloying additions and grain size of the steel. Figure 1.4 shows the effect of adding alloying elements and increasing grain size on the continuous-cooling transformation diagram for low-carbon steel [10].

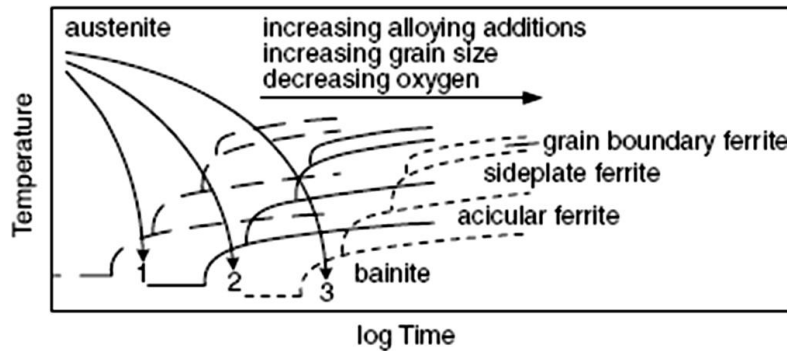


Figure 1.4 Effect of alloying element, grain size an, and oxygen on the CCT diagrams for weld metal of low-carbon steel [10]

HAZ is the region adjacent to the FZ where it is exposed to temperature high enough to induce microstructure and material properties change, but not high enough to cause melting. The metals most affected by the presence of the HAZ are cold-worked materials, as there is enough heat in this region to cause recrystallization and/or grain growth. The change in the microstructure and material properties can be better understood through thermal cycles. Figure 1.5 shows an example of thermal cycles and the change of grain size in the HAZ [10].

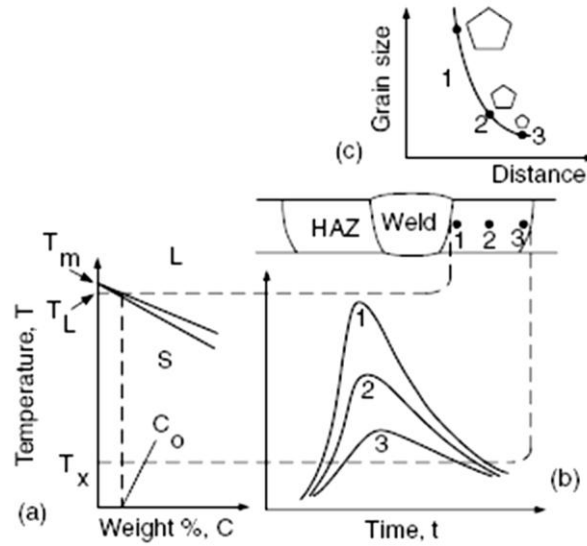


Figure 1.5 Grain growth in HAZ: a) phase diagram, b) thermal cycles, and c) grain size variations [10]

The peak temperature (well above the recrystallization temperature, T_x) closest to the fusion bound is the highest and the material in this area stays at this high temperature the longest. At a high temperature and with sufficient time, the grain grows. Moving away from the fusion boundary, the peak temperature decreases resulting in small grains. As a result, the HAZ can be made up of different regions, *i.e.* partial grain-refining (mix of coarse and fine grains), grain-refining (fine grains) and grain-coarsening regions (large grains) shown in Figure 1.6. Each region experiences different peak temperatures and has different microstructures as well as grain size. From this figure it is clear that welding causes inhomogeneity across the welded specimen.

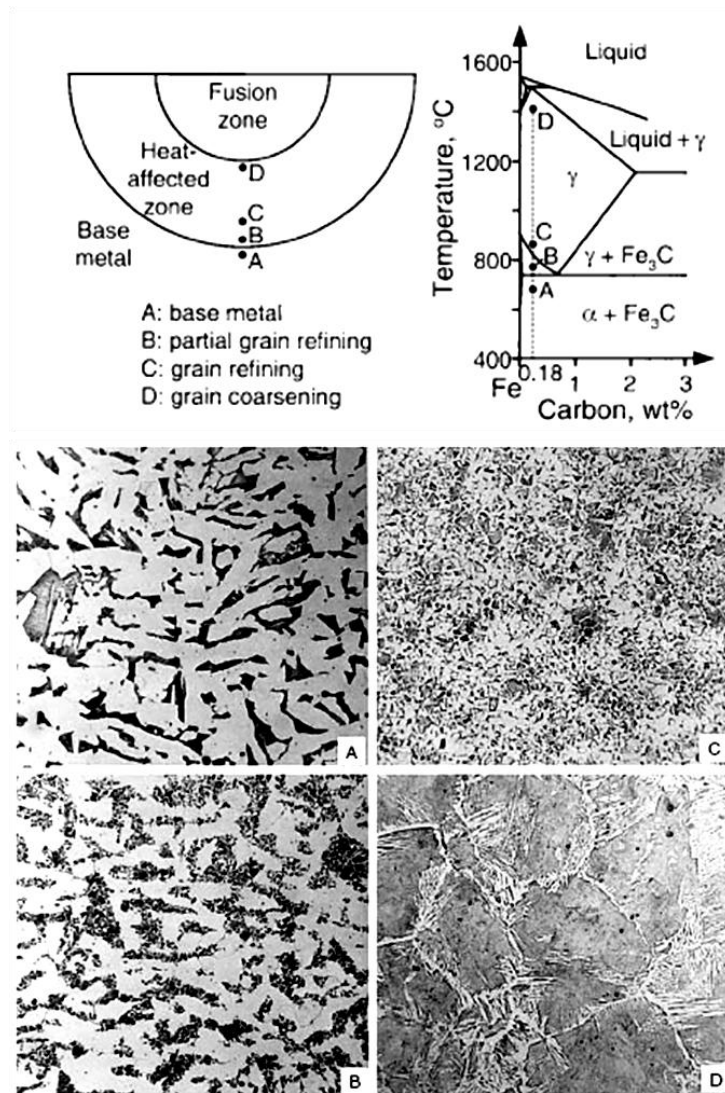


Figure 1.6 HAZ microstructure of a gas-tungsten arc weld of 1018 steel (magnification 200x) [10]

1.2 Advanced High Strength Steels

Various grades of steels are available for manufacturing stamped automotive components, and most of them have been incorporated into TWBs. Typical automotive grade steels include deep drawing steels (interstitial-free – IF, drawing-quality – DQ, extra-deep-draw – EDD), conventional high strength steel (high strength low alloy – HSLA) and the newer types of advanced high strength steels: AHSS, (dual phase, transformation-induced plasticity, complex phase and martensitic steels).

Deep drawing steels such as EDD, DQ and IF steels are used in TWB for complex stamping because of their very high formability *i.e.* stretchability and drawability [13]. The formability of these

steels is well understood [13,14,15,16]. However, these steels have low strength, which makes them poor for high local stress or high energy absorbing applications such as near the engine. On the other hand, high strength steel (HSS) have higher strength, but the ductility is sacrificed, where ductility is an indicator of formability. The use of HSLA in TWB is also significant because welding HSLA does not significantly change the forming behaviour of the TWB [17], high yield strength combined with reasonable ductility makes such TWBs good for forming operations. The formability of HSLA is also widely studied [2,18,19]. Figure 1.7 shows the relationship between strength and elongation for the conventional HSS and AHSS [20]. As seen in this figure, the low strength steels have excellent formability; however, they may not provide the structural integrity needed for similar thickness of HSS. In contrast, conventional HSS have a larger range of strength although as the strength increases the formability decreases, so they are suitable for applications where more strength is required. Notable in Figure 1.7 is the AHSS, especially lower strength DP steel which have similar formability as HSLA but the strength is much higher.

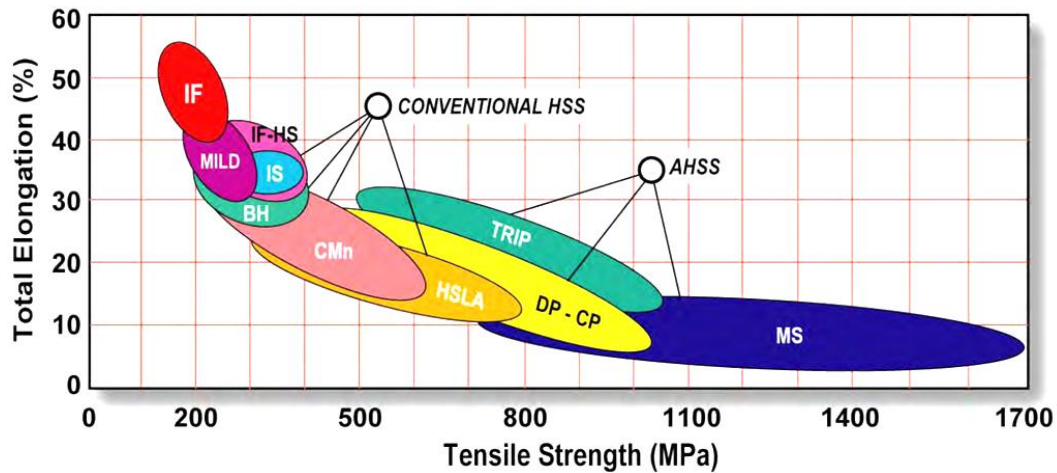


Figure 1.7 Tensile strength-total elongation relationship for low strength, conventional HSS, and Advanced HSS steels [20]

The main difference between conventional HSLA and AHSS lies in the microstructure. HSLA is a single-phase ferritic steel reinforced with second phase precipitates and strengthened by grain size reduction; while AHSS consists of more than one phase *i.e.* martensite, bainite, ferrite and retained austenite [20]. For example, dual phase steel (an AHSS), is made up of a soft ferritic phase reinforced with hard martensite islands. The martensite islands are produced by an intercritical annealing step followed by rapid quenching in the manufacturing process. It is during the quenching step that the austenite is transformed into martensite while the existing ferrite remains. As a result, the DP steels

have a good combination of ductility (offered by the continuous soft ferrite matrix) and high strength (depending on the volume fraction of martensite). The ductility of the DP steel makes it good for forming, while the strength is required to maintain structural integrity and improve crash performance. This uniqueness in DP steel lies in its material flow properties, DP steels tend to have relatively high work-hardening coefficients (n-values), K-values and R-values. Therefore, based on these properties, forming complex shapes with these high strength steel is possible [21].

Some applications where AHSS are used are the door outer, body structure, chassis frame applications, safety cage components, bumpers, and door beams [22]. Figure 1.8 shows the breakdown of the type of steels used in the TWBs for a vehicle [23].

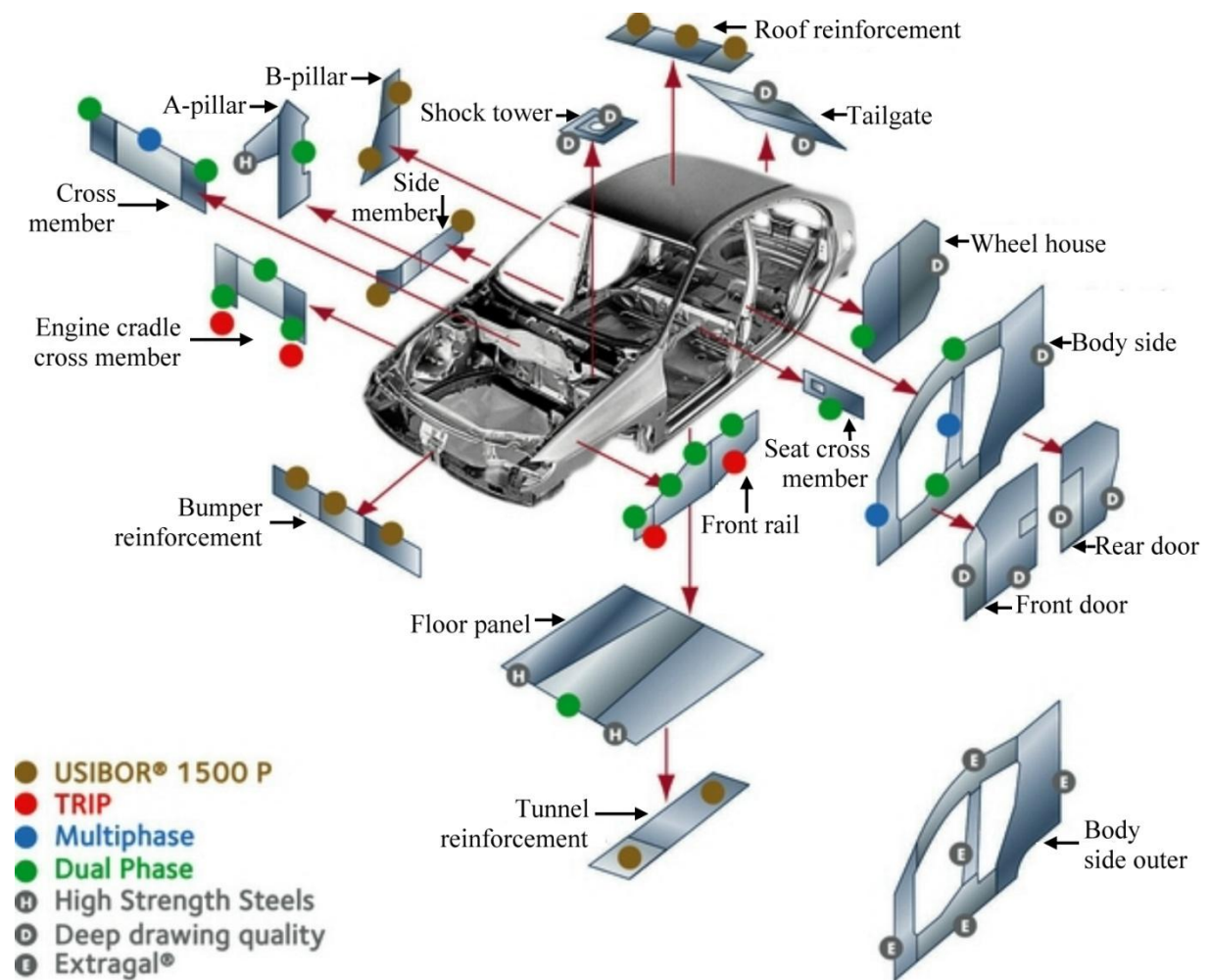


Figure 1.8 Materials breakdown in TWBs for a vehicle [23]

As seen in Figure 1.8, the majority of the TWB uses AHSS in areas where strength is required for energy-absorbing parts [21], while parts where formability is required use HSS and low strength steel. The use of AHSS, especially the lower tensile strength steels is advantageous to automotive manufacturers because for the same tensile strength DP, TRIP and complex steels give higher total elongation than the conventional HSLA. Thus, AHSS especially DP steel have the potential to replace HSLA in TWBs due to its high strength and comparable formability.

1.3 Formability

The formability of sheet metal is dependent on many factor such as its properties, microstructure, thickness and external factors. To understand formability of sheet metal is essential to define formability. Formability is loosely defined as a sheet metals ability to be mechanically shaped by plastic deformation without machining [24]. Sheet metal forming occurs when a sheet is clamped around the edge of a die and a punch forces the sheet (form) through a cavity where the sheet is stretched to conform to the shape of the tools [25]. To measure the formability of a metal, standardized sheet forming processes are used. There are many types of sheet metal forming processes used to measure formability, two well used forming operations are (1) stretch forming e.g. hemispherical punch test, and (2) deep-drawing.

The hemispherical punch test is a type of limiting dome height (LDH) stretch testing equipment that has a high degree of reproducibility when compared to other stretch forming tests, such as the Ohio State University test and the Swift round bottom test. In this test, draw-beads are used to hold the steel sheet firmly in place to prevent drawing in during forming process. The resulting form of the sheet metal is a rounded dome shape. There are also many studies [26,27,28,29] done using this test to determine the formability of metal. On the other hand, deep drawing is an operation that forms the metal by forcing the punch against the sheet metal over a die edge and into the cavity. The resulting part looks like a cup and this test is used typically for forming cups, shells, short tubes, automobile bodies, and gas tanks [30] with a flat plane on the bottom.

1.3.1 Analytical Methods Of Quantifying Formability

As there are different methods of characterizing formability, there are different methods of analyzing formability. The three most common methods are:

- (1) The height of the deformed specimen in the dome test
- (2) The strain distribution across the deformed blank (forming behaviour)
- (3) The forming limit diagram (FLD) based on the strains measured

These methods require the sheet metal to be deformed until necking occurs or when the metal reaches their forming limit. All materials have a forming limit, which is the maximum uniform strain adjacent to a localized neck or tear in a deformed specimen [31]. When the metal reaches its forming limit the test is stopped to allow for measuring of the dome height, strains across the deformed blank to be used in the strain profiles and the FLD. The following sections discuss in further details of each of the common formability measurements.

1.3.1.1 Limiting Height Of The Deformed Specimen

The first method of determining formability is finding the maximum height of the dome formed in a specimen in the hemispherical punch LDH test. Under simulative tests, the test is stopped when localized necking or fracture occurs and the resulting height is referred to as the limiting height. This limiting height is a measure of the maximum deformation the material experiences before failure and is often referred to as the forming limit and is used as a quantitative indicator of formability. In addition, the load required to obtain the LDH can be used as an additional definition of the limit of formability as it helps to indicate where plastic instability occurs [24]. Figure 1.9 shows a deformed sheet specimen that has been subjected to the limiting dome height test.

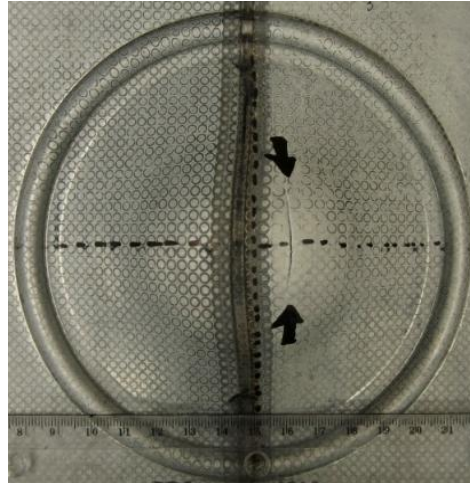


Figure 1.9 Deformed welded steel specimen under the limiting dome height test

1.3.1.2 Strain Distribution

The second method of analyzing formability or forming behaviour of the materials after deformation is the strain distribution, which can be used to generate a plot of the major and minor principal strain. Typically, true strains are used to plot the strain distributions because true strains are equivalent in tension and compression, except for the sign; true strains are additive; and due to the volume constancy, the combined normal strains are zero for the plastic portion of the total strain [32]. Figure 1.10 shows an example of a strain distribution profile of a bent sample [33]. As shown in this figure, as the bend radius reduces, the strain profile sharpens. The strain distribution is obtained after the simulative test on the gridded material is stopped at localized necking *i.e.* when the forming limit of the material is reached.

Also, the strain distribution profile illustrates the forming behaviour of the metal across the sheet material, high strain concentration areas (vulnerable regions where necking occurs), the amount of formability (area under the major strain curve) and the modes of stretching. The modes of stretching can be determined from the strain profiles by examining the major and minor strain curves and are categorized in the Table 1-1. The strain distribution profile may be used in TWB design is to determine areas prone to failure.

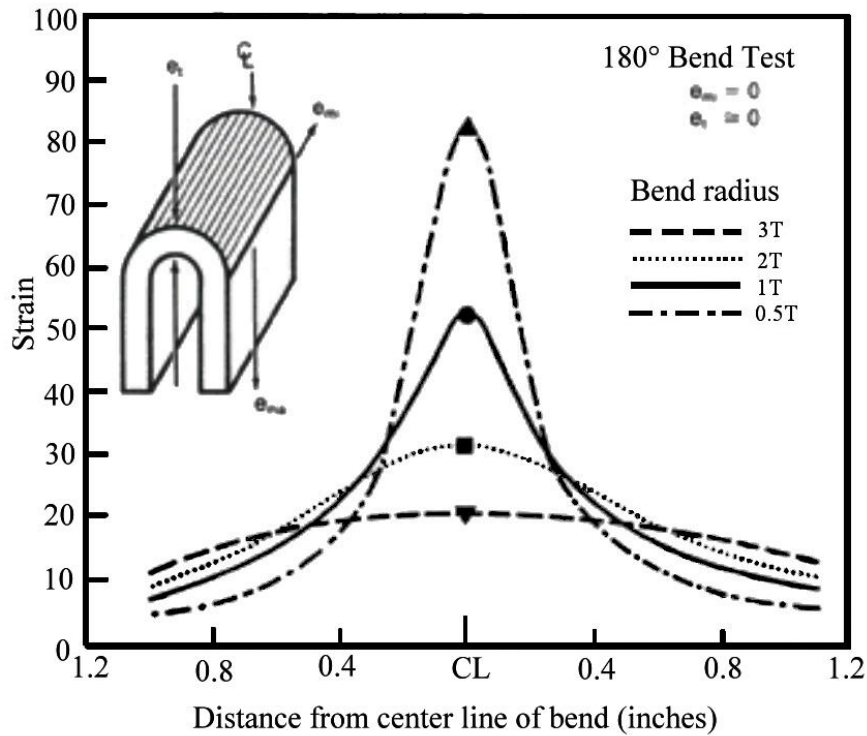


Figure 1.10 Strain distribution profile [33]

Table 1-1 Modes of stretch forming determined by the strain distribution profile

	Major strain	Minor strain
Biaxial stretch forming	Positive	Positive (close to major strain value)
Plane strain stretch forming	Positive	Zero
Tensile-compression stretch forming	Positive	Negative (compression)

1.3.1.3 Forming Limit Diagram

The third method of analyzing formability is the forming limit diagram (FLD), also known as the Keeler-Goodwin diagram shown in Figure 1.11, which can be used to determine critical areas of strain. Generally, the forming limit curve (FLC) of the material is plotted in the FLD, which refers to the forming limit of the specific material under a full range of strain states. A higher FLC (higher forming limit for a range of strain states) of the sheet metal results in better formability. FLC shape depends on the material properties (n -value, anisotropy), sheet thickness and size and the strain path and strain gradients [31].

The use of the FLD in formability analysis is to diagnose problems by comparing the failure-prone areas to the FLD. This approach is used to determine the severity of the potential problems due to factors such as lubrication, tooling, material properties and thickness. In addition, the nature of the problem can be assessed *i.e.* where the forming is performed under specific modes of stretching. For example, under dry conditions, a square blank will stretch under close to plane strain conditions where the forming limit of the metal is the lowest; however, with the use of lubrication the mode of stretching or strain path can be made more biaxial where there is more formability, as can be seen in Figure 1.11 .

The FLD shows that the strain path and the strain at localized necking are a function of the minor strain [33]. Some points of interest in an FLD are the modes of stretching; the right side of the FLD involves strains in both the major and minor direction in tension; while in the left side the minor strain is negative, similar to the uniaxial tensile condition; finally, the lowest point in the FLC occurs under plane strain stretching condition where the major strain is the lowest and the minor strain remains unchanged at zero. Figure 1.11 shows the strain path during punch stretching and the effect of applying lubrication and changing the blank width. Decreasing the blank width (so that the lateral edges of the blank are not uniformly clamped) results in a tensile-compression stretching (*i.e.* reducing the minor strain); while increasing the blank width results in a tensile-tensile stretching (*i.e.* increasing the minor strain).

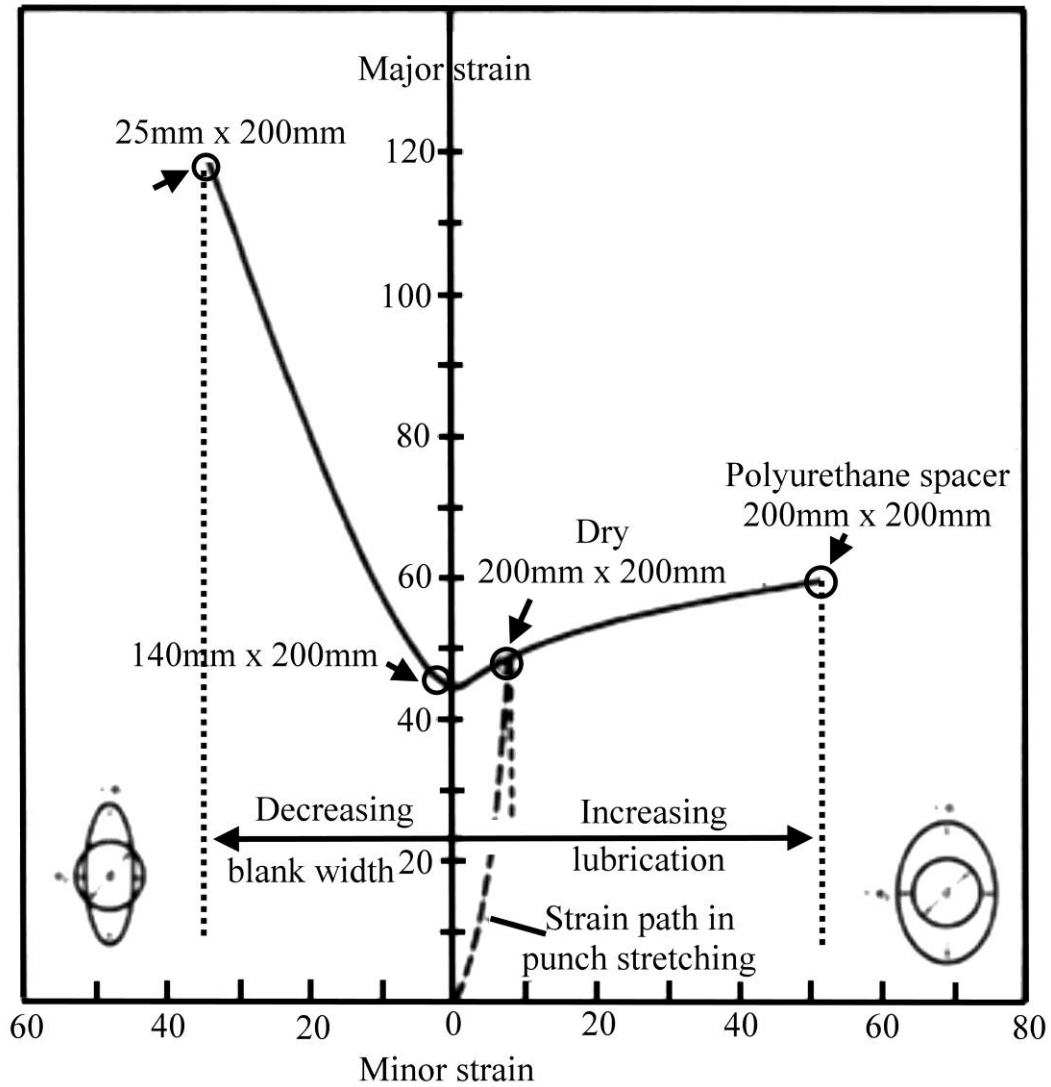


Figure 1.11 A forming limit diagram generated in laboratory tests by changing the width of the blanks [33]

There are also factors that shift the FLC, which are the thickness and the n -value since they change the FLD_0 (the lowest point on the FLD). The relationship of thickness, n -value, and FLD_0 is represented by the Keeler-Brazier equation [34] in Equation 1.1:

Equation 1.1 Keeler-Brazier relationship for FLD_0

$$FLD_0 = \ln \left[1 + \frac{23.3 + 14.13t}{100} * \frac{n}{0.21} \right] \text{ for } n \leq 0.21$$

An example of application of the FLD in the automotive industries is shown in Figure 1.12 [35]. For example, when stamping the front door and front fender, the material used for stamping experiences more biaxial stretch forming; while stamping the roof and trunk lid the strain path of the material will follow plane strain stretch forming. The FLD allows TWB designers to correct potential failures prior to the commencement of volume production.

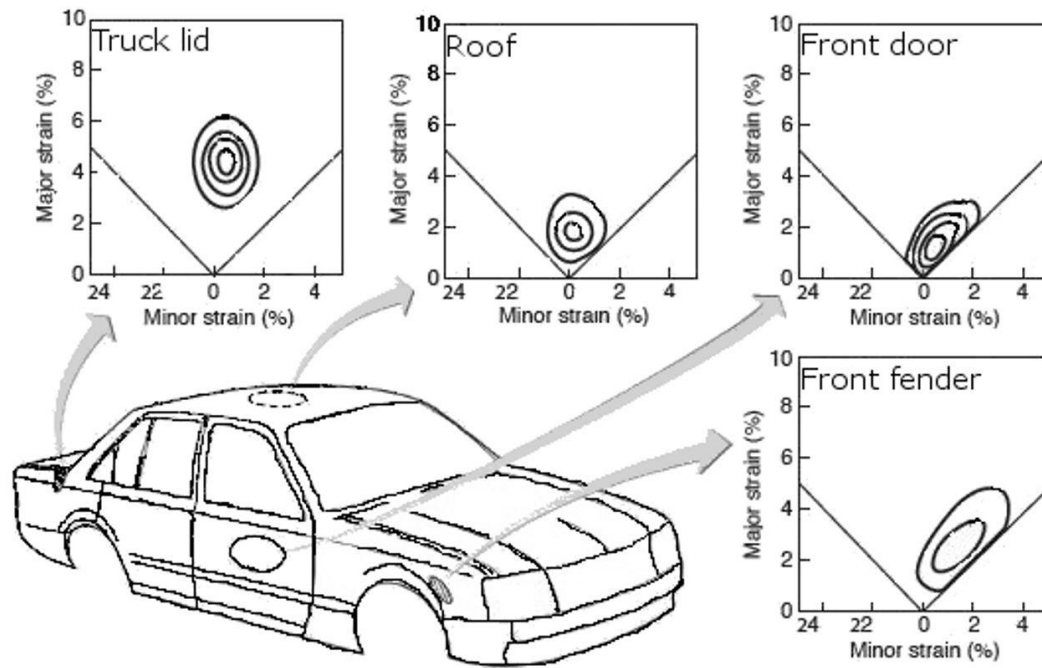


Figure 1.12 Major and minor strains (strain paths) of various automotive parts

1.4 The Problem

As mentioned in the section 1.1: Tailor Welded Blanks, assembly of blanks by welding has major effects on formability due to the inhomogeneity of the weldment and materials used. In addition, weld in DP steels may contain a softened zone at the outer edge of the HAZ [36,37,38,39]. This softened region is caused by the tempering of martensite, which reduces the hardness of this region during the welding thermal cycle. Significant softening may in turn affect the formability of welded DP steels by concentrating strains in this region during the forming process, resulting in premature failure. One method of improving the formability of TWBs involving DP steel is to combine it with HSLA steel. When deforming this TWB combination, the strain concentration location shifts to the weaker material (HSLA steel) as the hardness of HSLA steel is lower than the softened region in the DP steel [27]. Yet, the formability of TWBs with DP steel needs to be improved further.

Moreover, most TWBs used in the automotive industries contain more than one single straight weld (see Figure 1.1) and the interaction of multiple welds may also affect formability, but research results on the formability of these more complex TWBs are not available. In addition, TWB manufacturers orient multiple welds to simulate and accommodate components of curved shape, such as shock towers. However, this approach may also result in the presence of an inflection point, which during forming is the most likely area for failure. The study of the effect of curvilinear seams on formability is limited. Therefore, curvilinear seams need to be investigated further; in order to increase the application of more complex TWBs in the automotive industries.

1.4.1 Objectives

The objective of this thesis is to investigate methods to improve formability of DP steel by combining it with HSLA through weld geometry designs. The dissimilar TWB combinations studied involves DP600-HSLA and DP980-HSLA. The weld designs being investigated are:

(1) **Weld line positions, orientation and strain path.** Weld line positions are studied since weld line placement in areas of low strain concentration improves formability. For instance, in deep drawing applications, placing the weld close to the pole increases draw depth [40]. Weld orientations, tested under plane strain condition affect formability depending on weld ductility and material properties of the blanks

(2) **Curvilinear welds.** Although, the application of the curvilinear weld is limited to shock towers at present, there is potential for curvilinear welds. Curvilinear welds can decrease material usage, the number of weld requirements and offer possible opportunities to avoid defects when two welds intersect.

(3) **TWBs with multiple straight welds.** The interaction of more than a single weld may change the formability and many TWB applications involve multiple welds and multiple materials, e.g. vehicle floor plates [3].

In addition to weld designs, the TWBs with the exception of the curvilinear weld blanks are made of dissimilar thickness and dissimilar materials combination. It is the intent of this work to provide formability data for use in models, so predicting future failure locations while assessing forming behaviours of dissimilar thickness and materials combination TWBs with different weld designs is made easier. An understanding of the forming behaviour of dissimilar blanks with DP steel

promises to be beneficial to the weight reduction, crash performance and future vehicle design considerations. This thesis investigates the effect of blank designs (with DP600, DP980 and HSLA, specifically) and all other conditions *i.e.* factors that influence formability such as welding parameters and testing equipment designs are kept constant.

In this thesis, a literature review of factors that affect formability is given in chapter two. Chapter three features the experimental procedures, which includes the welding- and forming-parameters and the use of analytical tools. Chapter four examines the formability of the different weld position TWBs, orientation TWBs, failure locations and the strain distributions involved. Chapter five features curvilinear seam blanks and their effects on formability. Chapter six investigates the effect of two welds and their orientations on formability. Lastly, current conclusions and recommendations for future work are presented in chapter seven.

CHAPTER 2

2 LITERATURE REVIEW

This chapter reviews past studies on the effect of material properties, thickness differences, welding, weld positions and orientations and curvilinear seam welds on formability of TWBs.

2.1 *Factors Affecting Formability And Fracture Modes*

While the formability of TWBs has been widely studied with the introduction of new materials there are still many unknowns about the factors affecting formability. Some factors that affect formability are shown in Table 2-1. Some of these factors can be divided into three categories: 1) material, 2) process and 3) testing equipment design. For the purpose of this thesis, the process and testing equipment design remained constant.

Table 2-1 Factors that affect formability

Material	Process	Testing equipment design
Sheet thickness	Mode of stretching <ul style="list-style-type: none"> • In-plane • Out-of plane 	Draw bead
Material properties <ul style="list-style-type: none"> • Strain hardening coefficient (n) • Anisotropy (r) 	Strain path <ul style="list-style-type: none"> • Biaxial • Plane strain • Uniaxial 	Die corner radius
Grain size	Deformation speed	Punch corner radius
Inclusions	Blank holding force	Punch-die clearance
Welding	Lubrication	

As shown in Table 2-1, the material properties that affect formability include the strain hardening-coefficient, and anisotropy. Also, ductility contributes to formability, as it is an indicator of formability. These material properties are obtained through intrinsic tests *i.e.* uniaxial tensile test. The significance of: (1) strain hardening coefficient - *n*-value; (2) plastic anisotropy - R-value and (3) ductility of the material on formability is summarized in Table 2-2:

Table 2-2 Summary of the effect of the three material properties on formability

	Strain hardening coefficient	Plastic anisotropy (associated with rolled material)	Ductility
Relationship to formability	The material's ability to distribute strain during deformation and resistance to necking. Higher n -value = better ability to distribute strain	The material's ability to resist thinning. Higher R-value = higher resistance to thinning	Strengthening mechanisms that increase flow strength causes an increase in the stresses during forming
Represented by	Power-law hardening $\sigma = K\epsilon^n$ $\sigma = \text{yielding strength}$ $\epsilon = \text{induced strain}$ $K = \text{strength coefficient}$ $n = \text{strain hardening coefficient}$	$\bar{R} = \frac{R_0 + 2R_{45} + R_{90}}{4}$ $R = \frac{\epsilon_w}{\epsilon_t} = \frac{\epsilon_y}{\epsilon_z}$ $\epsilon_t = -(\epsilon_l + \epsilon_w)$	$\% \text{ elongation} = \frac{\Delta l}{l_0}$
Property associated with	UTS	Strain	Strain

2.1.1 Fracture Modes

Although the fracture does not affect formability, it is related to the ductility of the blanks being deformed, as fracture modes depend on the material combination. There are essentially three types of fracture modes seen in the forming of TWBs. The types of fracture are summarized in Table 2-3 and the two most common fractures are shown in Figure 2.1.

Table 2-3 Summary of the types of fracture modes

	Mode I	Mode II	Mode III
Fracture location	Across the weld	Parallel to the weld in the base metal	Parallel to the weld in the HAZ
Reason for fracture	Low weld ductility as the weld is stretched along the major strain direction	Base metal is stretched past its forming limit	Local drop in hardness in the HAZ [18]
Types of TWB combination fracture occurs	Similar thickness and material properties	Dissimilar thickness and material properties	Dual phase steels

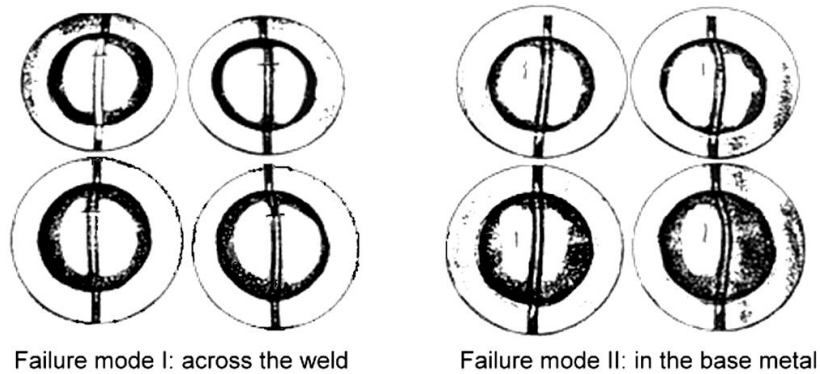


Figure 2.1 Failure modes: I) fracture across the weld, and II) fracture in the base metal [41]

2.2 The Effect Of Strain Hardening And Plastic Anisotropy

The two material properties that are related to the formability of a material are the n -value and the R -value. Their effects on formability are summarized in Table 2-2, where the n -value is the ability of the material to redistribute strain before necking and the R -value is the ability of the material to resist thinning during deformation. It should be noted that anisotropy may be introduced by the large deformation inherent in the steel sheet manufacturing process. For example, the initial rolling of the sheet metal will affect further deformation of the material [36]. Therefore, the studying of these two properties on the formability of material provides TWB manufacturers a point of reference in choosing materials based on the application.

Yang *et al* [29] studied the effects of the n -value and the R -value on the forming limit in the hemispherical-punch stretching test, numerically. They found that the n -value was proportion to the LDH; while the r -value was inversely proportional to the LDH, shown in Figures 2.2 a) and b), respectively. The numerical models showed that as the n -value increased and the r -value decreased, the strain distribution became more uniform with lower peak strains [29]. Thus, the strain-hardening and anisotropy affect the results of the standard LDH tests for formability.

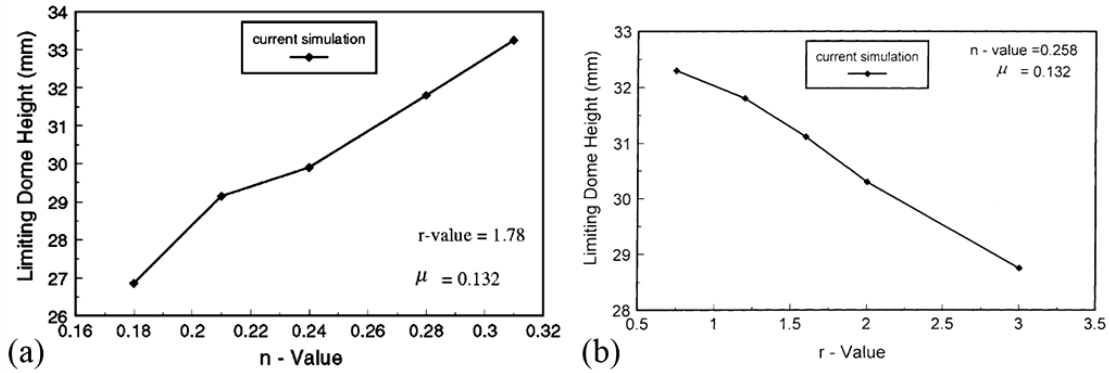


Figure 2.2 Numerical effect of a) n -value, and b) R -value on the limiting dome height [29]

On the other hand, Padmanabhan *et al* were interested in the effect of anisotropy under complex stress-strain state of the square cup deep-drawing process of mild steel welded to DP steel, numerically [36]. From the simulation, the thinner material experienced more deformation causing the weld line movement towards the stronger material. Significant weld line movement is undesirable as it may create problems such as wrinkling, tearing, and uncontrollable springback [42]. Anisotropic property behaviour was seen significantly in the mild steel side of the mild steel-DP steel TWB. In addition, the thinning along the weld line resembled an isotropic material combination more than an anisotropic TWB [36], which may indicate that the effect of anisotropy was erased during the welding process.

2.3 The Effect Of Thickness And Strength Ratios

TWBs made with dissimilar thickness and strength ratios are very common in vehicles especially where weight reduction and structural integrity are required, such as in a door inner panel. A number of studies showed that increasing the thickness and/or strength ratios decreases the formability of the TWBs [43,44,45]. A large thickness ratio forces more deformation into the weaker material and the strain is concentrated there, which results in premature failure. During deformation, the thinner material undergoes plastic deformation, whereas, the thicker material undergoes primarily elastic deformation. An increase in strength ratios has a similar effect on failure mode as the thickness ratio, whereby the weaker material deforms more and fails first. Failure may occur in the base metal *i.e.* the TWB experienced fracture mode II. In addition, due to non-uniform deformation, the weld line also tends to move towards the thicker/stronger materials [43,44,46]. Thus, to determine the effect of

thickness ratio Lee *et al* suggested forming TWBs comprised of materials with similar yield strength, but different thicknesses [47].

Shi *et al* [46] analyzed forming issues in terms of the strength ratio and the thickness ratio. The strength ratio (Equation 2.1) is described with the following relationship:

Equation 2.1 Strength ratio [46]

$$S_{TA}t_{OA} = S_{YB}t_{OB}$$

Where,

- S_{TA} is the tensile strength of material A
- S_{YB} is the yield strength for material B

The limiting strength ratio becomes (Equation 2.2):

Equation 2.2 Limiting strength ratio [46]

$$LSR = \frac{\text{Yield strength (ys) of the higher strength material}}{\text{Ultimate tensile (UTS) of the lower strength material}}$$

An application having a LSR of less than unity for the TWB provides better uniform stretching; however, in laser welded AHSS, the presence of the softened HAZ region and the increased hardness of the fusion zone as well as differences between those and the base metal hardness changes the formability of the TWB[39]. Conversely, the limiting thickness ratio does not change significantly. The limiting thickness ratio is given by Equation 2.3:

Equation 2.3 Limiting thickness ratio [46]

$$LTR = \left(\frac{t_{OB}}{t_{OA}}\right)_{limit} = \frac{S_{TA}}{S_{YB}}$$

Where,

- t_{OB} is the original thickness of material B
- t_{OA} is the original thickness of material A

When evaluating the effect of dissimilar materials TWB with dissimilar thickness and strength, the strength and thickness of material B should be the one with the greater thickness as well as greater yield strength. Based on these criteria, it was suggested that when failure mode I (fracture across the weld) was observed, the weld line should be positioned away from the major strain direction and/or

away from major strain concentration areas. When failure mode II (fracture parallel to the weld) was observed, the thickness/strength ratio was considered to be too large as the fracture occurred in the thinner or weaker material. Based on the failure modes, weld line movement or the amount of strain in the thinner/weaker material should be limited to improve formability [48].

Azuma *et al* studied the effect of strength ratio (thickness ratio) and its relationship to the maximum forming height [49], shown in Figure 2.3. In this study, two weld line orientations were studied, longitudinal and transverse, and compared to the parent unwelded material. The longitudinal weld orientation referred to the weld placed parallel to the major strain direction. During forming of the longitudinal TWB, the weld is being stretched. In the transverse weld orientation, the weld was placed perpendicular to the major strain direction and the base metal is stretched during forming.

This study showed that the forming height of the longitudinal and transverse welded TWB (with a strength ratio of 1.0) reduced by 30% and 8%, respectively when compared to the parent material. However, as the strength ratio increased the loss of forming height in the TWB with the weld in the transverse direction showed a steady drop until a ratio of 1.5 is reached. Comparatively, the drop in the maximum forming height for the longitudinal TWB was relatively small for the strength ratio of 1.0 to 1.8. This suggested that the ductility of the welds were similar. Surprisingly, the maximum height for the strength ratio of 1.5 for two loading directions was very close with a difference of approximately 10%.

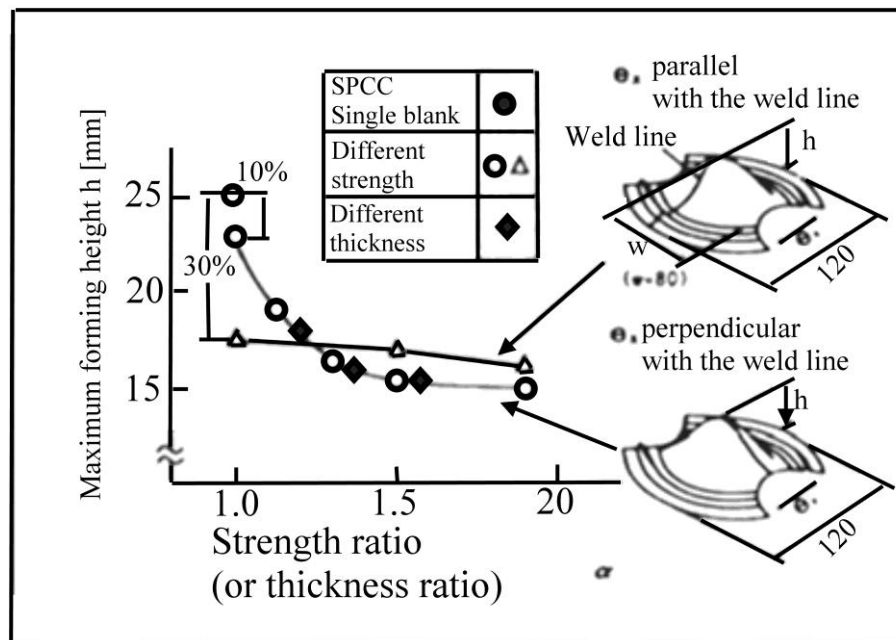


Figure 2.3 The relationship between the strength ratio and forming height for steel TWB [49]

From the study by Azuma *et al* it is clear that thickness ratio affects the forming height; however, the effect of thickness ratio on the strain distribution and its consequence on the FLD is unclear. Thus, Chan *et al* [45] investigated the effects of the thickness ratio of TWBs on the experimental FLC with varying TWB widths from balanced biaxial tension to uniaxial tensile with the weld line at the centre of the blank and perpendicular to the major strain direction; and also on the minimum major strain on formability. The results showed that the FLCs of the TWBs were lower than the base metal, which was expected; however, as the thickness ratio of the TWBs increased the FLC decreased. This relationship is shown in Figure 2.4, which compared the FLCs of the different thickness ratios to the base metal. The TWB FLC most similar to the base metal had the smallest thickness ratio. The small thickness ratio means that plastic deformation in the TWB for both sides of the weld was similar.

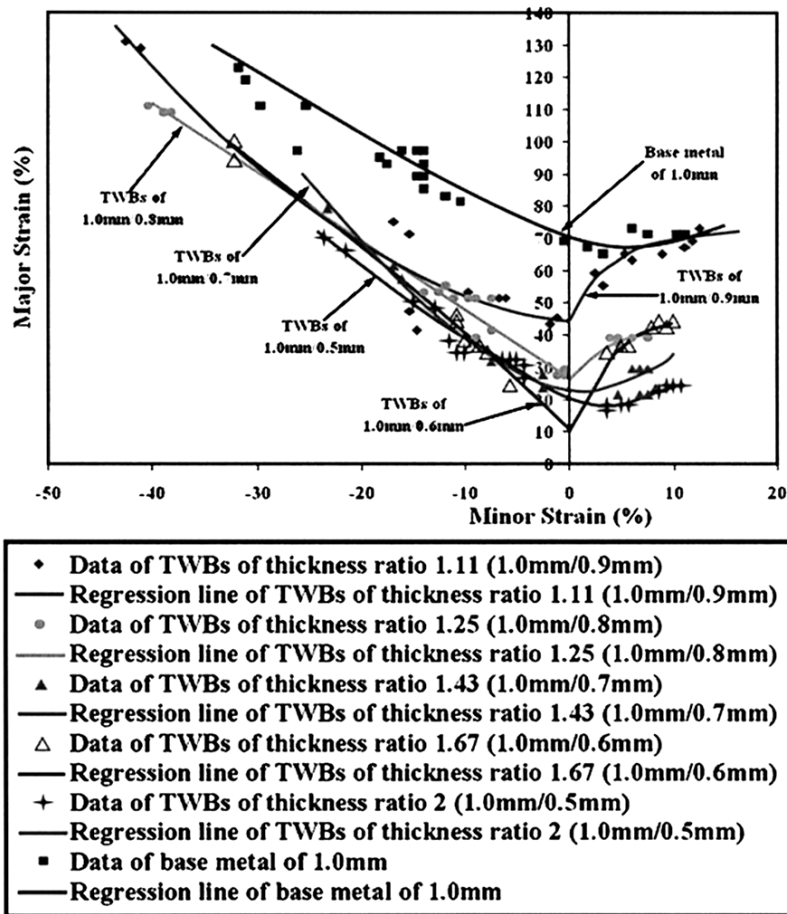


Figure 2.4 Comparison of the FLCs of the TWB with 1 mm base metals [45]

The study on the minimum major strain showed an inversely proportional relationship between the thickness ratio and formability of the TWB *i.e.* as the thickness ratio increased the formability decreased [45]. This relationship is seen clearly in Figure 2.5. As the thickness ratio increased the minimum major strain decreased, which implied that increasing thickness ratio decreased formability [45,47].

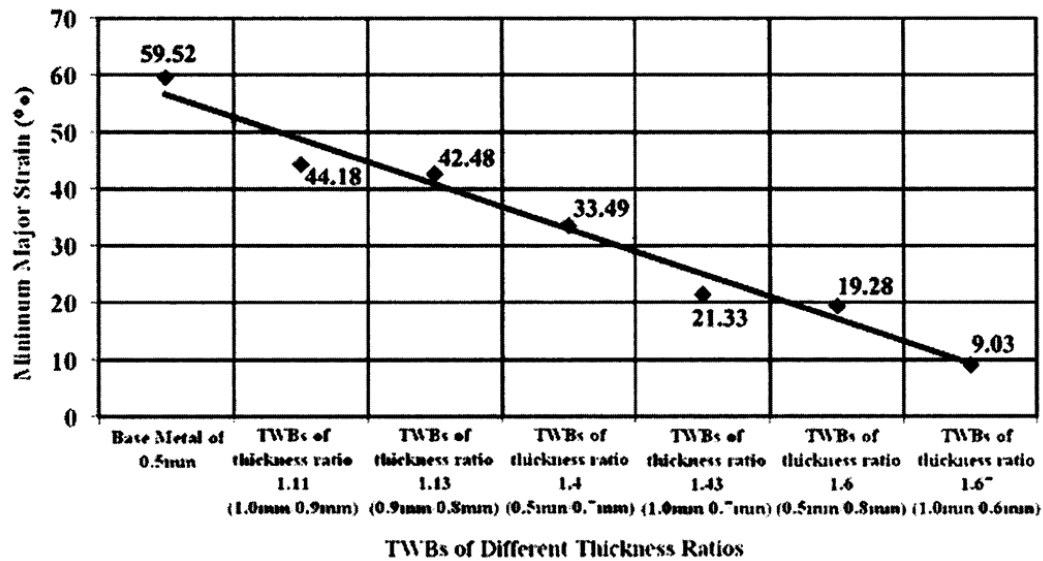


Figure 2.5 The relationship of thickness ratio to minimum major strain [45]

As seen in this section, these studies examined the formability of different thickness ratio; however, Heo *et al* took the investigation further by trying to control the amount of deformation by employing a draw bead during forming [50]. This investigation showed that by using the draw-bead to restrain the deformation in the thinner sheet, the drawing force increased. Consequently, increasing the draw force decreased the drawing depth of the blank as the deformation in the thinner material is restrained. From this study, the researchers reasoned that employing the proper use of draw-beads the draw depths of dissimilar material TWBs can increase; thus, suggesting the advantage of testing equipment design prior to the stamping process.

2.4 The Effect Of Welding

Fusion welding creates inhomogeneity across the TWB, such as a change in the microstructure in the FZ and the HAZ, which affects the formability of the TWB. Adonyi *et al* studied the effect of laser welded steel tailored blanks with automotive grade steels *i.e.* IF, HSLA and drawing-quality special-killed (DQSK) steels [51]. The TWBs studied were made up of similar thickness, material and coating combinations in plane strain stretch forming. Adonyi *et al* found the typical increase in the hardness of the TWB at the fusion zone, and forming the TWBs gave lower LDH than the parent materials. Upon investigation of the fracture surface of the plane strain specimens (transverse weld TWBs where the weld is perpendicular to the major strain direction compared to the longitudinal weld TWBs where the weld is parallel to the major strain direction), there was a strong correlation between the LDH variation and weld ductility for the longitudinal weld TWBs; however, the correlation between weld FZ hardness and formability remains unclear. To clarify the relationship between hardness and formability, the LDH of TWBs welded with GTAW was compared to that of laser welded TWBs. The weld FZ in the GTAW specimens was wider due to slower welding speed and higher heat input than the laser welded specimen, but the hardness of the GTAW was lower; however, the formability was lower in the GTAW welded specimens. This result led to the conclusion that weld-width (metallurgical inhomogeneous area) in a blank affected the formability and thus, weld ductility along with weld size and location are better indicators of formability than weld hardness [51,52].

Shao *et al* [53] studied laser blank welding of high-strength steels to mild steel of various dissimilar materials TWB combinations. Combining high-strength steels and mild steel caused a lowering of the cup height (quantitative indicator of formability) when the strength ratio of the dissimilar material TWB was higher than their LSR. Table 2-4 shows the LSR and the strength ratios of the different welded blanks and Figure 2.6 shows the cup height at fracture for the different parent material and TWB combinations. The TWB combinations that showed the strength ratio exceeding the LSR were MS + MS and HS3+ MS in Table 2-4, which corresponded to the higher cup height than the parent materials seen in Figure 2.6. From this observation, the authors reasoned that both base metals contribute plastic strain during the deformation process.

Table 2-4 LSR and strength ratio of different laser welded blanks [53]

Welded Blank	MS + MS	HS1 + MS	HS2 + MS	HS3 + MS	HS4 + MS
LSR	1.0	0.91	0.91	0.94	0.83
σ_Y of HS/ σ_T of MS	0.53	1.56	1.32	0.84	1.46

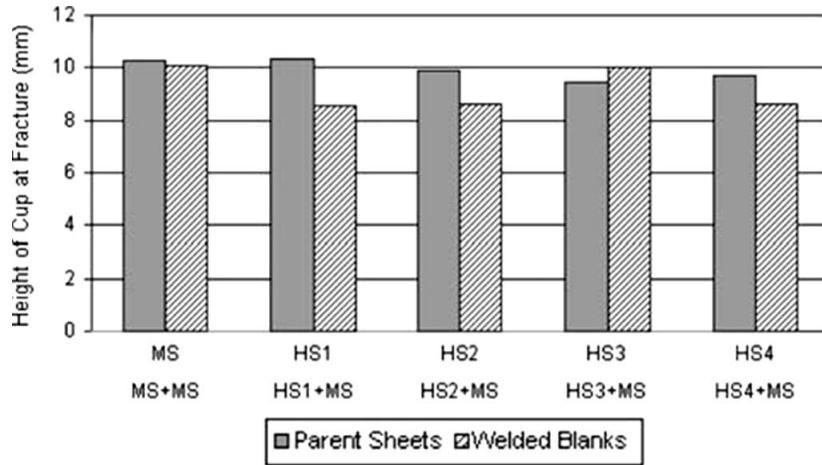


Figure 2.6 Comparison of equiaxial stretch formability between laser-welded blanks and the parent materials [53]

The formability of these TWBs as a whole was shown above; however, the distinctive effect of the weldment was not accounted. Cheng *et al* [54] investigated the effect of the weldment of the TWB on formability analysis experimentally and numerically. In order to study the mechanical properties of the weldment, specially designed tensile specimens where only the weld was present in the gauge length were used. The result showed typical increase in hardness in the weldment, and compared with the results in the standard tensile tests, the authors concluded that the tensile properties of the thinner material had a dominant effect on the formability [54]. The dominant influence of the thinner material in TWBs [44,45,46] was discussed in the previous section. To support this observation, the strain distribution across the weld was plotted (experimentally and numerically) in Figure 2.7. These results showed that in both the experimental and numerical simulation, twin peaks occurred across the weld; although, failure occurred in the thinner material because the peak strain was higher than the peak strain in the thicker material. However, the strain across the weld bead was nil despite the high strains in the adjacent areas. Therefore, the authors suggested that the minimum strain at the weld was due to its high strength and ability to withstand large applied stress [54].

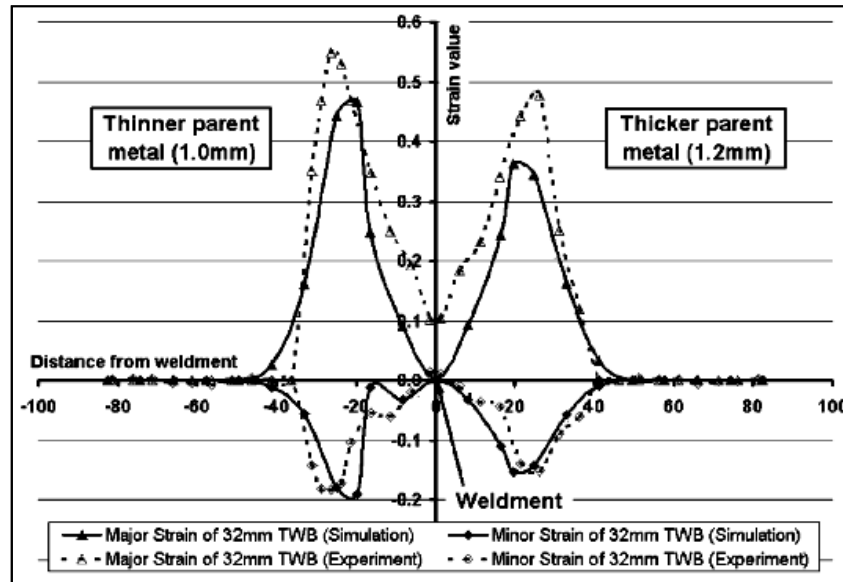


Figure 2.7 Strain distributions along the centreline perpendicular to the weld of the TWB with 32 mm width [54]

2.4.1 Welding AHSS

The interest in welding DP steel TWBs with laser has been focused mainly on the process and optimization [55,56,57]. The potential of integrating DP steel into TWB for automotive applications is high because of the combination of high yield strength and good formability (high work-hardening rate and high uniform elongation) for improving crashworthiness, mass reduction and overall performance of the BIW components. Therefore, with such interest in incorporating DP steel in TWB applications, researchers [18,58,59] have studied the effects of welded DP steel on formability.

Xia *et al* investigated the effect of welding of DP steels on formability as compared to similar weldments in HSLA steel. The welds on the DP980 steel and HSLA blanks were done by full-penetration bead-on plate welding then these blanks were formed and compared to the unwelded blank metal [38]. Figure 2.8 shows the hardness profiles of the welded DP980 and HSLA steels. The DP980 steel showed a significant drop in hardness in the HAZ compared to the base metal hardness, which was due to local tempering of the martensite phase. The hardness profile of HSLA steel did not show any drop in hardness and both these profiles are shown in Figure 2.8 a). In addition, the effect of welding speed was investigated and it was found that increasing the welding speed reduced both the width of the softening and its magnitude, shown in Figure 2.8 b). In general, increasing the welding speed decreased the heat input and produced narrower welds, which are desirable for TWBs [38,52].

Forming welded DP980 steel showed that failure initiated in the softened region *i.e.* strain concentrated there since this region was the weakest, causing fracture mode III. As mentioned in the previous section, during deformation the weakest material will experience plastic deformation while the stronger material experiences elastic deformation; hence, causing premature failure. This premature failure led to a significant decrease in the formability of welded DP980 steel compared to the base metal. This observation was further studied by Panda *et al* (2008) through numerical simulation of DP980 steel and the finite element analysis confirmed that the strength of the joint was significantly decreased with the formation of the soft zone [60].

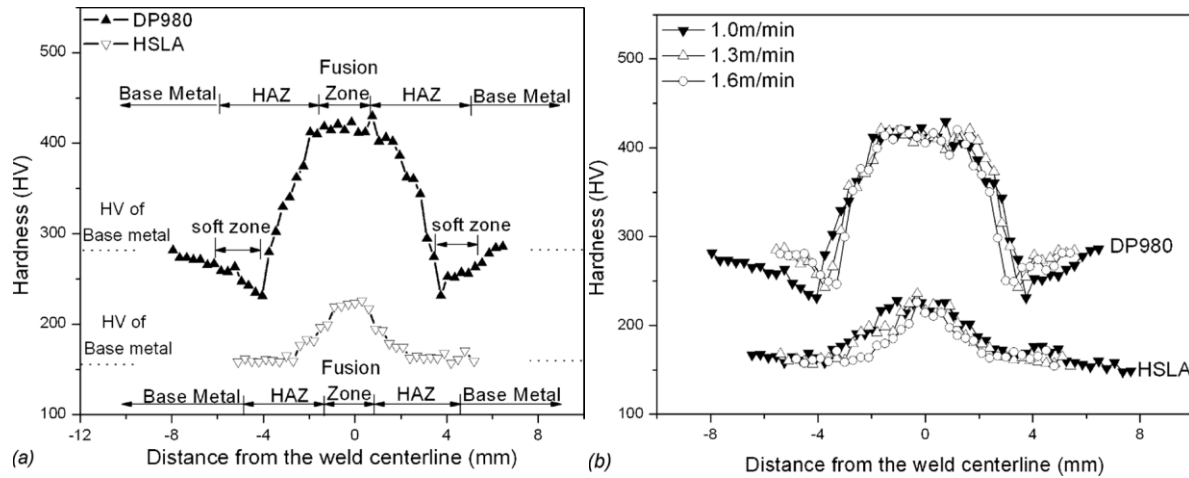


Figure 2.8 Hardness profiles of a) DP980 and HSLA at welding speed of 1.0m/min, and b) DP980 and HSLA welds at different welding speeds [38]

Xia *et al* (2008) further investigated the softening of different grades of DP steels (DP450, DP600 and DP980 steels) by forming bead-on plate blanks of these steels [39]. The softening seen in these steels was shown in the hardness profiles in Figure 2.9. The DP steel that showed the most softening was DP980 followed by DP600 and DP450 steels. According to the previous study by Xia *et al* (2007) [38] the severe softening in DP980 steel resulted in the most significant reduction in formability; while it is likely the softening in DP450 steel exert less influence on the formability. Thus, due to the high strength ratio, strain concentrated in the softened zone during, deformation will lead to premature failure. Increasing the heat input/decreasing the weld speed tends to increase the softened zone area; also, an increase in the initial martensite content affects the softened zone [39].

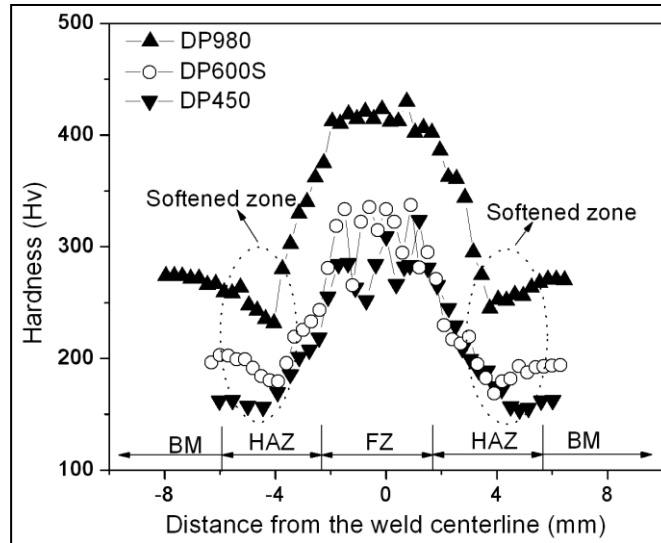


Figure 2.9 Hardness profile of diode laser welded DP steel [39]

Another study by Xia *et al* [61] considered the initiation of the failure during the forming of welded DP steel. Bead-on plate laser welded DP980 and HSLA steels were investigated. The failure observed in the DP980 welded blanks occurred in the HAZ region (corresponding to the softened region) parallel to the weld. The failure in the HSLA welded blank initiated at the welds and propagated perpendicularly to the weld line as shown in Figure 2.10. The resulting LDHs of the bead-on plate blanks compared to the parent base metal are shown in Table 2-5.

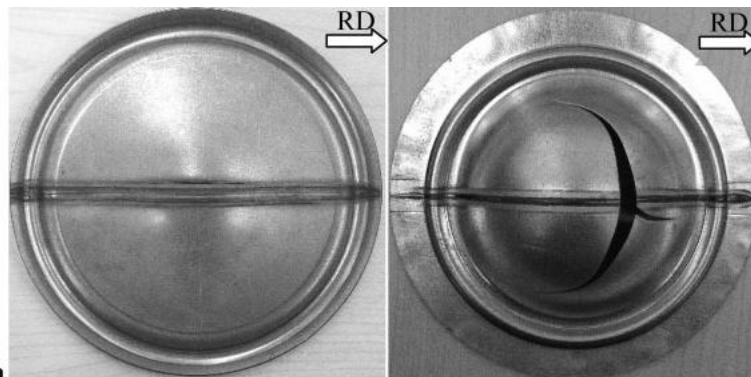


Figure 2.10 Top view of LDH of bead-on plate a) DP980, and b) HSLA fracture locations [61]

Table 2-5 LDH comparison bead-on plate DP980 and HSLA to parent base metal DP980 and HSLA [61]

LDH	DP980	HSLA
Parent base metal	30.4 mm	32.9 mm
Bead-on plate	13.2 mm	31.6 mm
% difference	~56.6%	~3.5%

From this table, it was concluded that welding affected the formability of DP980 steel. The underlying reason for the significant decrease in the formability of welded DP980 steel was the presence of the softened region in the HAZ. This softened region created an area for high strain concentration, due to its lower hardness; therefore, leading to premature failure in DP980 steel.

In the research cited so far, laser welding DP steel resulted in softening in the HAZ and the studies discussed so far studied and suggested methods to reduce the effect of softening on formability through material usage. Based on the softened region in laser welded DP steel blanks, Miles *et al* compared the formability of friction-stir (FSW) weldments of DP590 to laser weldments. FSW was of interest because the heat generated during this solid state process does not melt the material during the joining process and therefore, the weld nugget and HAZ could have more favourable properties [62]. The results of this study showed that the formability of the FSW-TWB when the weldment was oriented along the major strain direction increased ~20% compared to the laser welded TWB. However, the welding speed used in FSW was too low and not appropriate for production applications [62].

Conversely, Uchihara *et al* determined guidelines for choosing the appropriate welding type for materials used for TWBs based on the forming performance of the materials [57]. The welding processes investigated were laser welding, mash welding and arc welding. Three grades of DP steels were investigated, 590MPa, 780MPa and 980MPa. They were welded to equal strength grade and thickness materials to create the TWBs. Upon testing, it was apparent that laser welding was the best process for all grades of DP steel because of its narrow weld and small heat input [63,64], which cannot be duplicated with mash welding and arc welding. As a result of the smaller weldment and HAZ, the formability of the laser welded TWB showed the highest dome height. In addition, the authors suggested that plasma arc and mash welding should be limited to welding DP590 steels because of the large weld and HAZ. For any higher grades of DP steel, softening in the HAZ occurred

when welding with plasma arc and mash welding. Finally, the authors combined DP980 with low strength steel by the three welding processes and their results showed that the formability of these combinations was similar. Hence, welding high grade DP steel with low strength steel can be done with any welding process [57].

Panda *et al* [27] further studied the formability of TWBs made with different AHSS, namely DP980, DP800 and DP450 steels laser welded to HSLA. The formability was measured depending on the LDH and the best combination was determined. Their results shown in Figure 2.11 showed that combining DP steel with HSLA improved the formability when compared to the similar material TWBs, which was in accordance to [57]. In addition, failure location of the dissimilar TWBs was in the HSLA steel, which was the lower strength material, *i.e.* the higher strength and hardness of the soft zone in the DP steel caused the strain localization to occur in HSLA. This study also considered the formability of dissimilar TWBs numerically (without incorporating the soft zone) and found that the result was compatible to the experimental results. The soft zone was not modelled because the material properties in this region were still superior to the HSLA base metal [27].

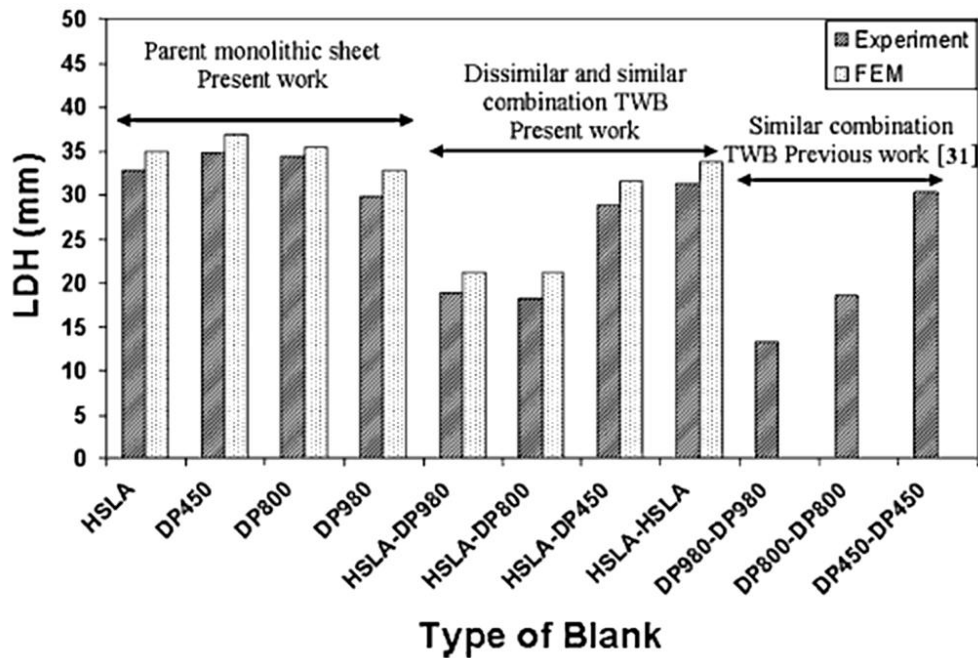


Figure 2.11 Comparison of LDH of parent metals and dissimilar TWB combinations [27]

2.5 The Effect Of Weld Positions

The formability of TWBs may change according to weld line position in critical areas. Studies have suggested that the best formability will occur when the weld line is placed away from areas of high strain *i.e.* place the weld far from the major strain direction [46]. Kridli *et al.* suggested that placing the weld closer to the thinner material in a dissimilar thickness TWB (*i.e.* decreasing the amount of thinner material in the TWB) increases the formability by allowing the thicker material to deform more [8]. However, weld line location does significantly reduce the forming-limit strains when compared to the unwelded blank as Narayanan [65] found, where increasing the weld line offset increases the forming limit reduction where the decrease in limit strain is in the stretching region.

Choi *et al* [40] studied the weld line movement and formability of dissimilar materials TWB with three different initial weld-line locations for a deep drawing process. This study showed that as the weld line was shifted farther from the centre of the blank, more weld line movement occurred. Heo *et al* [66] followed up on the study by Choi *et al* and studied the effect of different weld position in a deep drawing process and using a draw bead to limit the amount of weld line movement. Although, with the use of the draw-bead, the weld line movement was reduced, the same effect as found by Choi *et al* was observed where the maximum drawing depth and maximum drawing force were reduced as the weld line was placed farther from the centre of the blank.

2.6 The Effect Of Weld Orientation

Weld orientations affect the forming-limit strains of TWBs by adjusting the regions being affected by the major strain direction. Positioning the weld in the longitudinal orientation (the weld line is parallel to the major straining direction) where stretching is placing more emphasis on the weld as opposed to positioning weld in the transverse orientation (the weld line is normal to the major straining direction) where deformation is concentrated on the thinner/weaker material. Weld orientation also determines the mode of fracture as the weld only responds to uniaxial tensile deformation. In longitudinal welds, fracture occurs across the weld as the weld is being stretched (fracture mode I); in contrast, failure occurs on the weaker/thinner material when the weld is transverse to the major strain direction due to different work-hardening effects resulting in fracture mode II. Thus, the consideration of weld orientation is important in the TWB design process [42].

The effect of weld orientation on the formability of aluminum alloy 5754-O laser welded blanks showed that the longitudinal TWBs underwent significant forming limit reduction [67]. Narayanan *et al.* studied the weld orientations of steel bead-on-plate specimen to avoid the influence of

thickness/strength and material on forming. That study showed that welding in any orientation lowered the forming limit strain in the FLD; however, the forming limit strains (shown with the LDH tests) were similar in the longitudinal and transverse TWBs and it was concluded that there was negligible influence due to weld orientation in forming [65]. This study was followed by a numerical simulation by Narayanan *et al* of the TWB with different weld orientations to generate FLDs where forming limits could be predicted [68]. It was found that the simulated FLDs correlated to the experimental FLDs when failure occurred in the base metal of the TWB. Similarly, Kusuda *et al* [69] observed that when TWBs were formed near the weld; the strength ratio could be used to determine the formability.

A study by Panda *et al.* investigated three different TWB conditions (dissimilar thickness, dissimilar materials properties and dissimilar surface conditions) in plane strain stretch forming with different weld orientations and found that the formability of the longitudinal weld orientation was similar to the formability of the transverse weld orientation in the dissimilar surface condition TWB. While, thickness ratio and material properties resulted in lower LDH in the longitudinal condition by up to 11%. These results were consistent with finite element analysis [26]. Chatterjee *et al.* also found that the formability of longitudinal weld TWBs of IF-DP was comparable to the transverse weld TWBs with the longitudinal weld TWBs being only 10% lower [15]. These studies showed that weld orientation did not influence the formability of the plane strain TWB significantly when the materials properties of the blanks were similar. The weld orientation did affect the failure mode: in the longitudinal weld orientation failure initiated at the weld and propagated towards the base metals, while in the transverse weld orientation the failure initiated in the weaker/thinner materials [15,26,65]. Moreover, for these laser-tailored blanks with dissimilar thickness with transverse weld orientation, the forming limit (FLC) could be predicted based on the thinner/weaker steel in draw and plane strain conditions [70].

2.7 The Effect Of Curvilinear Welds

Curved seams have not been studied extensively as the number of applications is limited currently to shock towers as used mainly in North American automobiles [4]. However, the application of curvilinear welds can be expanded by proposed TWB designs for the inner doors. The inner door is made of multiple straight line welds, which change into broken lines after forming [71]. The problems of using multiple straight line welds to create curves are the inconsistency of the blank dimensions and the occurrence of inflection points where two welds meet [72,73]. The use of curvilinear welds eliminates the inflection. Recently, two studies were done on the formability of curvilinear seams. The

influence of curved weld radius, thickness ratio and different blank size was studied. The forming behaviours of curvilinear TWB with a radius of 76.2 mm with thickness ratio ≥ 1.5 is lower than the TWB with a thickness ratio of 1 in biaxial stretch forming. Increasing the radius produces a larger variation of the forming height during biaxial stretch forming. Interestingly, the formability of the TWB with a thickness ratio of 2.5 is higher than the blank with a thickness ratio of 1.5 [73].

A further study compared the formability of curved welds to straight welds and found that larger thickness ratio increased the forming height of the curved welds, while the straight weld TWB had the lowest forming height [72] as shown in Figure 2.12. From this figure, it is clear that when the thickness ratio is 1, increasing the curve radius does not affect the forming height. Also, with a thickness ratio of 1.5, curved weld blanks and straight weld blanks give the same forming height; however, increasing the curved radius is ideal when the thickness ratio is larger than 1.5.

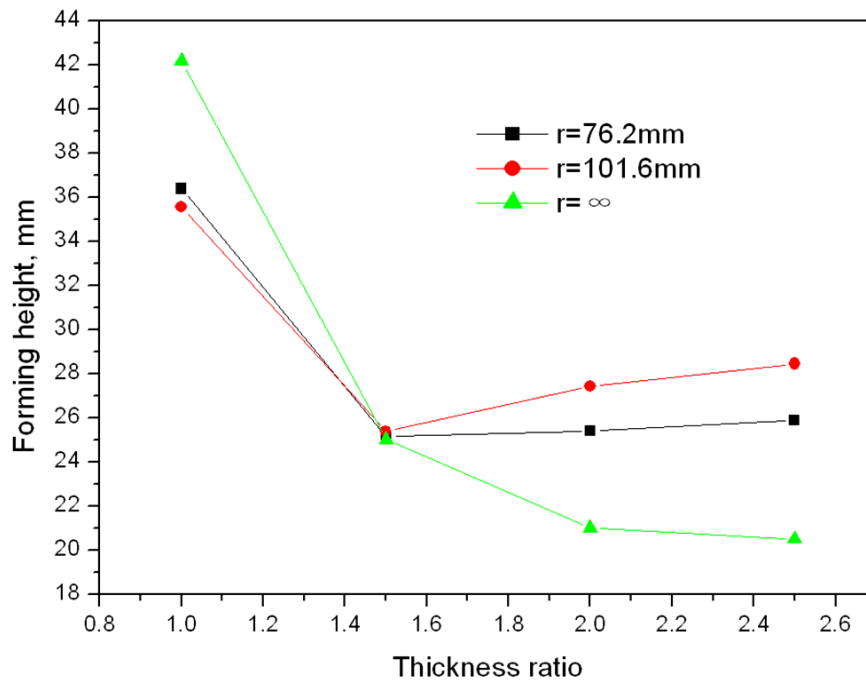


Figure 2.12 Relationship between formability, thickness ratio and curved weld radius [72]

CHAPTER 3

3 EXPERIMENTAL

The experiments in this thesis were divided into two parts. The general experimental techniques and methods used to characterize the properties of the base metals, and welding and forming of the laser welded blanks are described in this chapter. The dimensions and design of the tailored blanks for each section will be described in their corresponding chapters.

3.1 *Metallurgical Examination*

3.1.1 Base Metal

The materials used in this thesis were HSLA (high strength-HSS), DP600, and DP980 (both AHSS) steels with a nominal thickness of 1.14 mm, 1.2 mm and 1.2 mm, respectively. The thickness of the steel included the layer of galvanized coating (GI), GI, and galvanized coating (GA), respectively. These materials have been developed for automotive part manufacturing for structural exterior and applications in which improved crash and part performance is required.

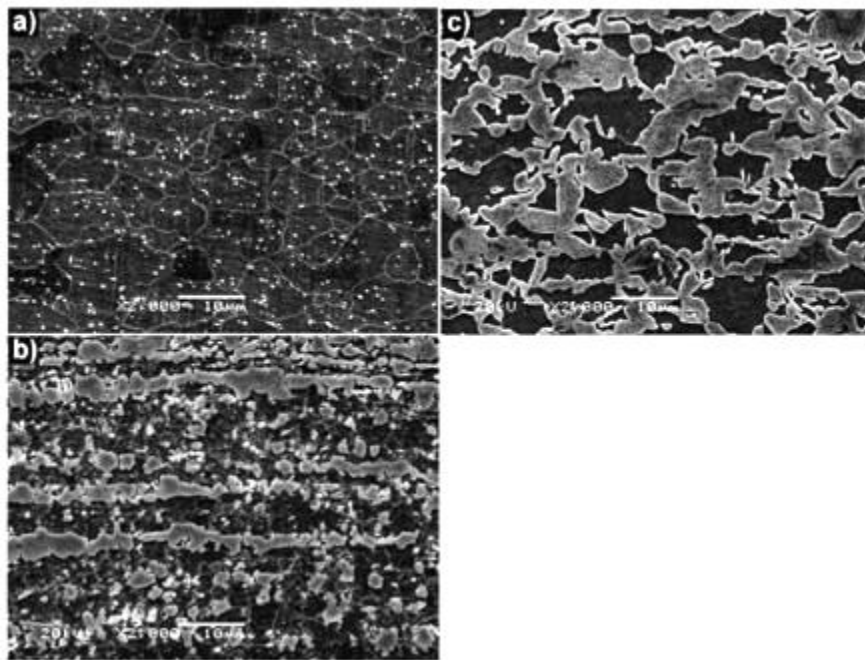


Figure 3.1 Microstructure of base metal a) HSLA, b) DP600, and c) DP980

Figure 3.1 shows the scanning electron microscopy (SEM) images of the microstructures of the base metals. Figure 3.1 a) shows the microstructure of HSLA steel, consisting of a ferrite matrix in which the grain boundaries are revealed, reinforced with sub-micron second phase precipitates through micro-alloying, these being the bright particles randomly distributed in the grains. Thus, the strength of the HSLA steel is obtained through grain size reduction and precipitation strengthening. Figure 3.1b) shows the microstructure of the DP600 steel, consisting of a ductile α -ferrite matrix reinforced with a volume fraction of 26% elongated banded martensite (M) islands. These martensite islands are aligned parallel to the rolling direction. Figure 3.1 c) shows the microstructure of DP980 steel, which has higher martensite content at a volume fraction of 54%.

3.1.2 Sample Preparation

The weld characteristics of dissimilar TWBs (Chapter 4) and curvilinear seams (Chapter 5) were evaluated through microhardness measurements and/or microstructure examination. Thin cross sectional specimens of the laser welded specimens were mounted, ground, and polished according to standard metallographic procedures to reveal the microstructure of the different zones in the welded specimens. After polishing the specimens were etched with 2% Nital. The specimens were observed under the optical microscope.

3.1.3 Optical Microscopy and SEM Analysis

Stereo-microscope images and optical micrographs for fracture analysis (Chapter 4) and the cross sections of the welded specimens (Chapter 5) were acquired with an image-analysis software. The weld profiles were observed at 50X magnification to reveal the different zones in the specimen. SEM examination of the formed fracture surfaces (Chapter 4) was performed on a Jeol JSM 6460.

3.2 Hardness Examination

The Vickers microhardness testing on the cross sections of the dissimilar materials combination (Chapter 4) and curvilinear seam at the curvature of the weld (Chapter 5) was conducted on etched specimens at a load of 300g with a loading time of 15s. Three rows of indentations with indentation spacing of 200 μ m apart (0.2 mm) were made across the weld zones, so the microhardness variations could be more clearly defined. The distance between each indentation horizontally was also 200 μ m.

3.3 Mechanical Testing

This section discusses the experimental techniques used to characterize the tensile properties of the parent materials and the TWBs, and also the formability of these welded blanks.

3.3.1 Uniaxial Tensile Testing

3.3.1.1 Parent Material

Uniaxial tensile tests were performed on the parent materials to obtain the standard tensile properties, such as 0.2% offset yield strength (YS), ultimate tensile strength (UTS), elongation percentage, strain hardening coefficient n , and strength coefficient K , where the strain hardening behaviour of the sheets can be described using the power-law hardening equation [32]. The tensile specimens were machined to ASTM E8M standard, Figure 3.2[74]. The specimens were tested along the three directions, where the tensile axis is parallel (0°), diagonal (45°) and normal (90°) to the rolling direction of the sheet, shown in Figure 3.3 and were machined to ASTM E571 standard. A uniform cross head speed of 2 mm/min was used.

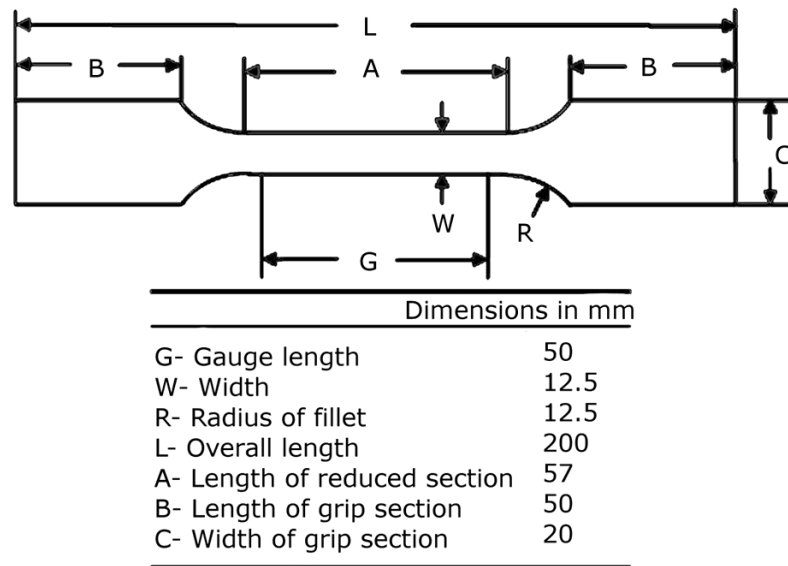


Figure 3.2 ASTM E8 schematic of tensile specimen

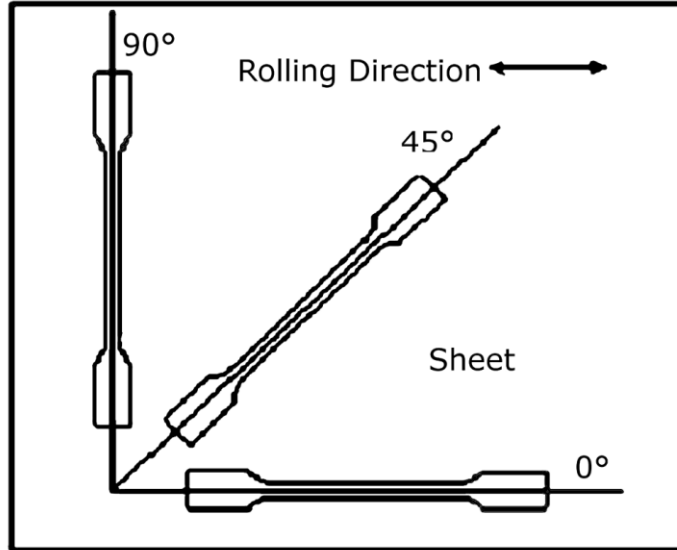


Figure 3.3 Tensile specimens of unwelded metal with different orientations relative to the rolling direction

Mechanical properties, shown in Table 3-1, of the parent materials for the three testing directions were obtained to determine the plastic strain ratio (R) of the parent materials. The R value was obtained when the specimens were elongated to 75% of the uniform elongation before the maximum load was reached. The R value was calculated using the final width and length of the specimen with the following equation for all three directions of the parent tensile materials [32].

$$R = \frac{\varepsilon_w}{\varepsilon_t} = \frac{\varepsilon_w}{-(\varepsilon_w + \varepsilon_l)} = \frac{\ln\left(\frac{w_f}{w_0}\right)}{\ln\left(\frac{l_0 w_0}{l_f w_f}\right)}$$

Where,

ε_w , ε_l , and ε_t : True width strain, true length strain, and true thickness strain, respectively

w_0 and l_0 : Initial width and length of the specimen

w_f and l_f : Final width and length of the specimen

Table 3-1 Tensile properties of various AHSS sheets present in this study

Steel grade	YS (MPa)	UTS (MPa)	Uniform elongation (%)	Total elongation (%)	n-value	K-value (MPa)	R-value		
							R ₀	R ₄₅	R ₉₀
DP600	365.2	631.4	16.0	25.6	0.21	1097.6	0.80	0.96	1.03
HSLA	421.0	511.2	13.5	25.6	0.13	760.9	1.02	1.23	1.16
DP980	672.3	1058.2	6.9	12.1	0.10	1505.4	0.83	0.91	1.05

3.3.1.2 Tailor Welded Specimens

Tensile specimens were cut from the laser welded TWBs in the transverse direction on the TWBs (*i.e.* the weld is normal to the tensile force direction) shown in Figure 3.4 as per ASTM E8M standard [74].

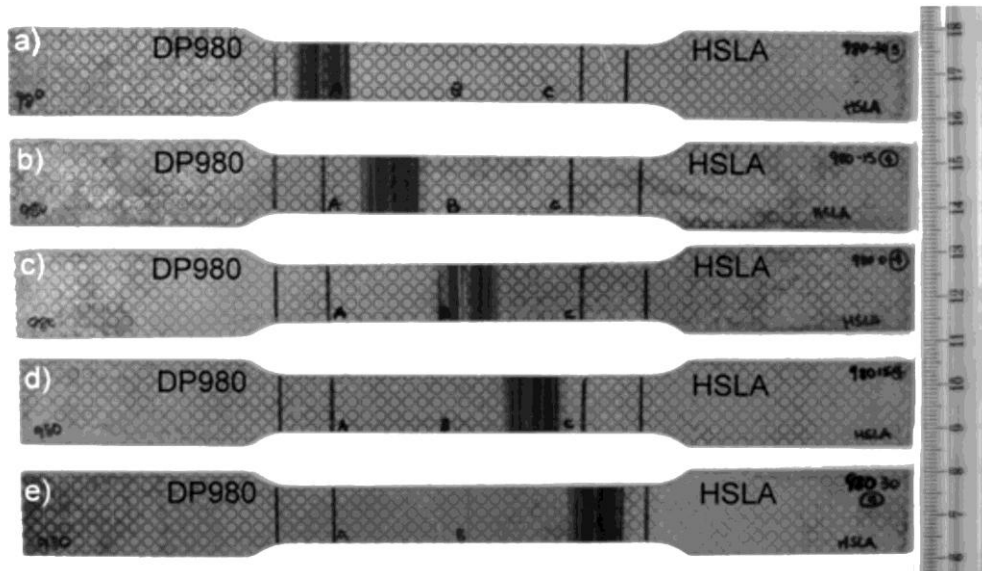


Figure 3.4 Tensile specimens with the weld placed a) -30 mm, b) -15 mm, c) 0 mm, d) +15 mm, and e) +30 mm offset from the centre

The purposes of testing these specimens were: 1) to determine the quality of the weld; and 2) to determine the formability effect of the weld locations under tensile loading. The same cross head speed used to test the parent metals was used to test these welded tensile specimens.

3.3.1.3 Sub-Size Tensile Specimen

Welding changes the materials properties of the weldment and it is necessary to determine the flow/mechanical properties of the weld bead for the dissimilar (DP600-HSLA and DP980-HSLA) and the similar (DP600-DP600 and DP980-DP980) materials combinations. The mechanical properties of the weld bead were determined by machining mini-tensile specimens where the weld bead was along the length of the gauge length, shown in Figure 3.5. The properties of these mini-tensile specimens were determined with the tensile Hopkinson bar (TSHB) test [75]. In this situation, only the weld bead was tested under tension. Table 3-2 shows the flow properties/mechanical properties of the weld zone.

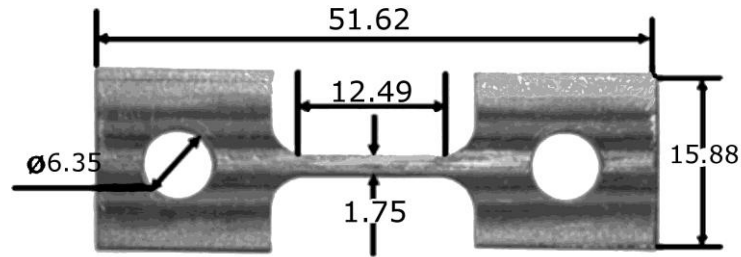


Figure 3.5 Sub-size tensile specimens used to evaluate the fusion zone of the TWB

Table 3-2 Flow properties of the weld bead

Tailor blank combination	YS (MPa)	UTS (MPa)	Uniform elongation (%)	n-value	K-value
DP600-DP600	250	1370.75	3.45	0.165	2398.4
DP980-DP980	406	1051.6	3.8	0.147	1734.75
DP600-HSLA	273	813	4.5	0.1343	1275.2
DP980-HSLA	344.9	851	4.9	0.137	1345.07

3.4 Laser Welded Blank Fabrication

The DP steels were laser butt welded to HSLA steel to create the dissimilar material TWBs for the different weld positions, orientation, and multiple-weld angles. The curvilinear seam weld was bead-on-plate. The specimens were mechanically edge sheared and the welding direction was perpendicular to the rolling direction of the sheet metal.

3.4.1 Diode Laser

Laser welds were produced using a Nuvonyx ISL-4000L High Power Diode Laser head (a 4kW AlGaAs diode laser with a wavelength of 805 ± 5 nm [76]) mounted on a Panasonic VR-16 robotic arm shown in Figure 3.6. The diode lasers operate on the same principles as the light emitting diodes, which are semiconductors with P-N junctions. These semiconductors are typically doped with GaAs, GaAlAs, and InGaAs [77]. In the laser diode, the light is reflected around between the cleaved ends of the semiconductor crystal; thus, changing the light to behave like a laser, the laser is emitted from a rectangular window in the active region [78]. Figure 3.7 shows a schematic of a typical laser diode.



Figure 3.6 Nuvonyx diode laser head mounted on a Panasonic robotic arm

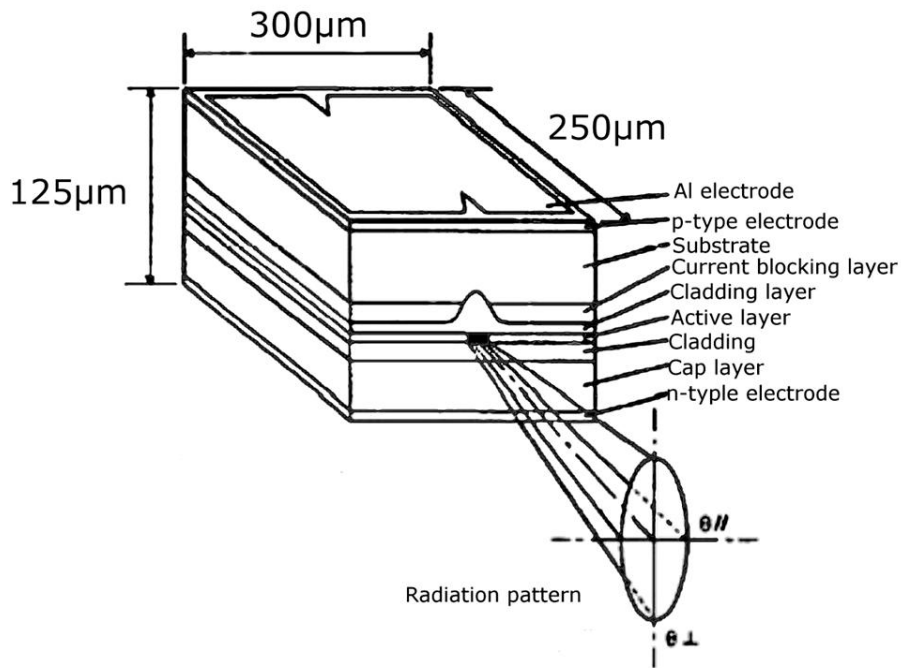


Figure 3.7 Schematic of a diode laser [78]

The output wavelength of the diode laser is dependent on doping concentration and the most common semiconductor is the GaAlAs. By adjusting the ratio of Ga to Al the wavelength can be adjusted from 808 to 810 nm [77]. During operation, the high power of the diode laser result in high heat output; therefore, a heat sink is necessary to prevent the degradation of the diodes. Adequate cooling is achieved by the design of the diode arrays. As seen in Figure 3.7 the diode is in actual a thin strip. When an array of these strips is mounted onto a heat sink, cooling is achieved. These thin strips act as planes where the photons reflect and the output beam is elliptical when it exits the active layer. The shape of the beam can be corrected with optics of different focussing properties, but is it difficult; as a result, the elliptical shape is not altered [77]. The Nuvonyx HPDL consists of four water cooled heat sinks with 20 individual diodes, which contains condensed optics to deliver a combined rectangular beam of 12 mm x 0.9 mm.

The laser system is made up of a system control unit that contains the current power supply, system control PLC modules and a touch-screen control interface; the laser head that contains the diode laser arrays, a focussing lens and output window; and a chiller that cools the laser by water flowing through the channels in the heat sinks where the diode bars are mounted [79].

3.4.2 Clamping Fixture and Shielding Gas

The sheet steels (*i.e.* DP600-HSLA, DP980-HSLA, DP980, DP600, and HSLA) were clamped down in a welding fixture and butt welded together with the weld bead transverse to the rolling direction. The welding speed ranged from 0.85m.min to 1.0m/min for full penetration for bead-on-plate conditions to dissimilar TWBs, respectively. The beam characteristics of the diode laser are summarized in Table 3-3. Due to the curvature of the curvilinear seams (Chapter 5), a new clamping fixture was designed, shown in Figure 3.9. This custom fixture had a widened back shielding gap to accommodate the weld curvature and an inlet for the back shielding gas to enter.

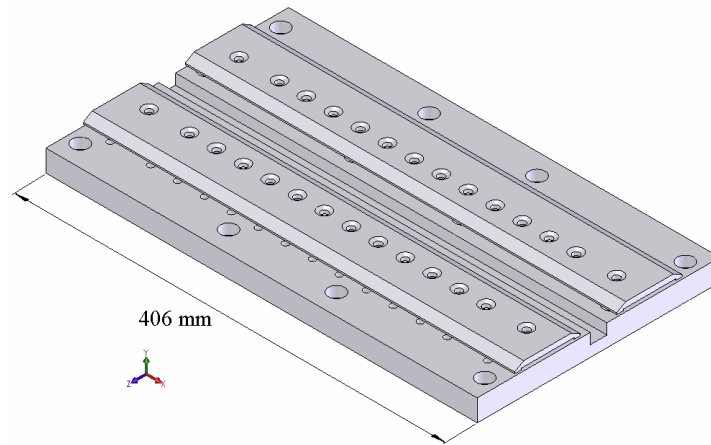


Figure 3.8 Clamping fixture for laser welding of TWBs [11]

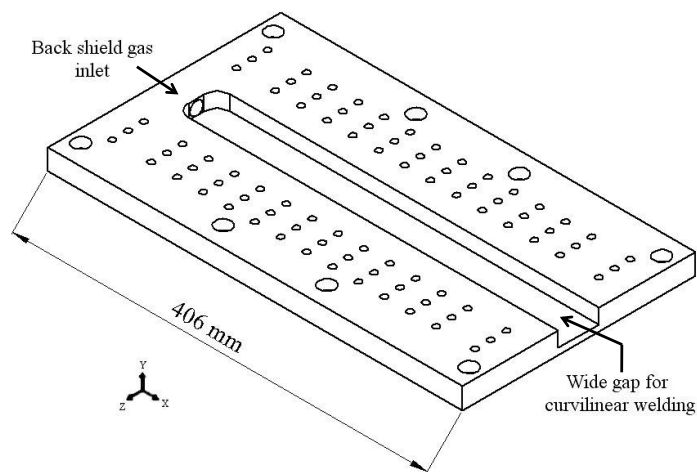


Figure 3.9 Clamping fixture for laser welding of curvilinear seam blank

Table 3-3 Beam characteristics of the diode laser

Welding Parameters			
	Welding speed (m/min)	Laser power (kW)	Beam size
Diode laser	0.85 and 1.0	4	12 x 0.9 mm

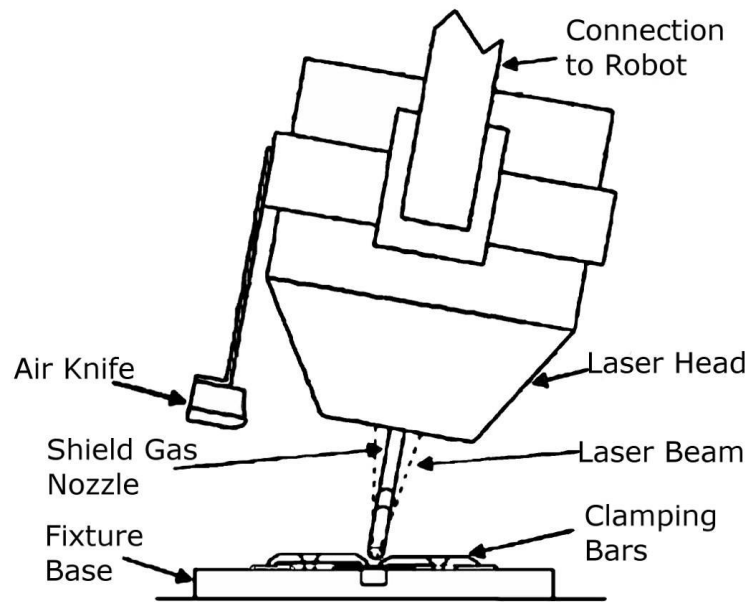


Figure 3.10 A schematic of the laser head configuration

The configuration of the laser head used is shown in Figure 3.10. During welding the air knife releases compressed air to blow away splatter from the process away from the shield glass lens protecting the laser. Argon shielding gases for top and back shielding is provided by the shield gas nozzle and the gas feed attached to the fixture base at a rate of 35 l/min to prevent blow holes and oxidization of the weld bead. During welding, the specimen was clamped using the clamping bars to the fixture base to prevent distortion and keep the specimen in place.

3.5 Formability Testing And Analysis

Welding caused variations in the mechanical properties across the weldment of the laser welded blanks. Therefore, the strain along the across the weld sample was expected to vary. To understand the local strain in the welded specimens after deformation the circular grid strain measurement method was employed. There are three parts to this strain analysis method:

1. Applying the circular grids prior to deformation;
2. Deformation; and
3. Measuring the deformed grids after testing

3.5.1 Gridding

The strains of the deformed blanks were analyzed with grids electro-etched on the unformed blanks. The circular grids had a diameter of 2.5 mm and were etched using a setup shown in Figure 3.11. This etching setup includes A) the power supply; B) the conductive roller through which current passes to etch the material; C) the specimen; D) the stencil for the grids; E) the wicking pad which is soaked with the electrolyte used in the etching process and to act as an insulator between the conductive specimen and the conductive roller; and F) the ground electrode.

The procedure of electro-etching involves passing an alternating current (for dark circles) or direct current (for white circles) through an electrolyte solution on the steel samples. The specimens were cleaned prior to electro-etching with a cleaning solution. The sheet surface was wet with the electrolyte with the (circular grid) stencil placed on top and connected to the ground electrode (F). A wicking pad (D) soaked with electrolyte was placed on top of this set-up to avoid shorting the circuit when the conductive roller (B) was applied. The conductive roller was connected to the power supply (A). The circuit was completed when the conductive roller rolled over the wicking pad until the grids were produced. During etching an AC potential of ~15V was applied; therefore, black grids were produced.

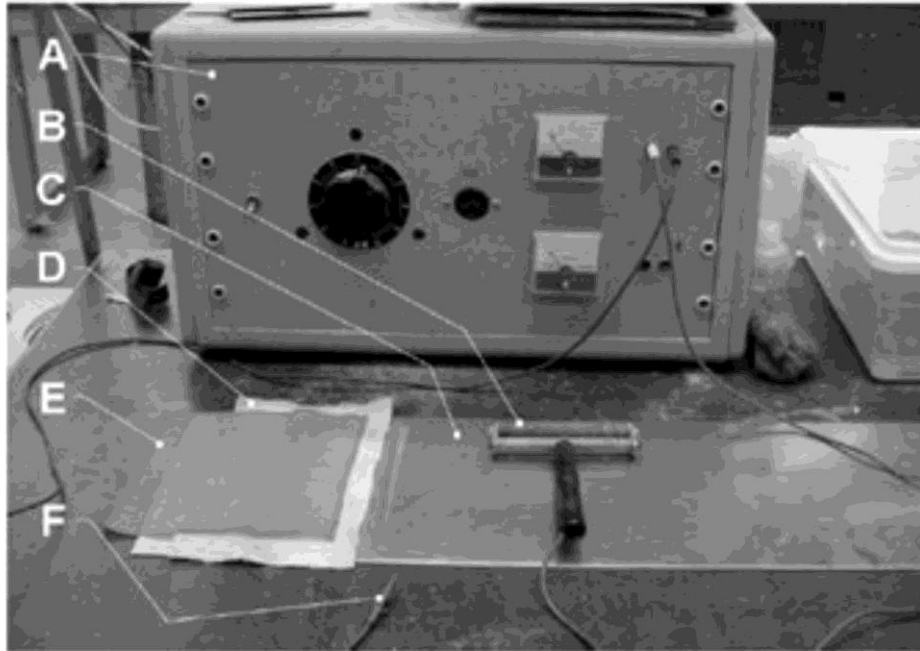


Figure 3.11 Grid etching system A) Power supply, B) conductive roller, C) specimen, D) wicking pad, E) stencil, and F) ground electrode [79]

3.5.2 Limiting Dome Height Test Equipment: Hecker's Hemispherical Punch

The limiting dome height tests were done according to the procedure documented by Hecker [80] using an MTS 866.02 hydraulic press (Figure 3.12). A schematic of the hemispherical punch with a diameter of 101.6 mm, and the upper and lower dies are shown in Figure 3.13. The upper and lower dies had a circular draw bead at a distance of 132 mm from the die centre.

During forming, the blank was placed at the centre of the lower die, so that the centre of the blank (marked with the guidelines) was at the centre of the punch. A clamping force of 135 kN was used to keep the blank in place so that no draw-in occurs in the flange region for biaxial stretch forming. Lubrication in the form of Teflon sheets and mill oil were used for the biaxial stretch forming blanks to yield smoother material flow during deformation. In plane strain stretching, the specimen size was narrower, so the draw-bead did not clamp the entire blank. During forming, the unclamped sides of the blank were allowed to draw-in to induce plane strain stretch forming condition and no lubrication was used. In addition, spacers were not used in the dissimilar materials TWB tests because there was negligible difference between the sheet thicknesses at 5%.

The punch velocity was maintained at 0.2 mm/s. Figure 3.12 shows the MTS formability press used in this research. The load progression and limiting dome height were obtained with an in-house developed data acquisition system consisting of a load cell and a rotary encoder to record the load-displacement data during the experiments. During testing, the load progression was monitored with the data-acquisition software. As soon as the load dropped *i.e.* when necking/failure occurred, the test was stopped and the load progression and LDH were obtained. After testing, the strain distribution or grid analysis measurements were done, described in the next section.



Figure 3.12 MTS 866.02 formability press [79]

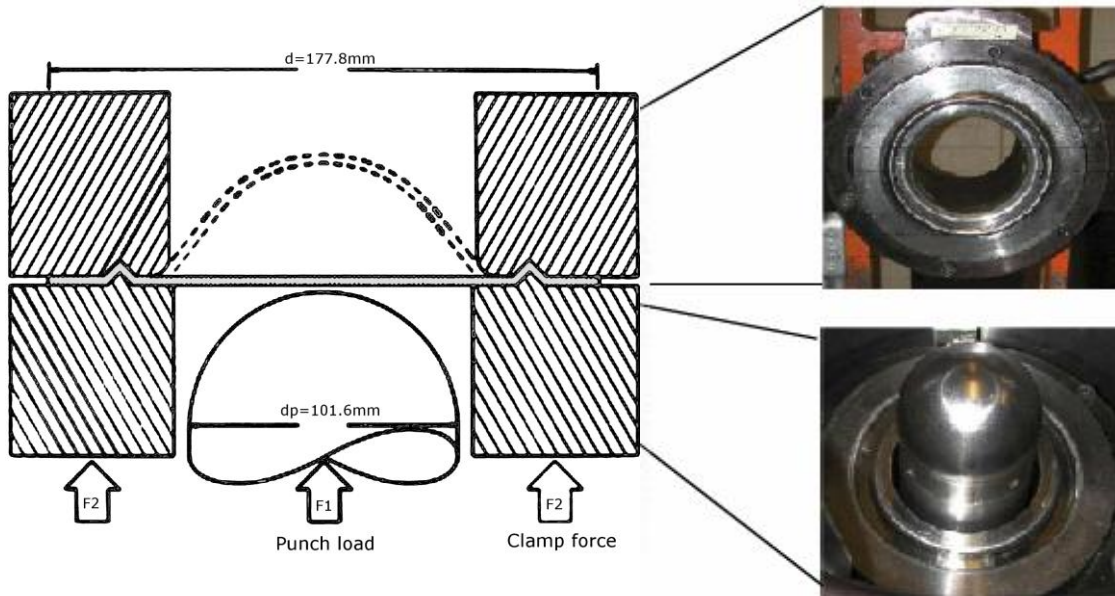


Figure 3.13 Hecker's hemispherical punch [41,79]

3.5.3 Strain Measurement

After forming, the deformed grids across the TWBs were measured for strain using an in-house developed camera and software shown in Figure 3.14. The circular grids of the unformed specimen were calibrated using the camera and software as a reference. After the calibration, the deviation was checked. The tolerance of up to approximately 6% strain is expected. After the specimens were deformed the grids were measured with the strain measuring system to calculate the strains in across the TWBs. To measure the strain, five points were chosen around the outer edge of each ellipse and the dimensions of the ellipse were calculated by the software.



Figure 3.14 Grid measuring system [79]

The calculations of the major and minor strains are shown with Equation 3.1 and Equation 3.2, respectively. The grids were used to develop strain distribution patterns and FLDs, which clearly showed the safe limiting strains from the unsafe zone with the failed and necked portions by plotting the major strains vs. minor strains. The change in the strains across each TWB was a good indicator of the forming behaviour and the influence of the material combination, thickness dissimilarity and the effect of the weld. Additionally, these strains could be plotted into an FLD.

Equation 3.1 Major engineering strain

$$\epsilon_1 = \frac{\text{Ellipse major axis length} - \text{calibration diameter}}{\text{Calibration diameter}}$$

Equation 3.2 Minor engineering strain

$$\epsilon_2 = \frac{\text{Ellipse minor axis length} - \text{calibration diameter}}{\text{Calibration diameter}}$$

CHAPTER 4

4 EFFECT OF WELD LOCATION, ORIENTATION AND STRAIN PATH

4.1 *Limiting Dome Height Testing*

The limiting dome height (LDH) test was performed according to the procedure in Chapter 3 for stretch forming. The dimensions of the biaxial TWBs with different weld locations and the plane strain TWBs with the different weld orientation are discussed in this section.

4.1.1 Weld Line Positions: Biaxial Stretch Forming

Five different weld line positions were studied with HSLA kept consistently on the right and DP steel on the left, shown in Figure 4.1. The biaxial blanks had a dimension of 200 mm x 200 mm and dotted guidelines were drawn to help identify the pole of the blank, and helped in aligning the blanks with the limiting dome height testing equipment. The centreline parallel to the weld line is referred to as the vertical centreline and the line normal to the weld is the horizontal centreline. The purposes of the centrelines were to assess the weld line position with respect to the vertical centre and to assist in aligning the blank to the die before forming.

Figure 4.1 shows the representative dissimilar materials combination TWBs (DP600-HSLA) with different weld locations. The other dissimilar materials combination TWB (DP980-HSLA) studied followed the same naming convention. The signs in front of each weld position indicate the side the weld line is on *i.e.* the negative numbers indicate that the weld is on the left side of the pole with more HSLA than DP steel in the TWB and positive numbers indicate less HSLA and more DP steel. The numbers refer to the distance away from the pole in mm.

Before testing these TWBs, parent unwelded blanks with the same dimensions were tested with the same conditions to determine if equi-biaxial stretch forming was achieved. The strain distribution patterns also showed areas of high strain concentration, *i.e.* where necking would likely occur. The results are shown the true strain distribution patterns of the parent materials for DP980, DP600 and HSLA steels in Figure 4.2.

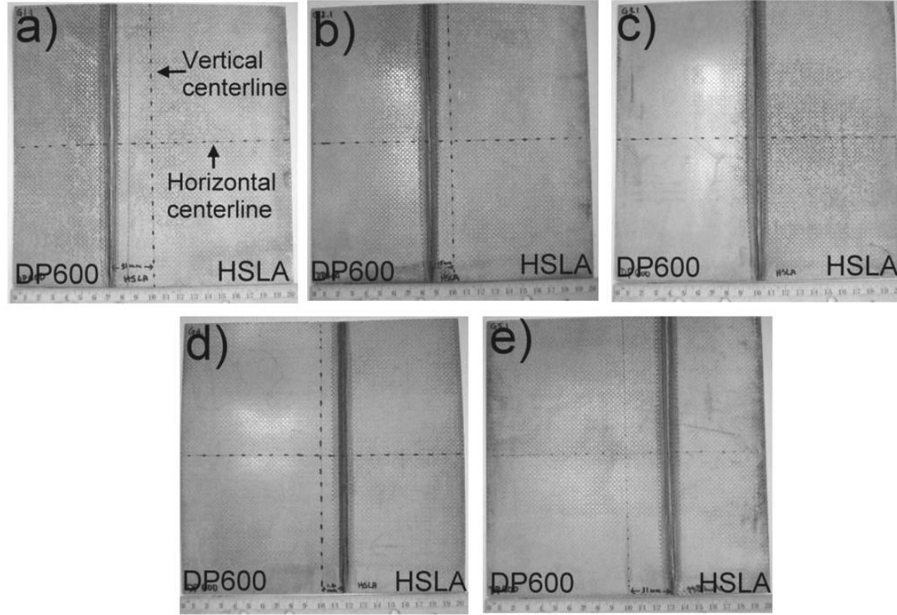


Figure 4.1 Biaxial TWBs with the weld placed a) -30 mm, b) -15 mm, c) 0 mm, d) +15 mm, and e) +30 mm offset from the centre

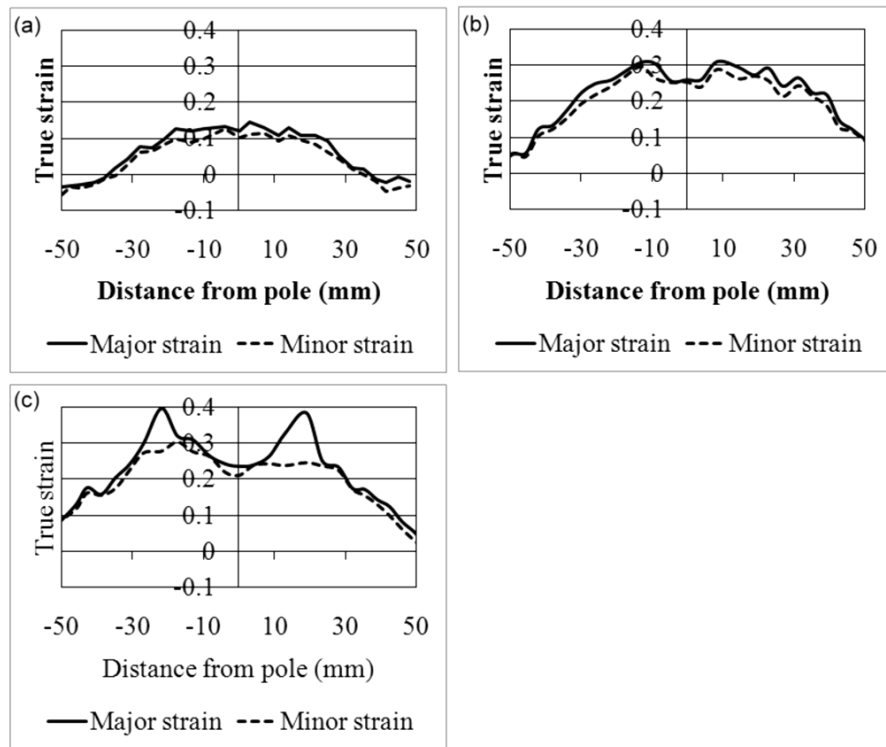


Figure 4.2 Strain distribution of the base unwelded metal in biaxial stretch forming a) DP980, b) DP600, and c) HSLA

These strain profiles showed that the major and minor strains were uniform and well developed, which indicated that the formability of these unwelded specimens was good. In addition, the major and minor strains were close together, which indicates biaxial stretch forming was achieved.

4.1.2 Weld Orientation: Plane Strain Stretch Forming

As mentioned in the literature review, plane strain stretch forming condition occurs when the minor strain is zero. Over 80% of failed stamping operations have been found to involve in this mode of deformation [81]. Therefore, the effect was studied of this mode of stretching on the formability of dissimilar materials. The dimensions of these TWBs, which results in near plane strain stretch forming under dry (no lubrication) condition, was determined after several trials of experimenting with various blank widths. The TWBs dimensions 120 mm x 200 mm were fabricated. The parent unwelded blanks were tested and the strains were plotted. Figure 4.3 shows the strain distribution profiles of the near plane strain stretched blanks, confirming that the minor strain was very close to zero.

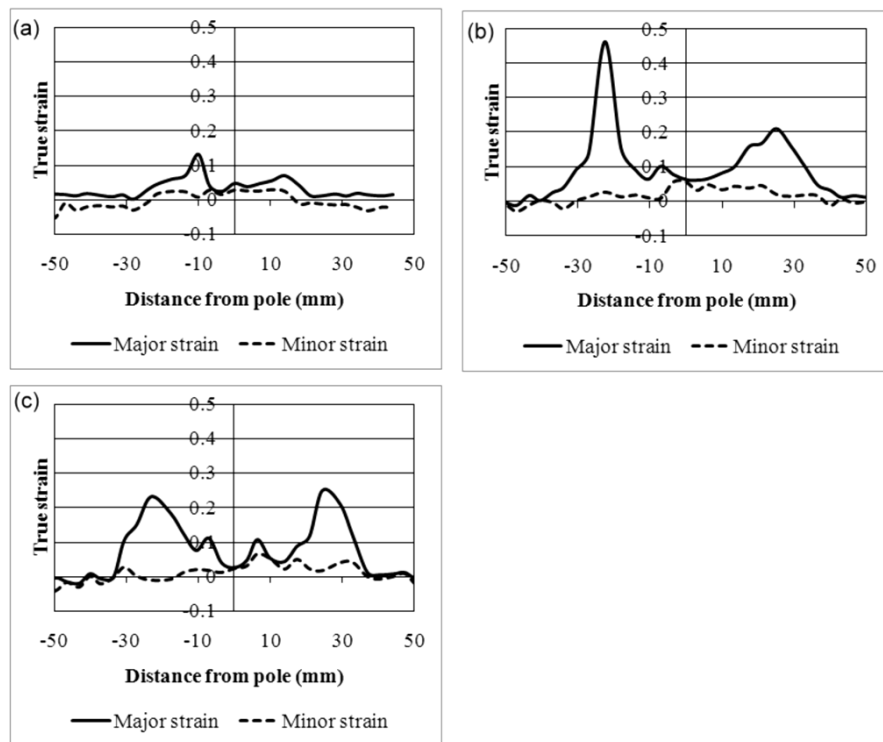


Figure 4.3 Strain distribution of the plane strain TWBs the base unwelded material a) DP980, b) DP600, and c) HSLA

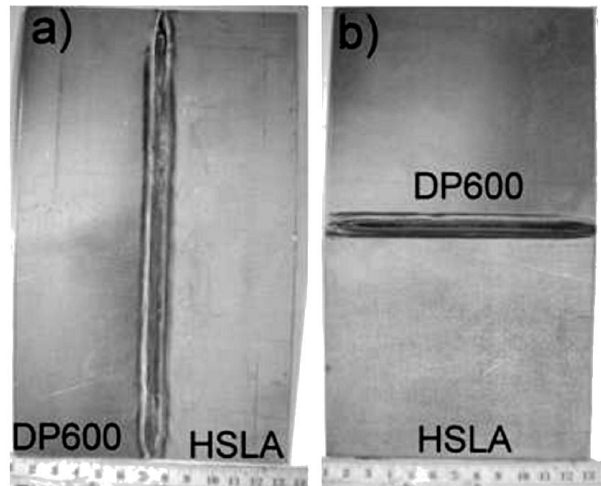


Figure 4.4 Plane strain TWBs with different weld orientations a) longitudinal TWB, and b) transverse TWB

Therefore, the dissimilar combination TWBs were created for two weld line orientations. Figure 4.4 shows the two weld orientations studied. Figure 4.4 a) shows the longitudinal weld, where the weld is parallel to the major strain direction and Figure 4.4 b) shows the transverse weld, where the weld is perpendicular to the major strain direction.

4.2 Hardness Measurements

Figure 4.5 shows the hardness profiles of DP600-HSLA (Figure 4.5 a)) and DP980-HSLA (Figure 4.5 b)) TWB welds. These profiles were obtained from an average of three rows of indentations across weldments of DP600-HSLA and DP980-HSLA. Figure 4.5 a) shows the increased hardness value (averaged 347 ± 17 HV) measured in the FZ of the DP600-HSLA TWB. The HAZ was characterized by the hardness values (350 HV for the DP600 steel side and 374 HV on the HSLA steel side) close to the fusion zone line and by a decreasing hardness along the HAZ towards their respective base metal. Interestingly, softening in the DP600 was not observable in the hardness profile.

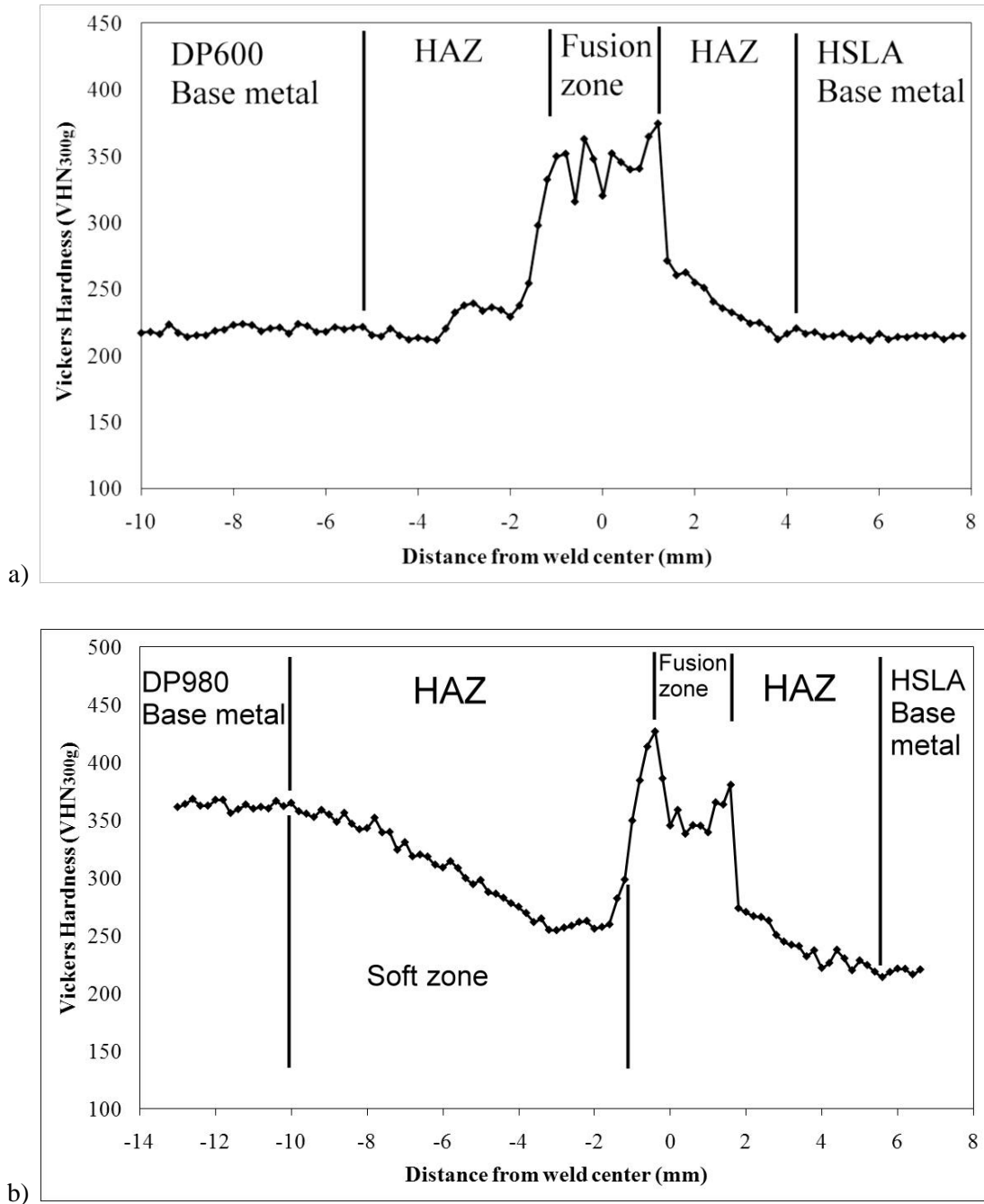


Figure 4.5 Vickers hardness profiles of dissimilar materials TWB: a) DP600-HSLA, and b) DP980-HSLA

The hardness profile of DP980-HSLA is shown in Figure 4.5 b). The average hardness in the FZ of this specimen was 363 ± 27 HV whilst the DP980 steel base metal hardness was measured to be ~ 363 HV and the HSLA steel base metal was ~ 220 HV. In addition, severe softening was observed in the HAZ of the DP980 steel in contrast, to the unobservable softening in DP600 steel. The peak

softening observed in the DP980 steel HAZ was measured to be 258 ± 3 HV. This trend observed in the hardness profiles was also seen in [27]. The general failure location during forming could be determined by examining the hardness profile across the weldment. Areas of low hardness results in strain concentrating in that area and failure to occur there. Low hardness indicates low strength of the material, when forming, this area of low hardness will fail first [43]. From the hardness profiles shown in Figure 4.5, it was expected that failure would happen in the HSLA steel for the DP980-HSLA TWBs, since HSLA is the weaker material. The HSLA steel, being weaker than the softened area of the DP980 HAS was expected to deform more and be the location of failure [27,43,44].

4.2.1 Uniaxial Tensile Test

Necking and fracture during the uniaxial tensile test for all the transverse TWB specimens occurred at the HSLA steel side. The failure location was dependent on the material combination and the weld location as shown in Figure 4.6. Figure 4.6 shows the representative tensile specimens for the tests with different weld locations.

Both DP600-HSLA and DP980-HSLA tensile TWBs showed similar trends of failure occurring in the HSLA steel. During deformation, the weld beads did not crack or fracture; this indicated that the welds were sound. In addition, failure did not occur in the softened region of the DP steel, which indicated that softening did not influence the deformation of the TWBs in tensile testing. This is confirmed that HSLA steel had a lower strength than the softened zone in the DP steels seen in Figure 4.6.

The comparison of the engineering stress-strain diagram of the transverse laser welded blanks where the weld location was the middle, with those of the three parent metals is shown in Figure 4.7. In this figure, the strength of the laser welded blanks was comparable to the HSLA steel parent material; however, the % elongation decreased as the weld line was placed towards the positive side, *i.e.* where there was less HSLA steel available, shown in Figure 4.8.

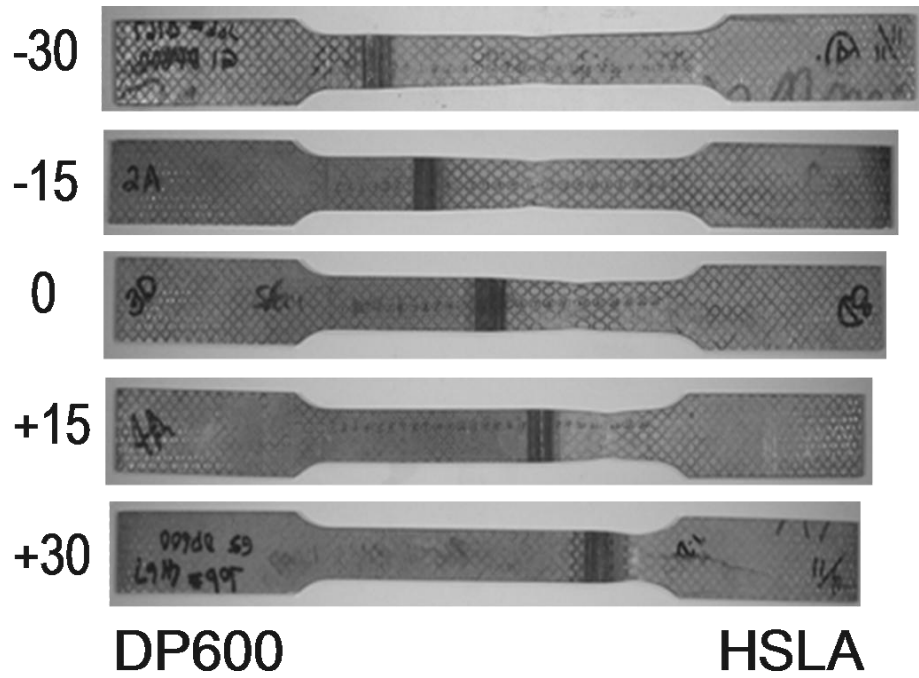


Figure 4.6 Deformed tensile specimens with different weld locations

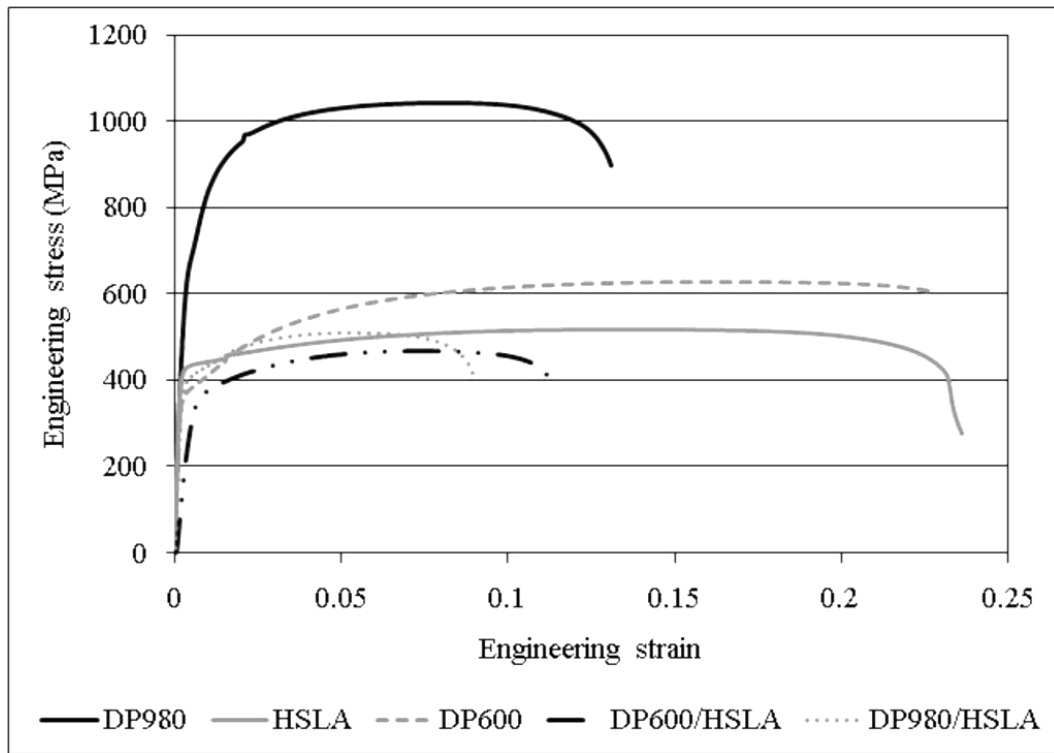


Figure 4.7 Engineering stress-strain graph of TWB (weld position at the middle) and parent materials

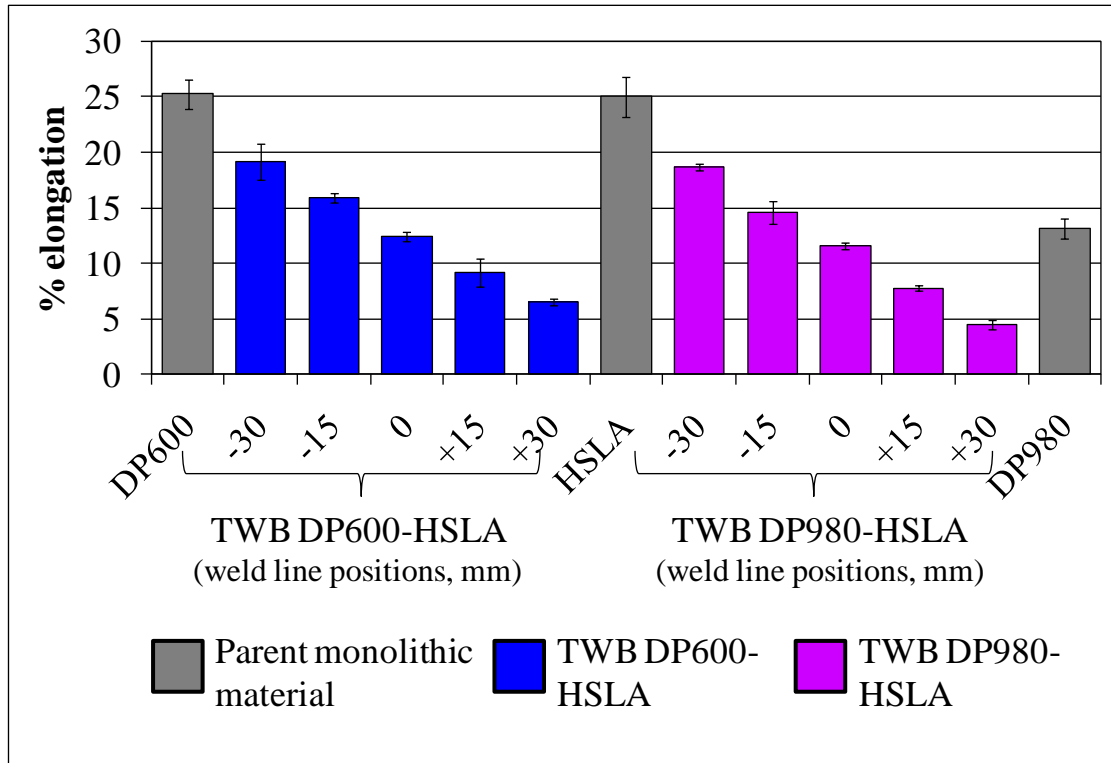


Figure 4.8 %elongation of tensile specimens with different weld position for DP600-HSLA, and DP980-HSLA

Figure 4.8 shows the % elongation of the different TWBs for DP600-HSLA and DP980-HSLA. As the weld line shifted from -30 mm offset to +30 mm offset, the elongation of the TWBs decreased. This trend was consistent with both types of TWBs; as the amount of HSLA steel decreased so did the elongation. Therefore, the amount of HSLA steel influences the elongation (deformation) of these TWBs. From this figure, during tensile deformation of these specimens, the stronger side (DP600 and DP980 steels) experienced negligible deformation. HSLA steel being the weaker material contributed the majority of the plastic deformation. The negligible deformation in the DP steel was due to the higher UTS and strength coefficient (K) compared to HSLA sheet steel.

4.2.1.1 Uniaxial Strain Distribution

The strain distribution profiles of the tensile TWBs showed the strain experienced by the tensile specimens during deformation. These profiles also exhibited the forming behaviour of the tensile TWB specimens for DP600-HSLA and DP980-HSLA.

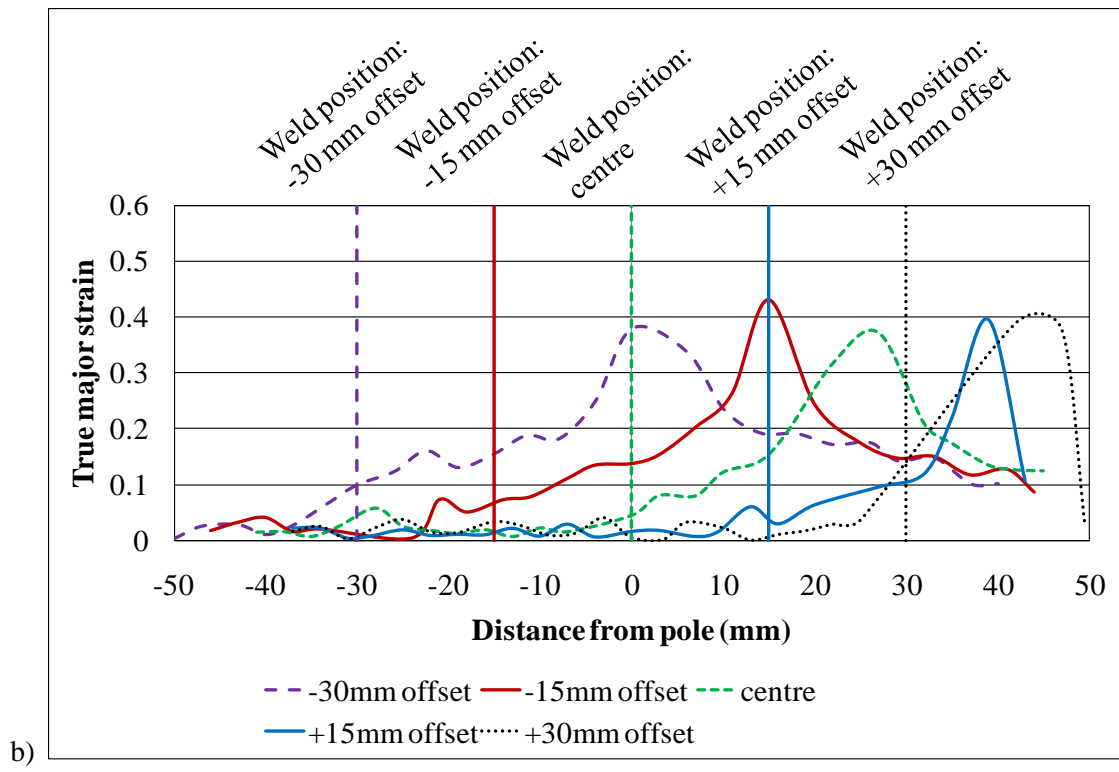
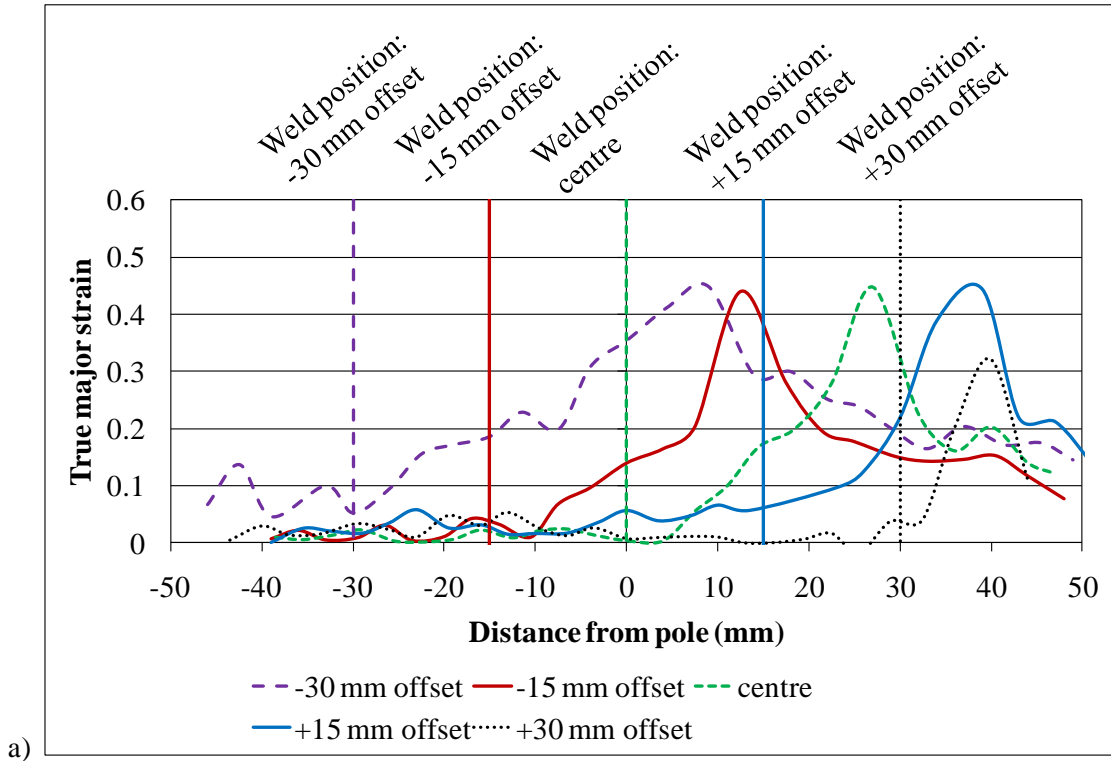


Figure 4.9 Major-strain distribution profiles of uniaxial tensile specimens with different weld locations: a) DP600-HSLA, and b) DP980-HSLA

Figure 4.9 shows the major strain distribution profiles of DP600-HSLA (Figure 4.9 a)) and DP980-HSLA (Figure 4.9 b)) tensile specimens with different weld line positions. As shown in these figures, as the weld line shifted from left to right, the amount of HSLA steel decreased, the major strain concentration peak (location of necking) shifted along with the weld position. The major strain concentrations were all located on the HSLA steel side, which corresponded with the necking locations on the specimen. Also, shown in this figure is the tail (trailing end) of the strain distribution pattern, which indicates the strain in the DP steel. From the minimal strain shown, there was negligible deformation in the DP steel and all deformation was in the HSLA steel; hence, the % elongation decreased (Figure 4.8). Both figures show the same trend of negligible strain in the stronger DP steel and most of the deformation in the HSLA steel.

4.3 Fracture Observations

4.3.1 Failure Locations

4.3.1.1 Biaxial Stretch Forming

The biaxial strain stretch formed specimens with different weld locations for DP600-HSLA and DP980-HSLA are shown in Figure 4.10 and Figure 4.11, respectively. The failure locations were identified on each TWB with arrows. Figures 4.10 a)- e) show failure occurred across the weld or in the HSLA steel and not on the DP600 steel side, ranging from 8-15 mm (Figures 4.10 c)- d)) away from the weld line. Failure did not occur in the softened region; consequently, the soft zone did not contribute to the failure these TWBs. Figure 4.11 shows the deformed DP980-HSLA TWBs with different weld line positions. Figure 4.11 a) shows the -30 mm specimen where failure occurred across the weld; while Figures 4.11 b) - e) show that the failure occurred on the HSLA steel side. The failure on the HSLA steel was parallel to the weld line position and very close to the weld (*i.e.* 3-5 mm). In all the specimens examined, failure did not occur in the soft zone in the DP980 steel side (see Figure 4.5 b) for the hardness profile); thus, indicating that the lower strength of HSLA affected the formability more than the softened region of the DP980 steel.

Comparing the failure locations in Figure 4.10 to Figure 4.11, the fractures occurred closer to the weld line in the DP980-HSLA TWB than in DP600-HSLA TWB. The closeness of the fracture location in the tailored blank was the result of the larger material properties difference in DP980 and HSLA steels compared to DP600 and HSLA steels.

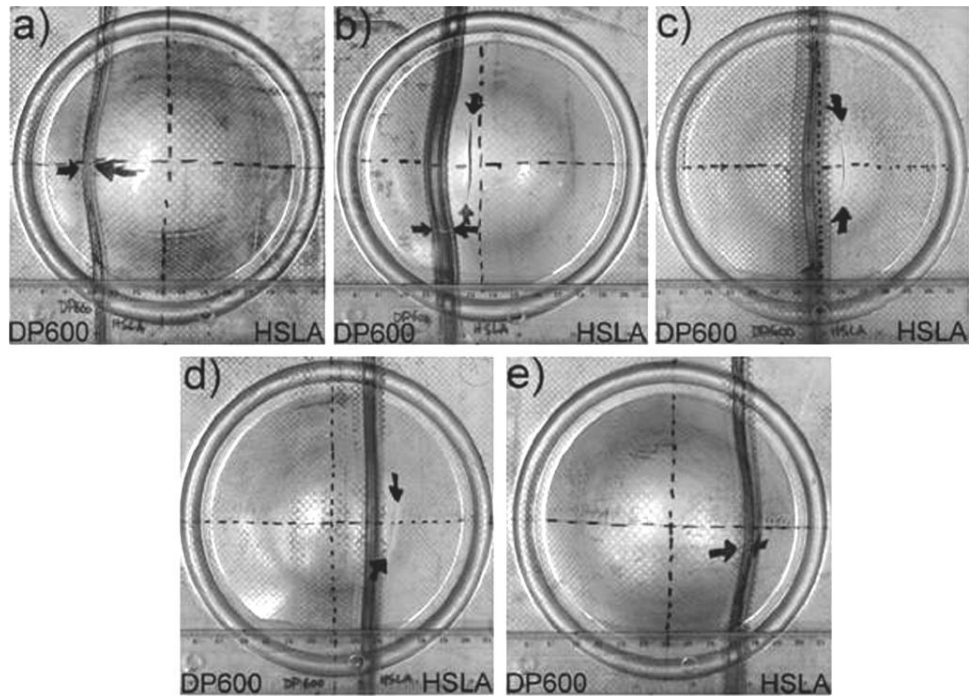


Figure 4.10 Deformed DP600-HSLA biaxial specimens with different weld positions a) -30 mm, b) -15 mm, c) 0 mm, d) +15 mm, and e) +30 mm offset from centre

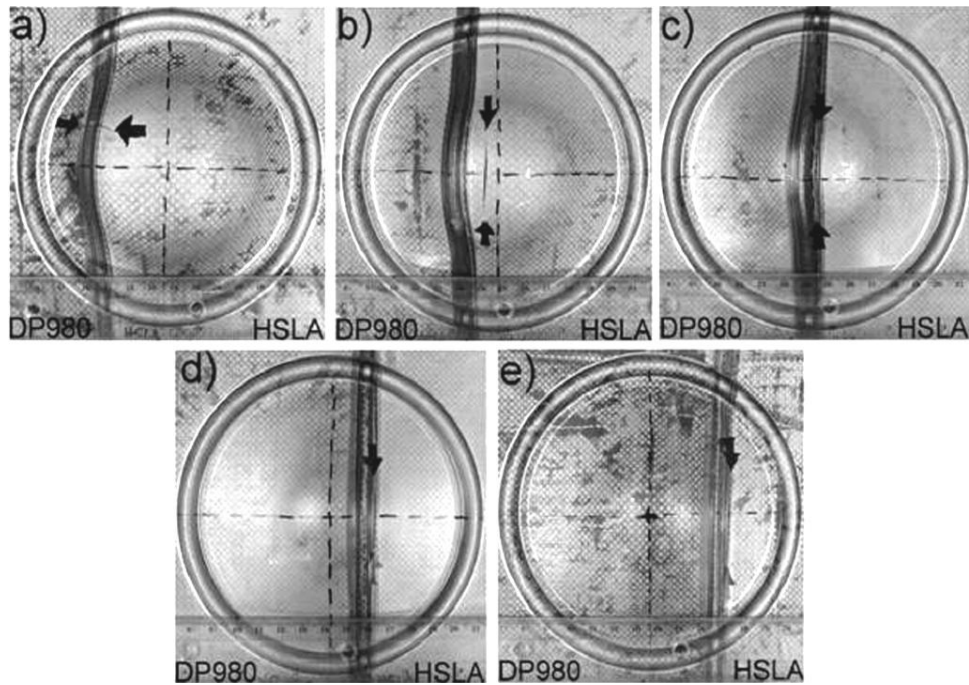


Figure 4.11 Deformed DP980-HSLA biaxial specimens with different weld positions a) -30 mm, b) -15 mm, c) 0 mm, d) +15 mm, and e) +30 mm offset from centre

4.3.1.2 Plane Strain Stretch Forming

The plane strain stretch formed TWBs are shown in Figure 4.12 with the fracture locations: TWBs with longitudinal and transverse weld orientations for DP600-HSLA in Figures 4.12 a) - b) and DP980-HSLA in Figures 4.12 c) - d), respectively. In the longitudinal weld orientations, Figures 4.12 a) and c) failure occurred across the weld – fracture mode I; while in the transverse weld orientation, Figures 4.12 b) and d), failure occurred in the HSLA base metal – fracture mode II. Failure occurred across the weld in plane strain stretch forming for the longitudinal TWBs because the major strain direction was parallel to the weld line *i.e.* the weld was being stretched. The formability of a longitudinal TWB thus depends on the ductility of the weld line. On the other hand, failure occurred in the base metal in the transverse orientation because the weld line was normal to the major strain direction, which caused the base materials to deform. Also, the FZ at the pole experiences much less deformation, which will be discussed in the strain distribution section. In the case of dissimilar material combinations, the weaker material HSLA steel failed first as strain concentrated in this area. From these observations, the formability of transverse weld orientation TWBs is dominated by the formability of the weaker material, while the weld ductility dominated in the longitudinal weld orientation TWBs.

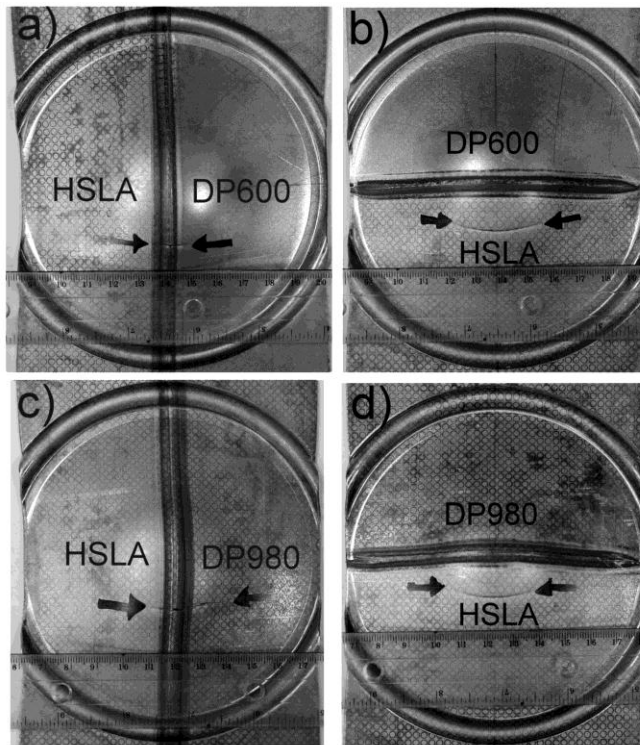


Figure 4.12 Deformed plane strain TWBs a) DP600-HSLA longitudinal TWB, b) DP600-HSLA transverse TWB, c) DP980-HSLA longitudinal TWB, and d) DP980-HSLA transverse TWB

4.3.2 Fracture Modes

The fractures of the specimens in biaxial stretch forming and plane strain stretch forming for the longitudinal and transverse weld orientations are shown in Figure 4.13, Figure 4.14 and Figure 4.15, respectively. Each figure is composed of three parts: a) the macrostructure of the cross-section at the failure location; b) the optical microscope image of the microstructure beside the failure; and c) the SEM image of the fractured surface.

4.3.2.1 Biaxial Stretch Formed Specimens

Figure 4.13 a) shows the general fracture appearance of the TWB in the HSLA steel a few millimetres from the fusion zone (the dissimilar TWB combination shown is DP980-HSLA).

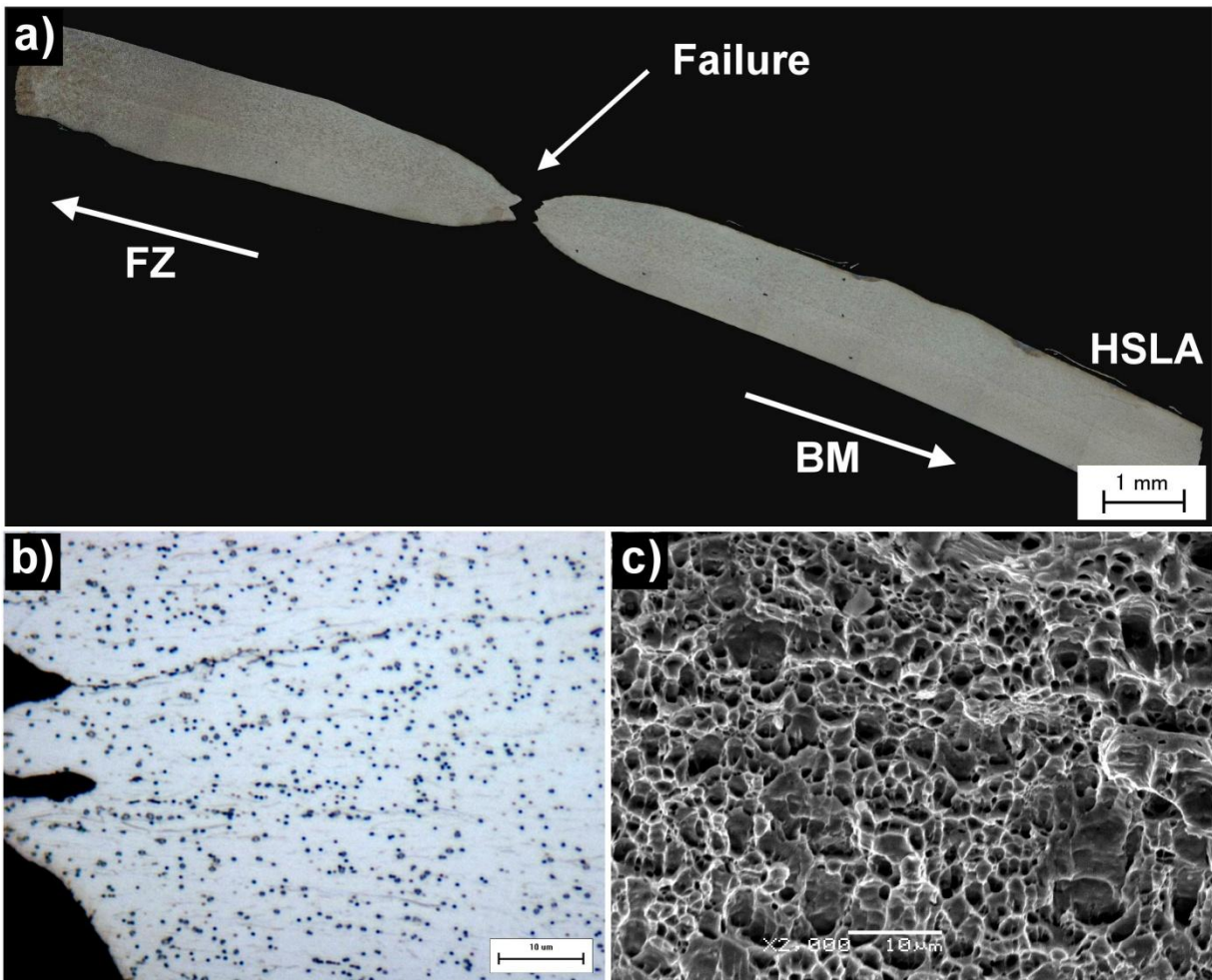


Figure 4.13 Representative images of the biaxial stress forming specimen showing a) cross section macrostructure at the failure location, b) microstructure at the tip of failure, and c) fracture surface

Shown in this figure is the necking observed at the failure and the reduction in the sheet thickness at the tip. This reduction was approximately 75% and the final thickness was 0.27 mm beside the tip. Figure 4.13 b) shows the magnified failure area of the deformed HSLA steel at the region of necking. This figure shows clearly elongated α -grains and dark second phase particles. The second phase particles appeared to be aligned to the prior rolling direction of the sheet. Figure 4.13 c) shows the fracture surface under SEM. Observable cup-like depressions in this figure indicate dimple fracture mode. The dimples appeared to be equiaxed and their distribution was uniform along the fractured surface. The appearance of dimples is characteristic in ductile fracture and this mode of fracture is predominating in biaxial stretched specimens for both dissimilar materials TWBs (DP600-HSLA and DP980-HSLA). The initiation of the fracture may be started by the second-phase particles in the HSLA steel sheet as is typically found in this type of fracture [82,83].

4.3.2.2 *Transverse Plane Strain Stretch Specimens*

Figure 4.14 a) shows a macrograph of the transverse plane strain stretched specimen (DP600-HSLA combination, but also representative for DP980-HSLA combination). Failure in this figure showed necking on the HSLA steel side and the thickness reduction of this necking region was 70% (*i.e.* 0.36 mm at the tip). A closer look at the material adjacent to the fracture, showed elongated α -grains and second-phase particles as illustrated in Figure 4.14 b). While the fracture surface in Figure 4.14 c) revealed the presence of dimples; these dimples were sparsely distributed along the apparent sheared surface. Despite the presence of dimples in the transverse plane strain TWB, the observable sheared surface indicated a distinct difference in failure mechanism when compared to the biaxial strain stretched TWBs.

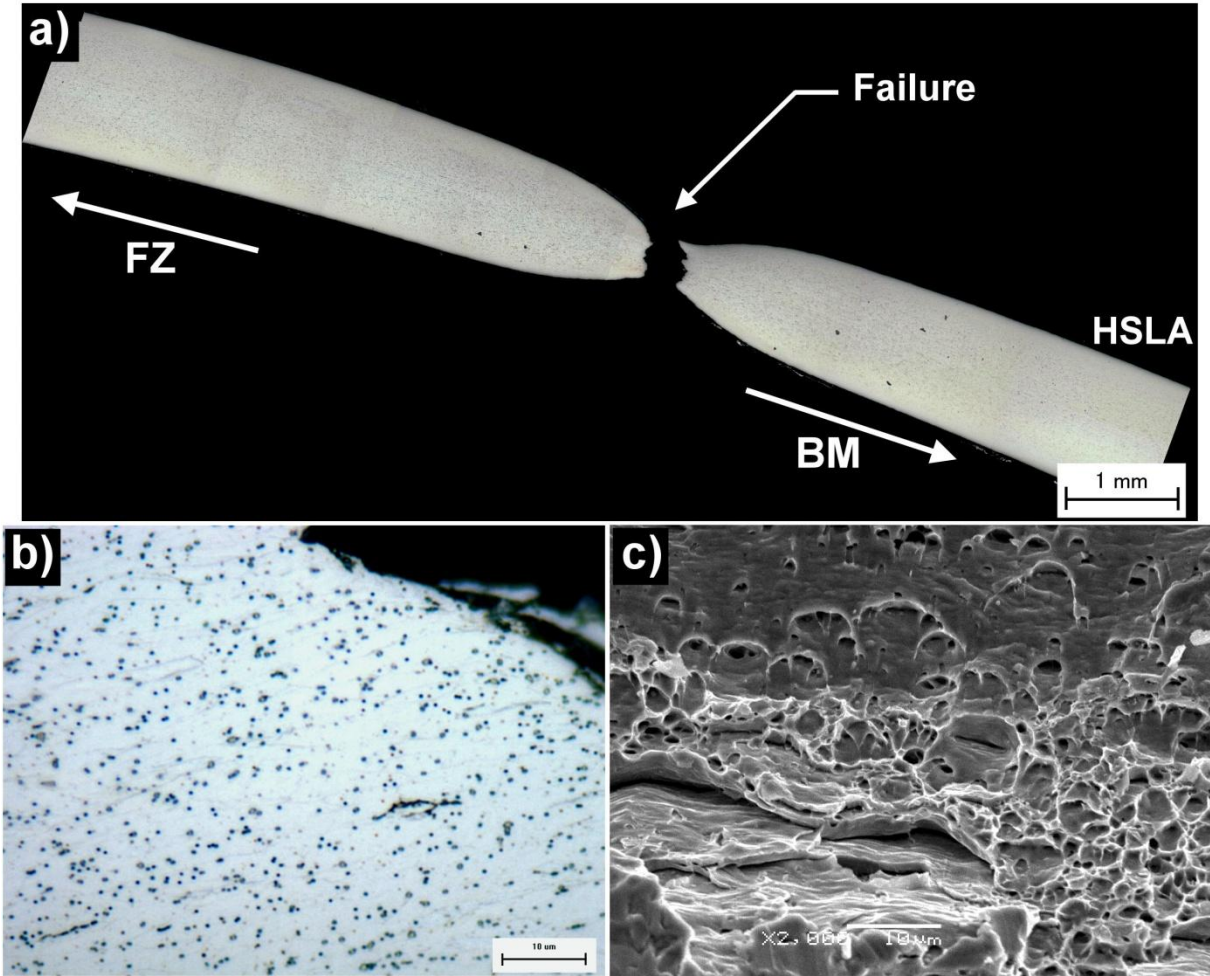


Figure 4.14 Representative images of the transverse plane strain forming specimen showing a) cross section macrostructure at the failure location, b) microstructure at the tip of failure, and c) fracture surface

4.3.2.3 Longitudinal Plane Strain Stretch Formed Specimens

The fracture mechanism in the longitudinal plane strain stretch formed specimens was similar in both the dissimilar materials combination conditions (DP600-HSLA and DP980-HSLA). A representative figure is used; the representative dissimilar combination TWB used was DP600-HSLA.

The failure location in the longitudinal plane strain TWB was in the FZ as seen in Figures 4.15 a) and b). The macrostructure in Figure 4.15 a) did not reveal any apparent necking. The fracture in this specimen appeared to propagate from a 45 degree path angle with respect to the sheet surface. Failure initiated in the fusion zone and extended through the HAZ and then through to the base metal seen in Figures 4.12 a) and c). The optical microscopy image of the fusion zone microstructure

Figure 4.15 b), which was beside the fracture location, exhibited mainly martensite, some bainite phase and also some fractions of ferrite side plate, allotriomorph structure. The fracture surface of the longitudinal plane strain stretch specimen showed few shallow dimples and a large number of trans-granular cleavage-shaped fractured regions [84]. The trans-granular fracture was observable at the edge of the fracture as shown in Figure 4.15 b).

According to the observations in this section it is possible to infer that fracture mode of the stretched formed TWBs is dependent on the weld orientation and strain state (biaxial or plane strain) caused by the different forming test constructions.

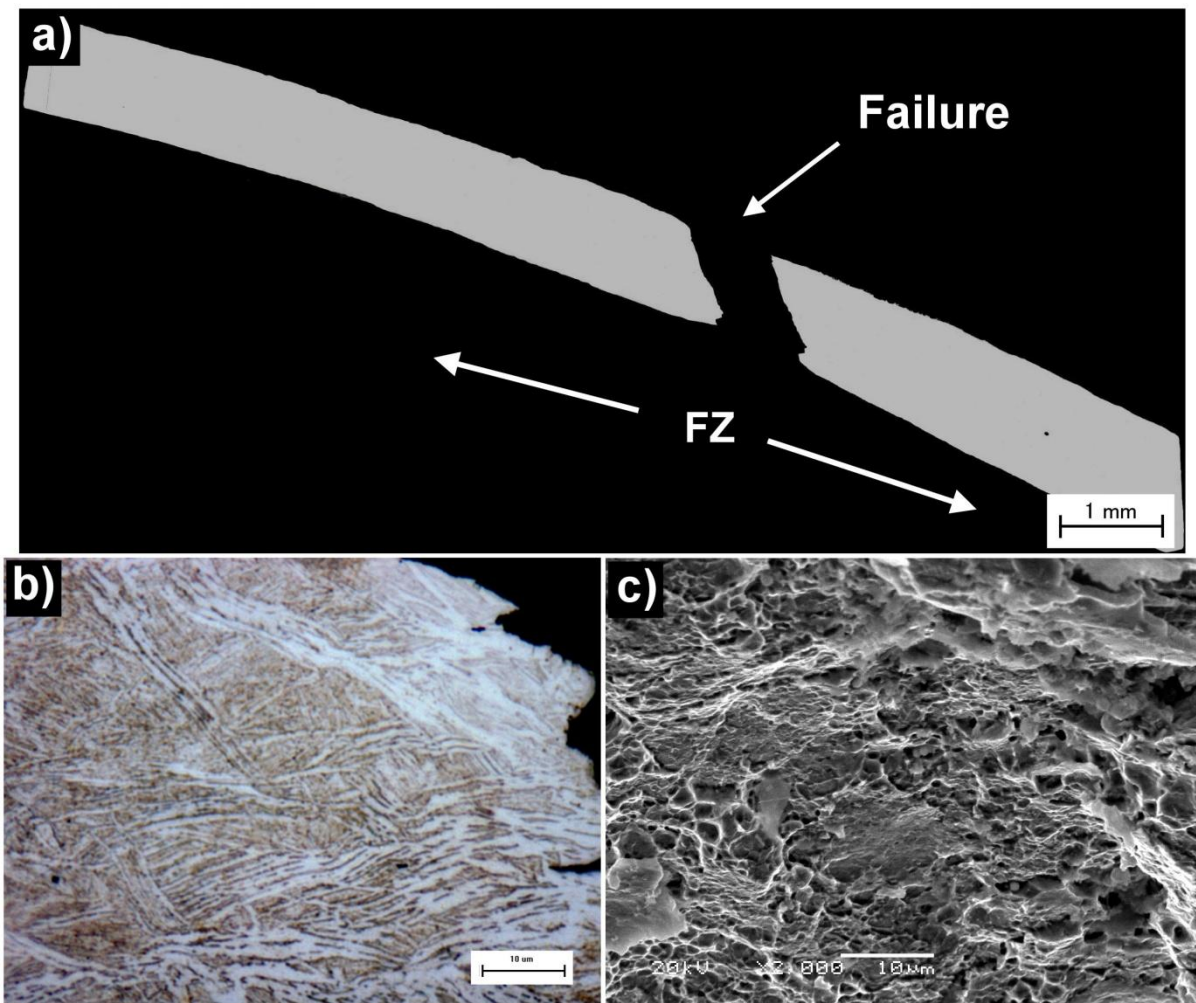


Figure 4.15 Representative images of the longitudinal plane strain forming specimen showing a) cross section macrostructure at the failure location, b) microstructure at the tip of failure, and c) fracture surface

4.4 Limiting Dome Height

4.4.1 Effect Of Material Properties On Weld Location

Figure 4.16 shows the comparison of the LDH of the biaxial TWBs with different weld locations for DP600-HSLA and DP980-HSLA. All the welded specimens showed lower LDH than the base metal, this effect was due to the presence of the weld zone and the different material properties of the TWB. The difference in the material properties led to non-uniform deformation, where the larger the material properties difference between the parent materials the lower the formability, as seen in the DP980-HSLA TWBs compared to the DP600-HSLA TWBs.

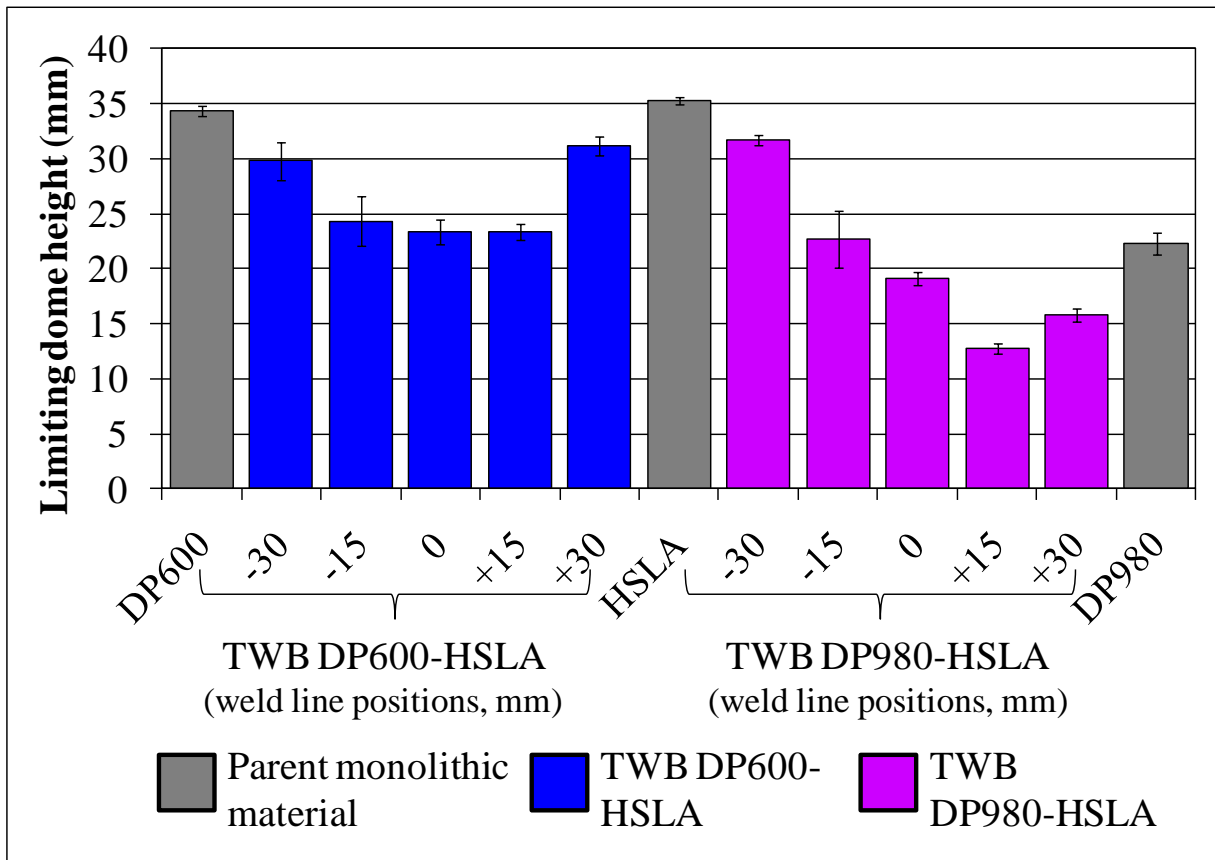


Figure 4.16 LDH of the biaxial TWBs with different weld positions for DP600-HSLA, and DP980-HSLA

Another trend shown in this figure is that as the weld position shifted from the extreme (± 30 mm offset) to $+15$ mm the LDH decreases by 27-33% in the DP600-HSLA combinations. In the case of the DP600-HSLA TWBs the LDH values of the specimens placed at the extremes (-30 mm and $+30$ mm) had comparable LDHs. The weld positions that showed the lowest formability occurred in the

TWBs with the weld positions closest to the centre (-15, 0 and +15 mm offset) with LDH of 23 mm to 24 mm. Comparatively, DP980-HSLA showed the lowest LDH at weld position +15 mm. The LDH increased significantly in this combination when the weld line was placed at -30 mm away from the vertical centreline; the increase was 147.7% compared to the TWB with weld position +15 mm. This result indicates that weld line location affects the formability of dissimilar TWBs significantly and placing the weld furthest from the pole results in improved formability. In spite of this, the amount of increase in the formability with respect to weld position is dependent on the material combination.

Since, there was a change in the LDH as the weld positions shifted; it was likely that the load carrying capacity of each TWB changed. Thus, the load progression curve for each TWB was investigated. The effect of the material combination on the load progression of the different weld location TWB during biaxial stretch forming for DP600-HSLA and DP980-HSLA TWBs is shown in Figures 4.17 a) and b). In both figures, the load progressions of the laser welded blanks were within the parent materials (DP600, DP980, and HSLA steels) load progression curves. Moreover, the slope of the curve depended on the amount of DP600/HSLA and DP980/HSLA in the TWB. The peak load depended on the slope of the curve as well as the dome height achieved. The biaxial stretching load progression curves and the LDH of the laser welded blanks with the different weld locations did not correspond to the uniaxial tensile percentage elongation (Figure 4.8). Consequently, due to the inconformity of the uniaxial percent elongation to the biaxial LDH, the uniaxial tensile test is not a good indicator of the actual press performance of the laser welded blanks. In a previous finding by Heo *et al* [66], the formability in deep draw decreased as the weld line shifted away from the centre. The reasons why the uniaxial tensile test is not a good indicator of formability are: (1) during the uniaxial tensile test, the specimen is stretched in one direction only; and (2) only one material is deformed in the dissimilar materials TWB, unlike the LDH test where both materials are being deformed. Therefore, the LDH is a better indicator of formability; however, it does not reveal the forming behaviour of the TWB. Therefore, the strain distribution patterns are discussed later as part of the effects of the weld placement on the formability.

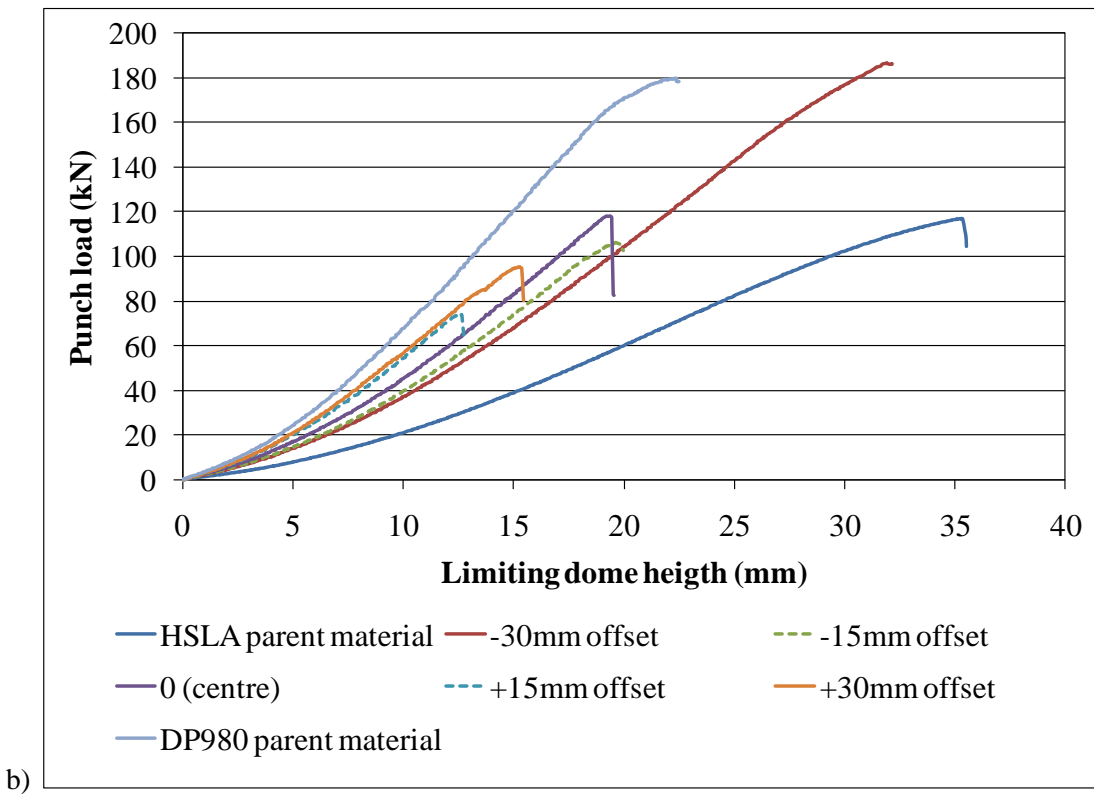
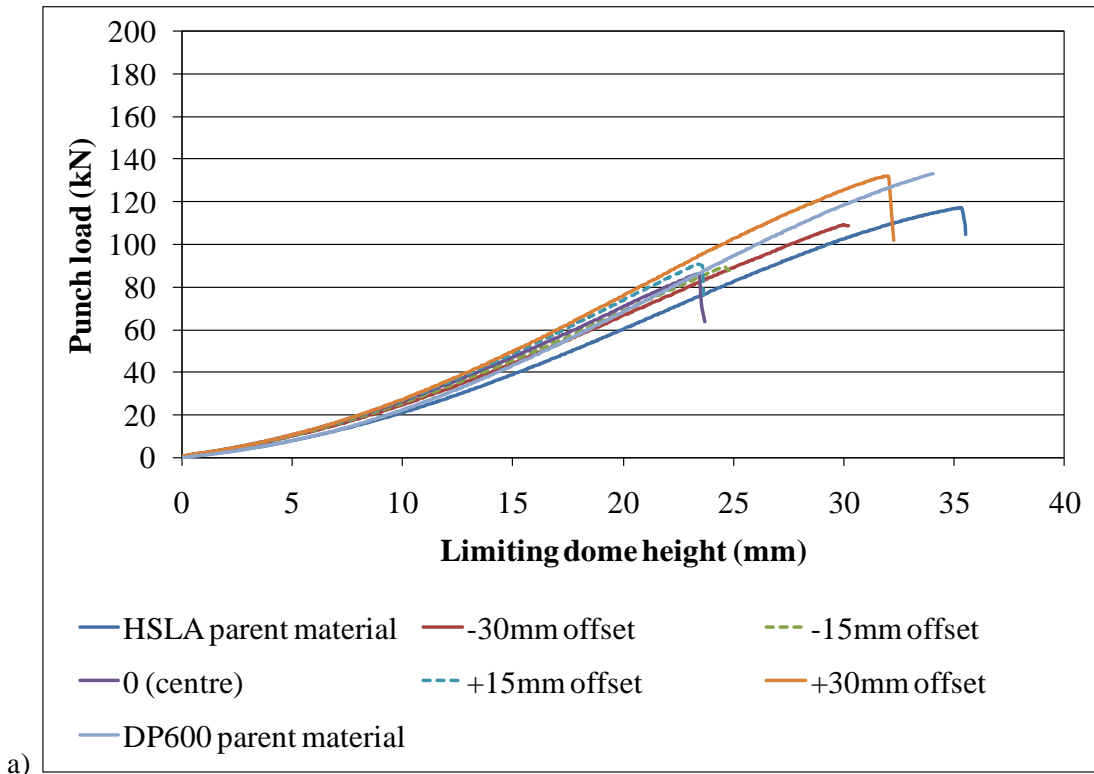


Figure 4.17 Load progression curves of TWBs with different weld line positions: a) DP600-HSLA, and b) DP980-HSLA

4.4.2 Effect Of Weld Orientation And Strain Path (Strain Ratio)

The LDH of the plane strain stretch formed TWBs with different weld orientations are compared to the parent unwelded materials in Figure 4.18.

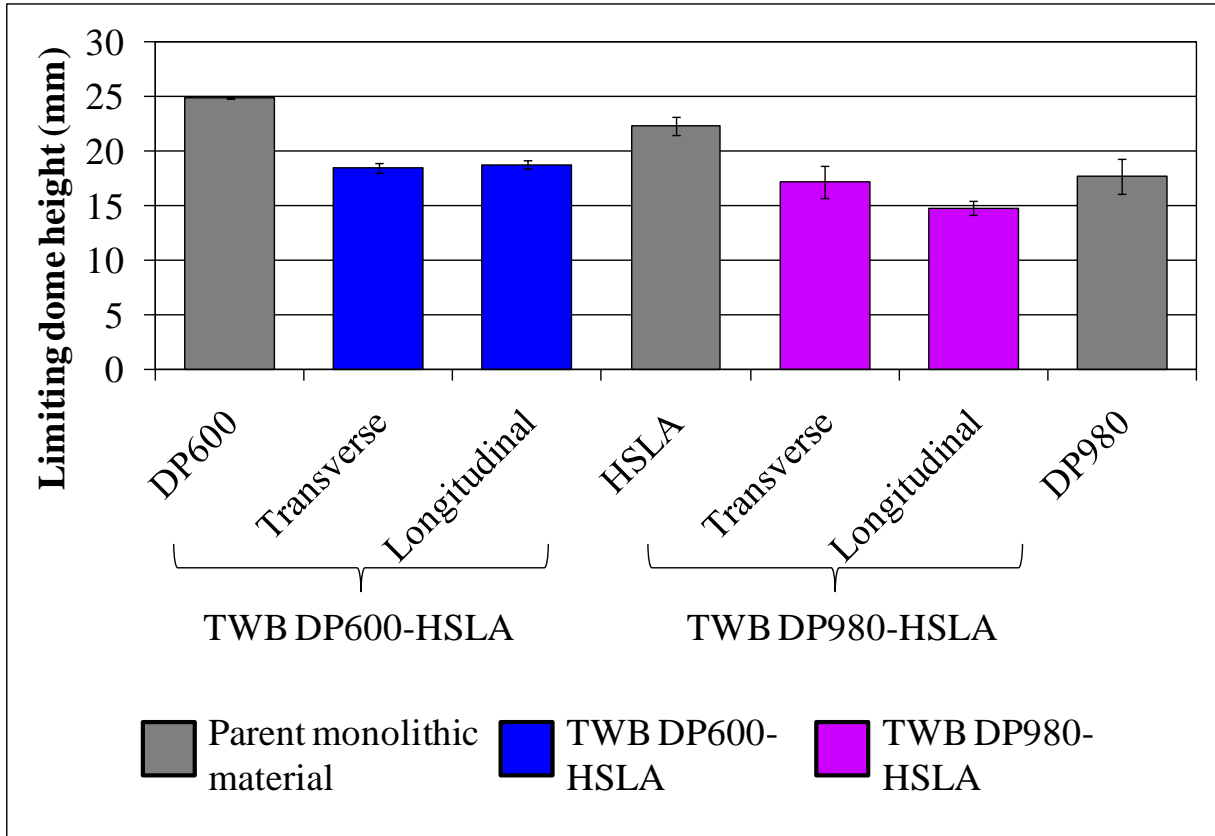


Figure 4.18 LDH of the plane strain TWB with different weld orientations for DP600-HSLA, and DP980-HSLA

First, all of the plane strain stretched specimens had a lower LDH when compared to the biaxial stretch formed specimens. This decrease in LDH is due to the lower forming limit during plane strain condition [85], which induces different fracture morphology (shown in Figures 4.14 and 4.15 and compared to the biaxial stretch mode Figure 4.13). Second, the lowered LDH of the welded blank when compared to the parent material in the plane strain stretch formed condition was due to the presence of the weld and the difference in the material properties. Finally, observable in this figure, the longitudinal and transverse weld orientations LDH of DP600-HSLA were similar at ~18 mm (the difference in LDH was 1.54%); however, in the DP980-HSLA TWBs, the LDH of the longitudinal weld (at 14.79 mm) was significantly lower by 20% than the transverse weld (at 18.49 mm). The

similarity of the formability in the DP600-HSLA combination maybe attributed to the similar material properties; hence, the effect of the weld orientation was insignificant compared to the weld location on the formability of the dissimilar TWBs. Weld orientations significantly affected the formability of the DP980-HSLA TWBs and the decrease was attributed to the large difference in the material properties in the laser welded blanks. The difference in material properties in the DP980-HSLA combination increased the hardness of the weld zone, Figure 4.5, which also decreased the ductility of the weld. Thus, when the weld was being stretched in the longitudinal condition early failure occurred and gave a lower formability compared to the higher LDH in the transverse TWB due to the large material properties.

The load progression curves of the plane strain stretched dissimilar tailored blanks are shown in Figure 4.19. The similarity of the DP600-HSLA TWBs with the different weld orientations is reflected in the load progression curves in Figure 4.19 a). The load progression curves of the DP980-HSLA TWBs are shown in Figure 4.19 b). The load carrying capacity of the longitudinal DP980-HSLA TWB was significantly lower than the transverse DP980-HSLA TWB. Hence, the weld line should be oriented transversely to the major strain direction when stretching DP980-HSLA combinations in TWBs.

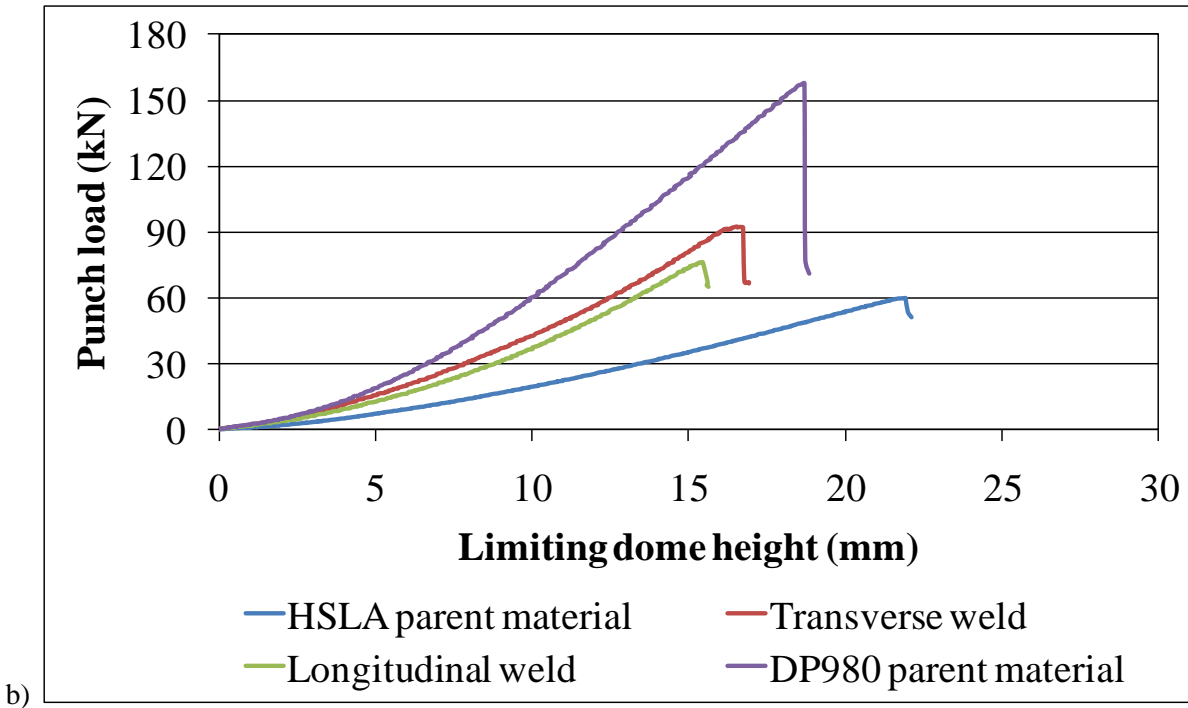
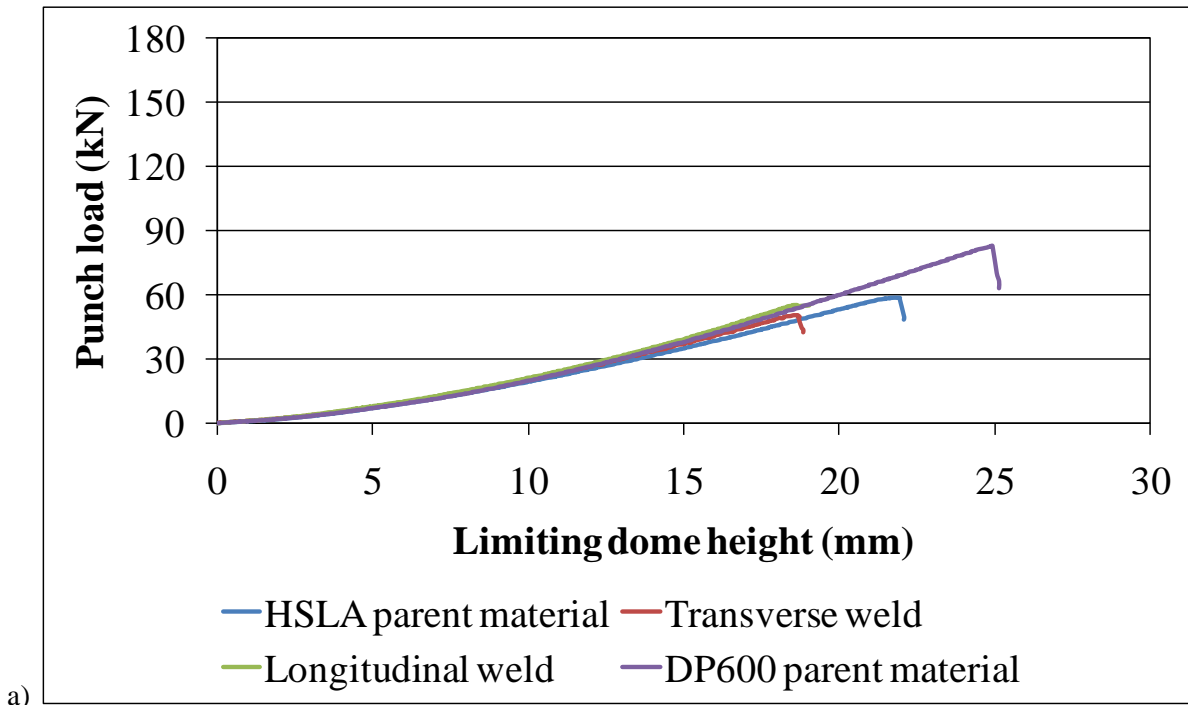


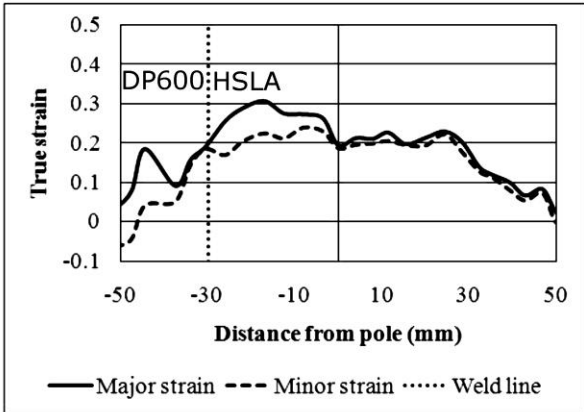
Figure 4.19 Load progression curves of plane strain TWB specimens: a) DP600-HSLA, and b) DP980-HSLA

4.5 *Strain Distribution*

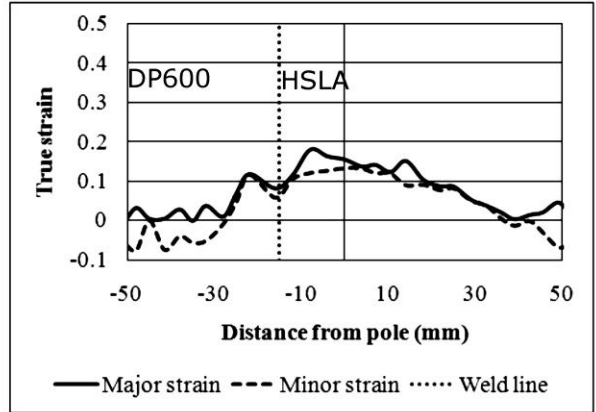
The strain distribution profile indicates the forming behaviour across the TWB. These profiles are composed of the major and the minor strain on the dome plotted with respect to the pole. The strain paths with respect to the experimental FLDs of the parent materials are shown in Appendix B.

4.5.1 *Biaxial Stretch Forming*

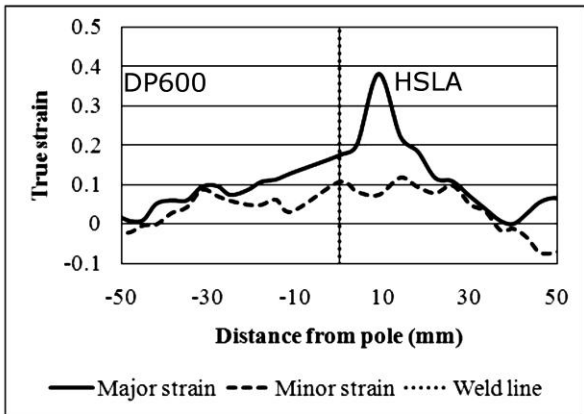
The major and minor strain distribution profiles across the deformed TWBs at different weld locations for DP600-HSLA and DP980-HSLA are shown in Figure 4.20 and Figure 4.21, respectively. In both dissimilar TWB combinations (DP600-HSLA and DP980-HSLA) non-uniform strain distribution was observed when the weld was placed near the centre (Figures 4.20 b)- d) and Figures 4.21 b)- e)). The most non-uniform distribution pattern in DP600-HSLA and DP980-HSLA TWBs occurred when the weld position was at the +15 mm offset location, Figure 4.20 d) and Figure 4.21 d), respectively. As seen in all the specimens with the weld positions -15 mm, 0 mm and +15 mm, the weaker material, HSLA steel, deformed more compared to the stronger DP steel during the forming process. The concentration of the peak strain that led to failure occurring on the HSLA steel side. The strains of these laser welded blanks were unlike the parent material strain distribution in biaxial and plane strain stretch forming shown in Figure 4.3 and Figure 4.4, which showed uniform strain distribution.



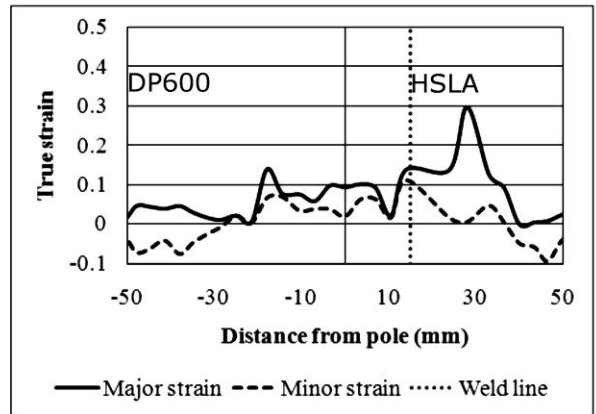
(a) DP600-HSLA and weld position: -30mm



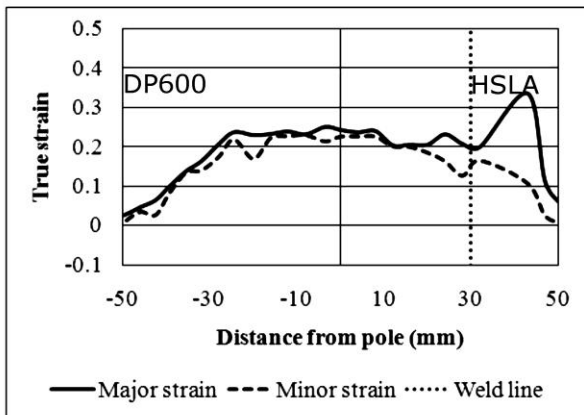
(b) DP600-HSLA and weld position: -15mm



(c) DP600-HSLA and weld position: 0mm



(d) DP600-HSLA and weld position: +15mm



(e) DP600-HSLA and weld position: +30mm

Figure 4.20 Strain distribution patterns of DP600-HSLA TWBs with different weld locations

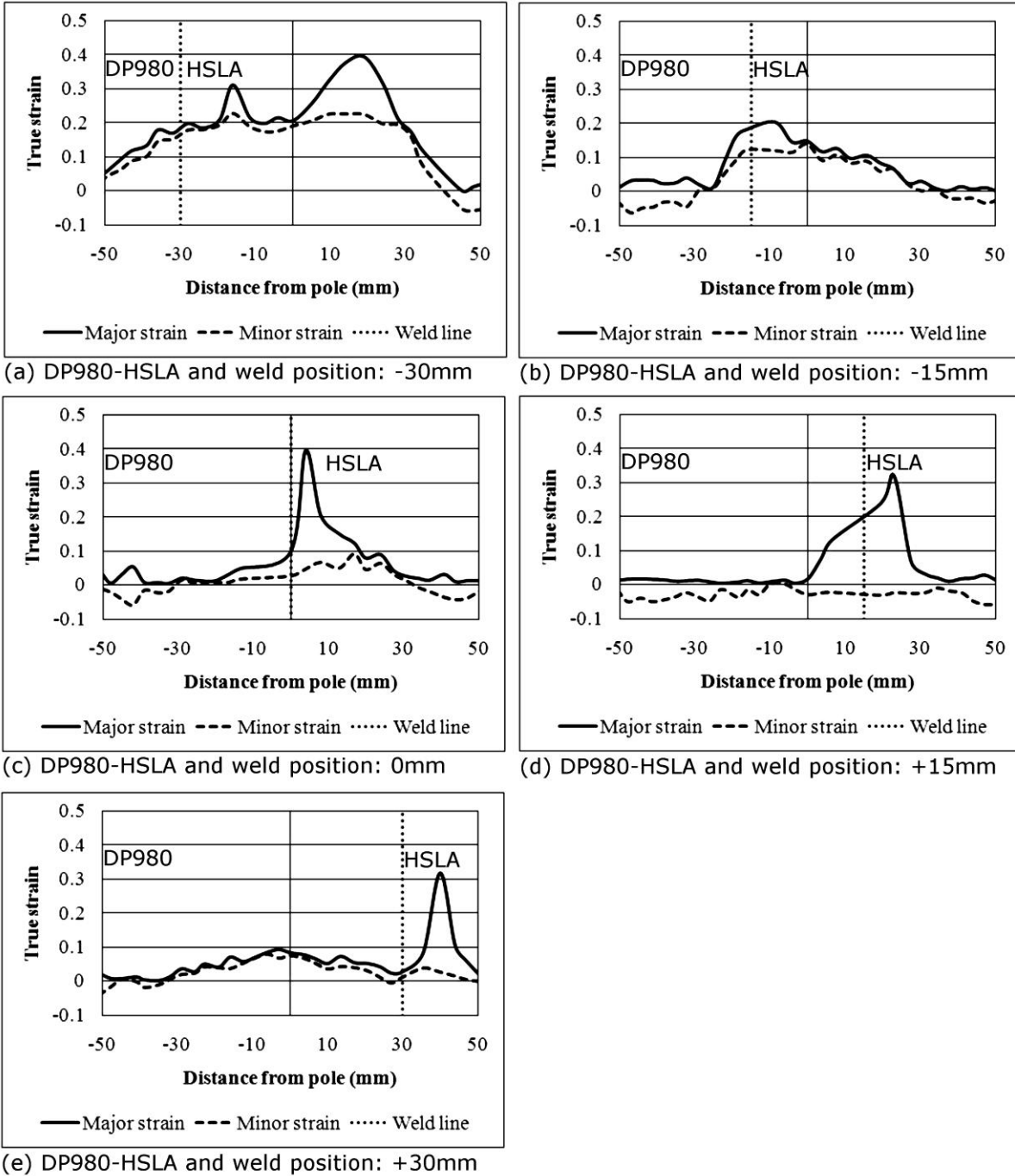


Figure 4.21 Strain distribution patterns of DP980-HSLA TWBs with different weld locations

The major strain distribution patterns of the TWBs with the weld position of -30 mm offset (Figure 4.20 a) and Figure 4.21 a)) were more uniformly distributed. In addition, the minor strains were

well developed indicating a strain path that was more equi-biaxial during deformation when compared to having the weld at the centre of the blanks. For this reason, the LDH at the weld position -30 mm was higher than those of the tailored blank with the weld at the centre. As to the weld position +30 mm offset from the centre of the TWB, uniform strain distribution with well developed minor strain occurred in the DP600-HSLA combination, Figure 4.20 e). In contrast, the major strain distribution was non-uniform in the DP980-HSLA combination with the weld at +30 mm, Figure 4.21 e). The peak strain in the DP980-HSLA combination occurred in the HSLA steel and the minor strain at less than 0.1. The strain in the DP980 steel was limited. With more DP980 steel than HSLA steel material and the large difference in the materials properties (unlike the DP600-HSLA combination) the LDH and strain distribution were both limited.

Therefore, the strain distribution and LDH of dissimilar material combinations is dependent on the weld position and the material properties of the TWB. The larger the material properties difference in the TWB, the lower the formability. Hence, it is desirable to keep the amount of stronger material in the blank low to get a laser welded blank with higher formability.

4.5.2 Plane Strain Stretch Forming

The major and minor strain distribution of the plane strain TWBs (with a blank width of 120 mm) with different orientations (longitudinal and transverse) for DP600-HSLA and DP980-HSLA combinations are shown in Figure 4.22. In the profiles seen in Figure 4.22, the minor strains were close to zero similar to the parent materials stretched in plane strain condition in Figure 4.3.

The strain profile along the weld line in the longitudinal weld TWB of DP600-HSLA is shown in Figure 4.22 a). The peak strains in this figure were comparable on both sides and there was negligible strain at the pole, since the major strain was close to zero. Conversely, the strains in the transverse tailored blank for DP600-HSLA Figure 4.22 b) showed that there was more strain in the HSLA steel than in the DP600 steel. Comparatively, the strain distribution profiles of the DP600-HSLA longitudinal TWB and the DP600-HSLA transverse TWB (Figures 4.22 a) and b)) were similar. Therefore, the LDH of the longitudinal specimens was comparable to the transverse specimens.

While comparing the strain distribution of the DP980-HSLA longitudinal specimen to the transverse specimen (Figures 4.22 c) and d)), there was only one peak in the longitudinal TWB with insignificant amount of strain elsewhere along the weld. In the DP980-HSLA transverse specimen there was more strain due to the presence of another minor peak in the DP980 steel. This peak

indicated that there was some deformation in the DP980 steel side, which resulted in the higher LDH when compared to the longitudinal DP980-HSLA specimen. This difference in LDH also indicated the influence of weld orientation.

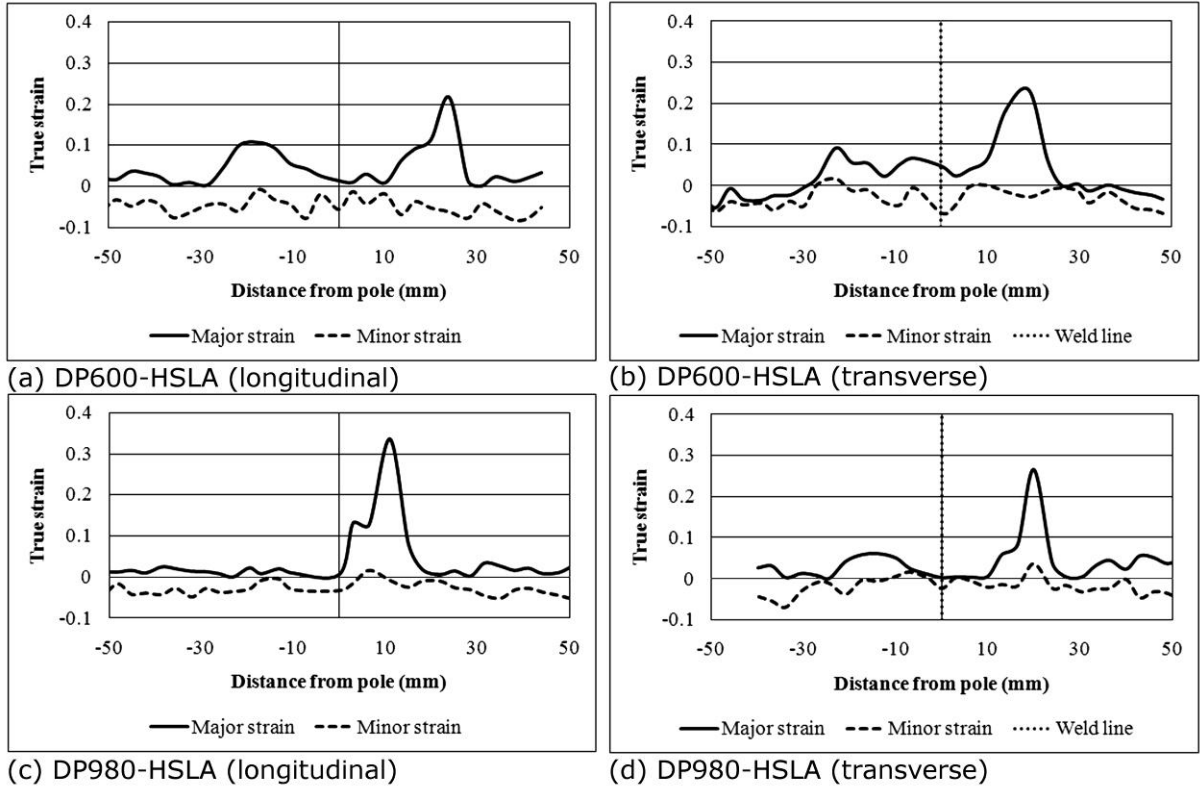


Figure 4.22 Strain distribution patterns of TWBs with different weld orientations for DP600-HSLA, and DP980-HSLA

4.6 Summary

Welding DP steel causes the formation of a soft zone and reduces the formability of the welded blank, but combining DP steel with HSLA steel improves formability [27]. In this study, the effect of weld line position and weld orientation on dissimilar materials TWB (DP600-HSLA and DP980-HSLA) on formability was investigated. It was found that despite the materials combination or the severity of softening in DP980 steel compared to DP600 steel, failure occurred in the HSLA steel and changing the weld position did not cause failure to occur in the DP steel. However, weld position affected the formability of the TWB, especially in the TWBs with similar materials properties. The decrease in formability was observed in the forming behaviour indicated by non-uniform strain patterns. When changing the stretching mode to plain strain stretch forming, it was found that effect of weld orientation was negligible when the materials properties of the TWB were similar. This was observed in the forming behaviour, where the strain profiles were similar for the longitudinal and transverse TWB for DP600-HSLA. In addition, analysis of the fracture topography may imply a change in the formability (forming mode) of the blank.

CHAPTER 5

5 EFFECT OF CURVILINEAR SEAMS WITH DIFFERENT WELD POSITIONS ON FORMABILITY

Chapter 4 explored the effects of weld line position and orientation on the formability of dissimilar TWBs. In this chapter the effects of weld geometry and weld placement on HSLA, DP600, and DP980 steels are explored. In most past research, the weld geometry studied was focused on linear welds as used in TWB applications. For applications that benefit from nonlinear welds, manufacturers have generally used multiple welds to accommodate the blank fit up without the welding complexity of a nonlinear/curvilinear weld. One potential disadvantage of this method is the occurrence of a blow-hole or comparable process defect at the inflection point where two welds meet; hence, the study of non-linear or curvilinear welded TWBs is considered important. Therefore, the work recorded in this chapter investigates the effect of curved welded blanks on formability and compares it to straight welded blanks at different weld locations for HSLA, DP600, and DP980 steels.

5.1 *Limiting Dome Height Testing*

The curvilinear bead-on plate blanks had dimensions of 200 mm x 200 mm. The welds had a radius of curvature of 220 mm as shown in Figure 5.1. The testing of these blanks was done according to the procedure described in Chapter 3. The curvilinear seam was placed at distances, 0 mm, 15 mm, and 30 mm to the right of the centre. In the figure, the left (concave) side of the curvilinear seam was labelled the inner region and the right side of the weld was labelled the outer region for simplified reference. During welding, each sheet was clamped in a custom fixture where the bottom opening for the back shielding gas was 40 mm in width, shown in Figure 3.9. The welding speed used was 0.85 m/min to ensure full penetration.

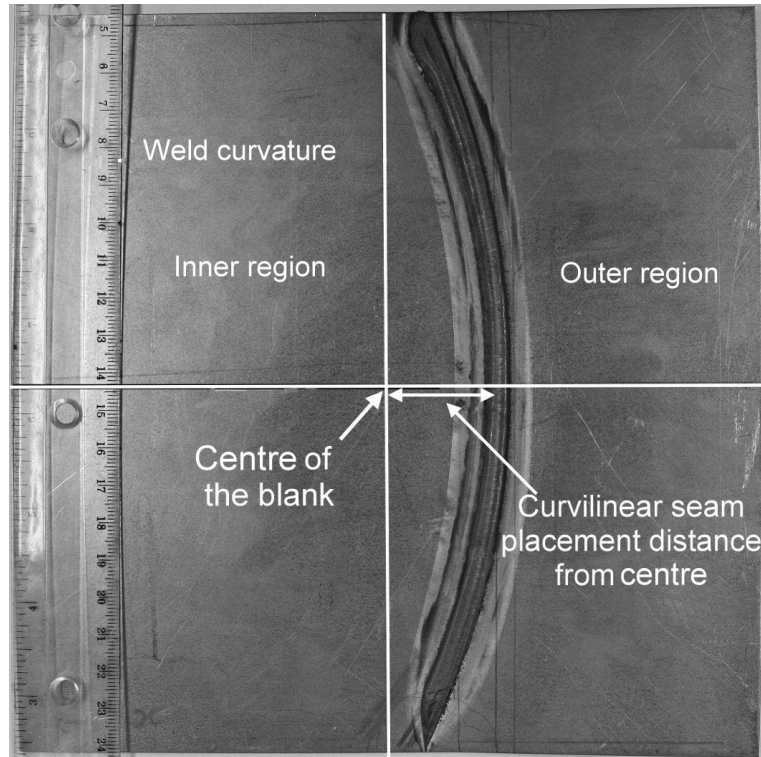


Figure 5.1 Curvilinear welded TWB

5.2 Hardness Measurements And Microstructures

The cross section specimens used for the hardness profiles were taken as sections normal to the local weld path, near the horizontal arrow shown in Figure 5.1. The hardness profiles of the curvilinear welded HSLA, DP600 and DP980 sectioned blanks are shown in Figures 5.2 a), b), and c), respectively and Figure 5.2 d) illustrates a representative cross-sectional macrograph (DP980). The macrograph illustrates the different regions of the weldment, such as the FZ, HAZ and the base metal (BM). It should be noted that the left side of the cross-sectioned weldment (with respect to the FZ as the baseline), in Figure 5.2 d) corresponds to the inner region of the bead-on plate seam curvilinear weld shown in Figure 5.1.

Figure 5.2 a) shows the typical pattern of weld hardness for HSLA. The average FZ hardness value measured was 246 ± 5 HV in the HSLA steel. The HAZ was characterized by the relatively high (but lower than the FZ) hardness value of ~ 245 HV close to the fusion zone line and then followed by a drop in hardness in the HAZ toward the base metal. The base metal hardness was measured at an average of 179 ± 2 HV. The extent of the HAZ in the HSLA steel in the inner region compared to the

outer region was 14% longer (at 3.2 mm and 2.8 mm, respectively). Softening was not observed in the HAZ of the hardness profile of the HSLA.

In the DP600 steel weld cross section, the measured hardness average at the FZ was approximately 330 HV. The HAZ was characterized by high hardness values (*i.e.*, approximately 320 HV) close to the fusion zone line and by a decreasing hardness along the HAZ towards the base metal. Within the HAZ there was a slight reduction in hardness (softening) with respect to the base metal. The base metal hardness averaged at 200 HV, while the peak softening value on the inner region was ~188 HV and the peak softening value on the outer region was ~191 HV. The total extension of the HAZ and softening region varied according to the location of the indentations across the weld. The extension of the HAZ on the left side of the profile is longer than the right side HAZ (Figure 5.2 b)) similar to the HSLA steel. For instance, the extension of the softening region on the left side (~3 mm) was 33% longer than that of the right side (~2 mm).

Figure 5.2 c) shows the hardness profile of the DP980 steel weldment; the average measured hardness in the FZ was 386 ± 22 HV, whereas, the BM hardness was measured to be 335 ± 5 HV. The softening in the HAZ of the DP980 steel was severe in contrast to the softening in DP600 steel (Figure 5.2 b)). Notably, the peak softening was larger on the left side (210 ± 3 HV) compared to the right side (221 ± 3 HV) of the DP980 steel. In terms of the HAZ length, the DP980 steel (Figure 5.2 c)) showed a similar trend as the DP600 steel, *i.e.* the extent of the softened region for DP980 steel was ~8 mm on the inner region whereas the extent of the softened region on the outer region was ~5 mm on the hardness profile. The difference in the widths of softened region was ~38%. This trend regarding the extent of the HAZ is shown in the macrograph of the cross-sectioned DP980 steel weldment in Figure 5.2 d).

It is clear from these results that curvilinear seam weld had a significant effect on the extent of the HAZ, seen in the hardness profiles of HSLA, DP600, and DP980 steels (Figures 5.2 a) to c), respectively). Although, softening was not observed in the HSLA steel, the extent of the HAZ in the inner region was longer than the outer region. The extent of the softened region in both the DP steels' hardness profiles was longer in the inner region of the curvilinear seam welded blank. More importantly, the maximum softening in both DP steels was observed in the inner region of the curvilinear seam welded blank. It is very probable that these two effects (the extent/width of the HAZ and the severity of the softened region) might be caused by the increase in heat/thermal cycle and heat distribution due to the geometry of the weld. The curvature of the weld could cause the heat to

concentrate in the inner region whereas in the outer curvature region there is a larger area for heat dissipation because heat transfers in the radial direction for curved geometries [86].

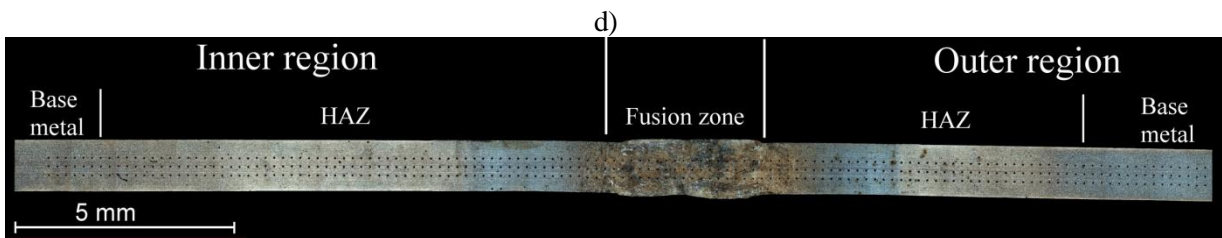
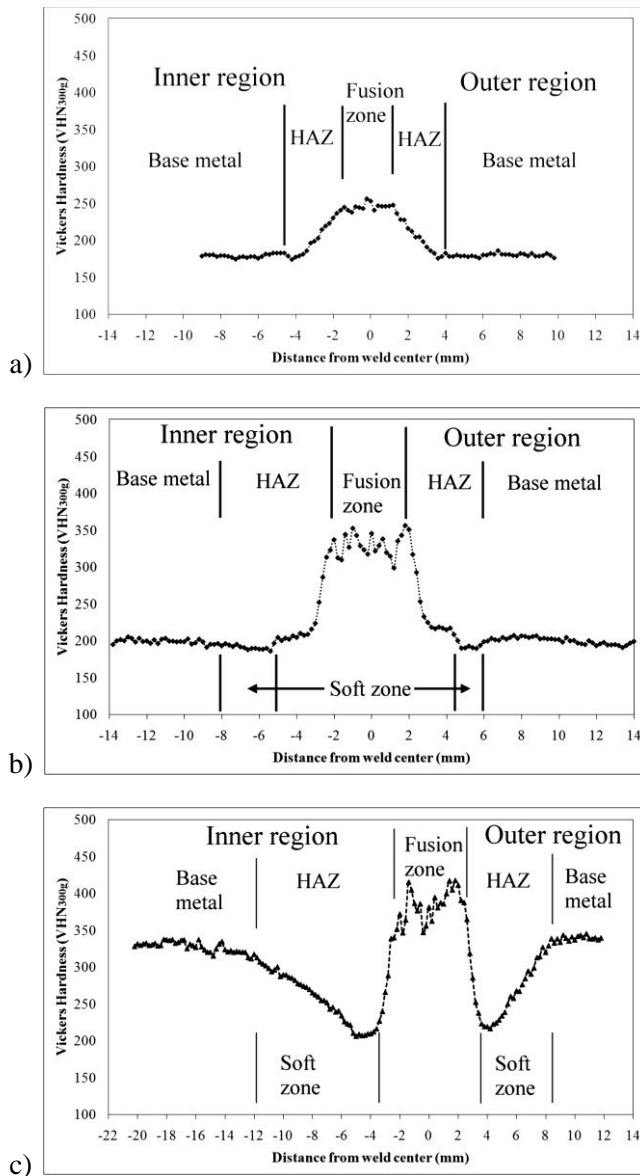


Figure 5.2 Vickers hardness profiles of curvilinear welds: a) HSLA steel, b) DP600 steel, c) DP980 steel, and d) macrograph of cross-section (DP980)

5.3 Strain Distribution Profiles

The strain distribution profiles show the forming behaviour observed across the deformed TWBs. These profiles show areas of high strain concentrations, the amount of deformation at the pole and the effect of the weld on the overall forming behaviour. To understand the effect of the curvilinear weld, the strain profiles of the curved weld were compared to the strain profiles of comparable straight welds for the same material and weld position.

Figures 5.3, 5.4, and 5.5 show the strain distribution profiles for HSLA, DP600, and DP980 steels at different weld placements. Each figure is divided into six parts: a) to c) show the strain profiles of the straight line welds at different weld locations; and d) to f) show the strain profiles of the curvilinear welds at the comparable locations.

In all the strain profiles of the HSLA steel blanks in Figure 5.3, the major and minor strains were found to be very close, indicating biaxial stretch forming condition. The strain profiles of the curvilinear blanks were similar to the straight line blanks in terms of the strain distribution, amount of strain at the pole, and peak strain locations. The peak strains in the HSLA steels were located approximately 15-20 mm away from the weld. The similarity between the strain profiles at the respective weld placements indicated that the weld geometry did not significantly influence the formability of the welded blanks. Also, noticeable from these figures was the change in the amount of strain as the weld position shifted. The strain profiles were best developed *i.e.* had the highest strain occurring, when the weld was shifted away from the pole.

The strain distributions in Figure 5.3 (despite weld geometry) for welded HSLA steel at weld positions 0 mm and 30 mm show twin peaks similar to the parent unwelded HSLA steel (Figure 4.2) and the peak locations were also similar. The strain profile most resembled the unwelded HSLA steel was when the weld position was placed 30 mm from the pole. It is likely that the similarity was due to the weld being placed far from high strain locations; hence, the formability of the blank with weld position 30 mm was similar to the parent unwelded material.

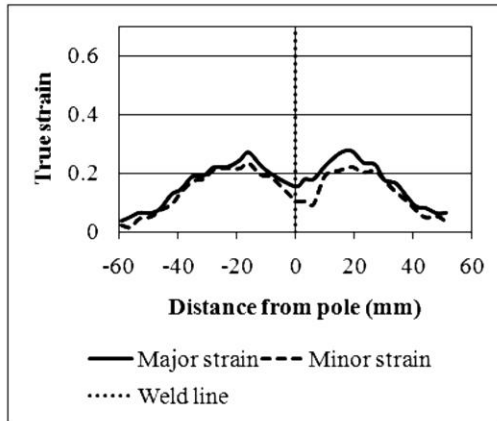
Figure 5.4 shows the strain profiles of the welded DP600 steel. The strain distribution profiles of the straight line welds were generally similar, shown in Figures 5.4 a) to c). The strain profiles for the straight line weld position at 0 mm and 15 mm were similar. However, when the weld was at 30 mm from the pole, the amount of strain increased as did the strain at the pole indicating that the formability of the blank with weld position farthest from the pole gave the best formability. The shapes of all the straight line welded blank profiles at different weld locations resembled the parent unwelded DP600 steel (Figure 4.2); but, the height (the amount of strain) of the profiles were lower. This

indicated that the formability of welded DP600 steel was lower than the parent unwelded blank. The strain distribution profiles of the curvilinear welds when the welds were placed 0 mm and 15 mm from the pole gave similar non-uniform strain profiles. These profiles showed the peak strains on the left of the pole in the inner region of the blank and within the softened region as shown in Figure 5.2 b). The curvilinear welded blank with weld position 30 mm from the pole showed an increase in the overall strain and the strain at the pole when the weld was shifted to the farthest position indicated that the formability of the curvilinear welded blank was affected by weld position.

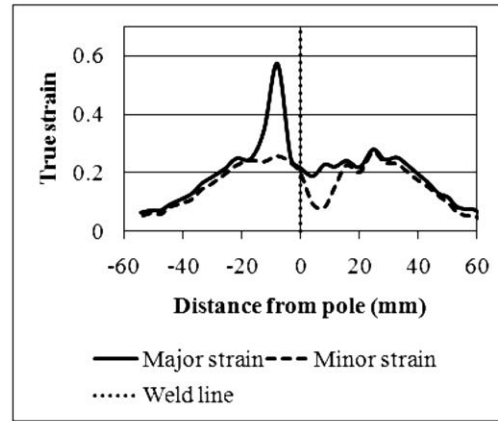
The DP600 strain profiles for the curvilinear welded blank with weld position close to the centre differed from the profiles of the linear welded blanks in terms of overall amount of strain measured and the strain at the pole. The amount of strain on the outer region (right side of the weld) was also reduced when compared to the linear welded blanks at similar weld positions. However, the strain profile of the 30 mm offset DP600 curvilinear welded blank was similar, but not as developed as the linear welded blank at the comparable location. These observed strain behaviours indicated that the weld geometry affected the formability of the DP600 welded blanks unlike the case of HSLA steel as shown in Figure 5.3. Moreover, even though the strain profiles of the parent unwelded DP600 and HSLA steels were very well-developed (Figure 4.2), the strain profiles of the welded DP600 steels were not as well-developed as the welded HSLA steels. This indicated that the formability of the weld affected DP600 steel more than HSLA steel, since welding created softening in the HAZ of the DP600 steel shown in Figure 5.2, which was not present in the HSLA steel.

Figure 5.5 shows the strain profiles of the welded DP980 steel blanks. These profiles show that the amount of strain present in welded DP980 steel was low despite the weld geometry, with the smallest strain magnitudes at the 15 mm location. The limited strains in welded DP980 steel were also seen in dissimilar material combination TWBs in Figure 4.11. When these DP980 steel strain profiles were compared to the HSLA steel (Figure 5.3) and DP600 (Figure 5.4), welded DP980 steel showed the lowest formability and the cause of this was attributed to the effect of the softening seen in the hardness profile in Figure 5.2 c).

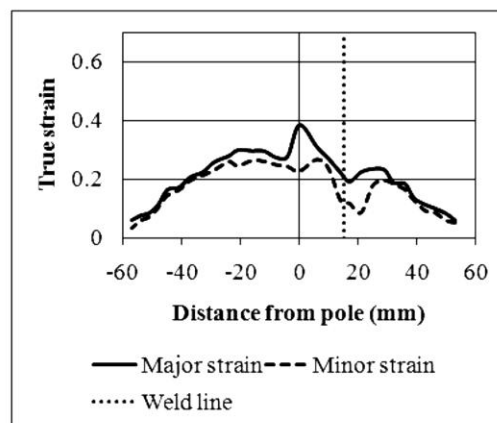
Therefore, according to the strain distribution profiles of the welded steels only DP600 steels showed a significant effect of weld geometry on the formability. Both welded HSLA and DP980 steels showed comparable strain profiles in the straight-line welded blanks as compared to the curvilinear welded blanks. In HSLA steel, weld geometry did not affect formability [18]; while HAZ softening effects dominated over the weld geometry effects in terms of formability in DP980 steel [38,39,60,61].



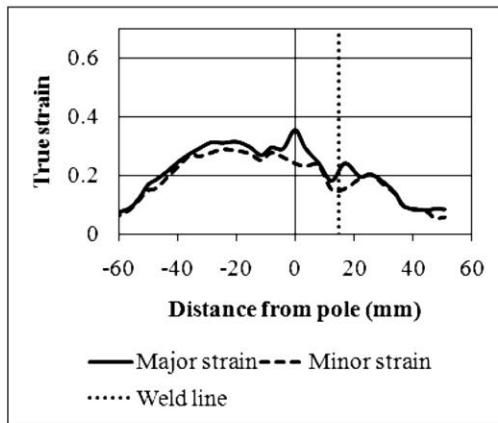
(a) HSLA straight weld and weld position: 0 mm



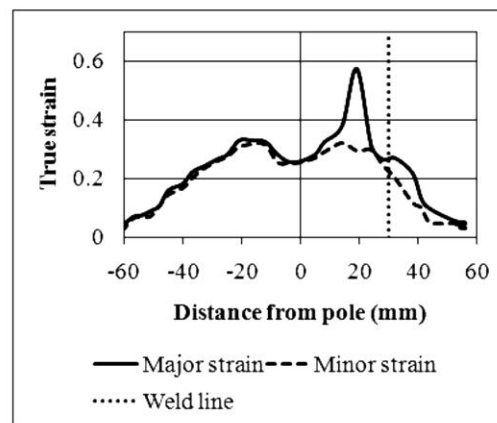
(d) HSLA curvilinear weld and weld position: 0 mm



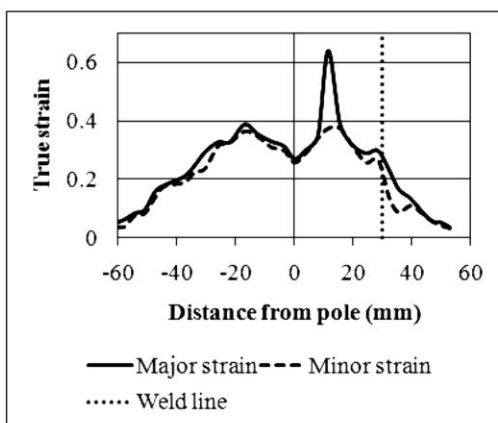
(b) HSLA straight weld and weld position: 15 mm



(e) HSLA curvilinear weld and weld position: 15 mm

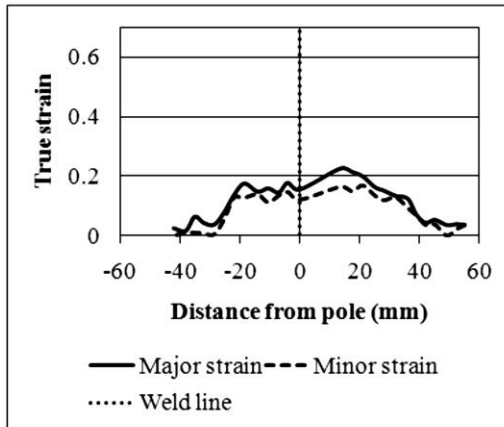


(c) HSLA straight weld and weld position: 30 mm

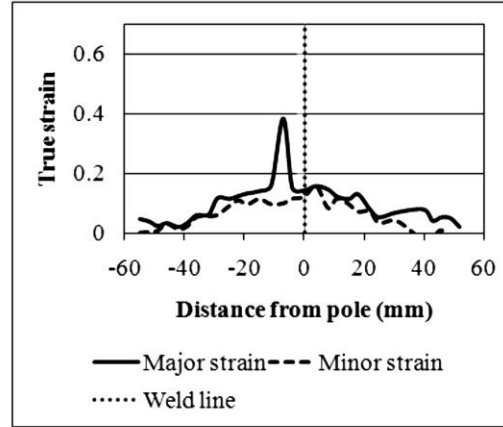


(f) HSLA curvilinear weld and weld position: 30 mm

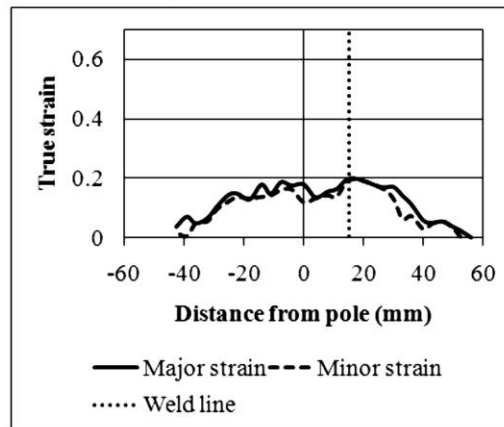
Figure 5.3 Strain distribution profiles of HSLA linear and curvilinear welded blanks with different weld placements



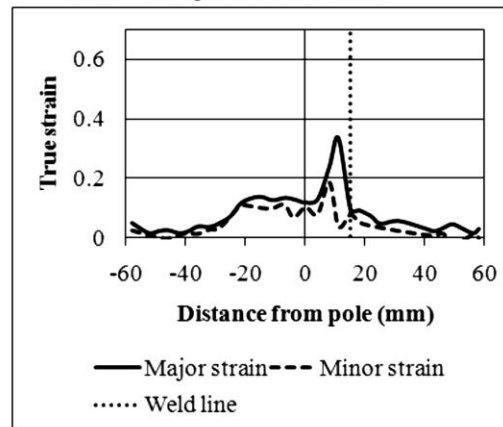
(a) DP600 straight weld and weld position:0 mm



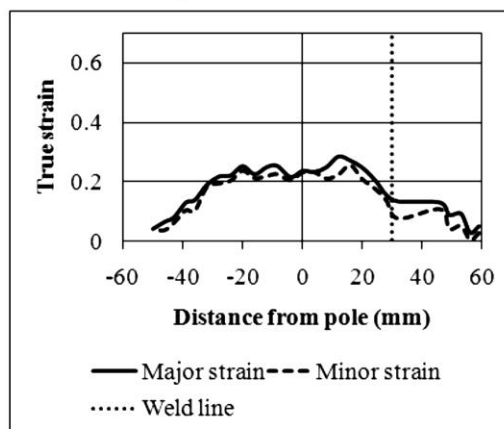
(d) DP600 curvilinear weld and weld position:0 mm



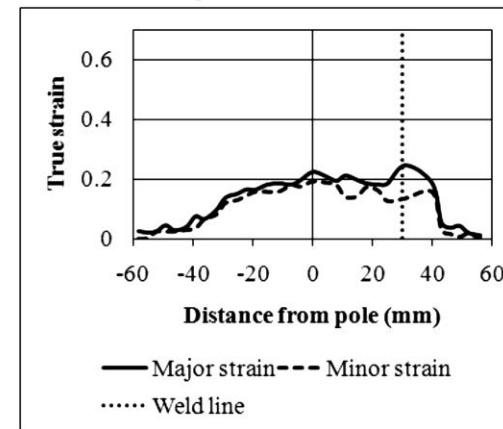
(b) DP600 straight weld and weld position:15 mm



(e) DP600 curvilinear weld and weld position:15 mm



(c) DP600 straight weld and weld position:30 mm



(f) DP600 curvilinear weld and weld position:30 mm

Figure 5.4 Strain distribution profiles of DP600 linear and curvilinear welded blanks with different weld placements

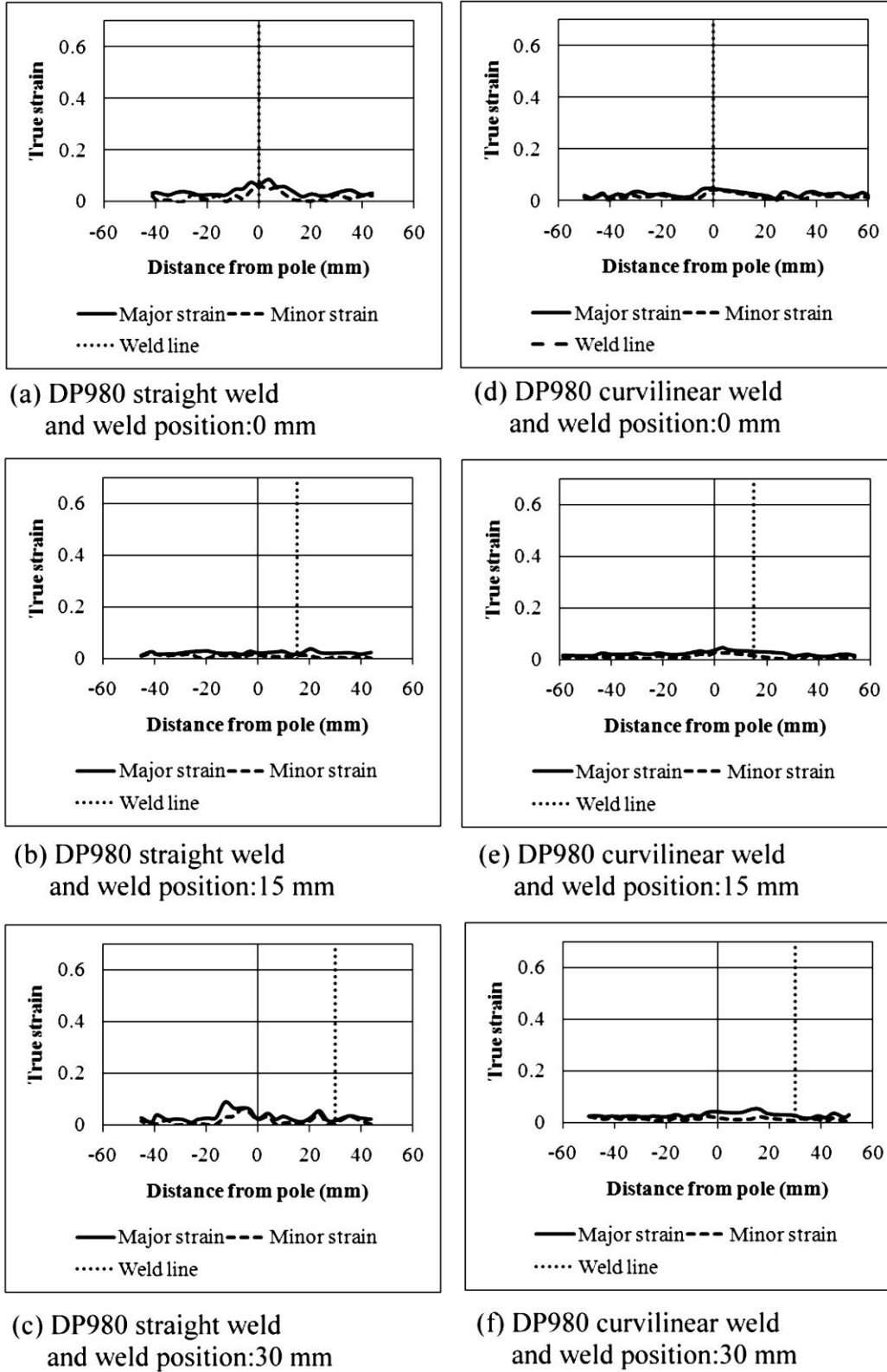


Figure 5.5 Strain distribution profiles of DP980 linear and curvilinear welded blanks with different weld placements

5.4 Fracture Locations

The biaxial strain stretch formed linear welded blanks and curvilinear weld blanks in HSLA, DP600, and DP980 steels with different curve weld positions (0, 15, and 30 mm from the centre of the blank) are shown in Figures 5.6, 5.7 and 5.8, respectively. The curvilinear welded blanks are all displayed with the inner region on the left side and the outer region on the right side like in the blank shown in Figure 5.1.

The failure locations were indicated in each specimen. The failure locations in the linear welded HSLA blanks were located either across the weld (Figure 5.6 a)) or in the base metal (Figures 5.6 b) and c)). The failure location in all of the HSLA steels was located 10-20 mm away from the pole in Figures 5.6 a) and c). These failure locations were consistent with the high strain concentration peaks seen in the strain distribution profiles in Figure 5.3 when the welds were placed in the 0 mm and 30 mm positions and corresponded to the twin strain peaks seen in the parent unwelded HSLA steel strain profile in Figure 4.2.

The failure locations in the linear welded DP600 steels occurred either across the weld (Figures 5.7 a) and c)) or in the HAZ (Figure 5.7 b)). From these observed failure locations, softening in the HAZ did not significantly affect the formability of these blanks. The failure locations in the curvilinear welded DP600 steels occurred very close to the weld, ~5 mm from the centre of the weld (Figures 5.7 d) to f)) on the inner region, which indicated the influence of softening.

The failure locations of the linear and curvilinear welded DP980 steels occurred in the HAZ despite weld placement or weld geometry were located ~3-5 mm from the weld centre as shown in Figure 5.8. The failure locations of the curvilinear welded DP600 and DP980 steels occurred on the inner region of the blank corresponding to the soft zone as shown in the hardness profiles in Figures 5.2 b) and c). Failure occurred in the softened region because it was the weakest part of the blank and during the deformation process strain concentrated in this area: this failure location in welded DP980 was consistent with past research results [17,27,39].

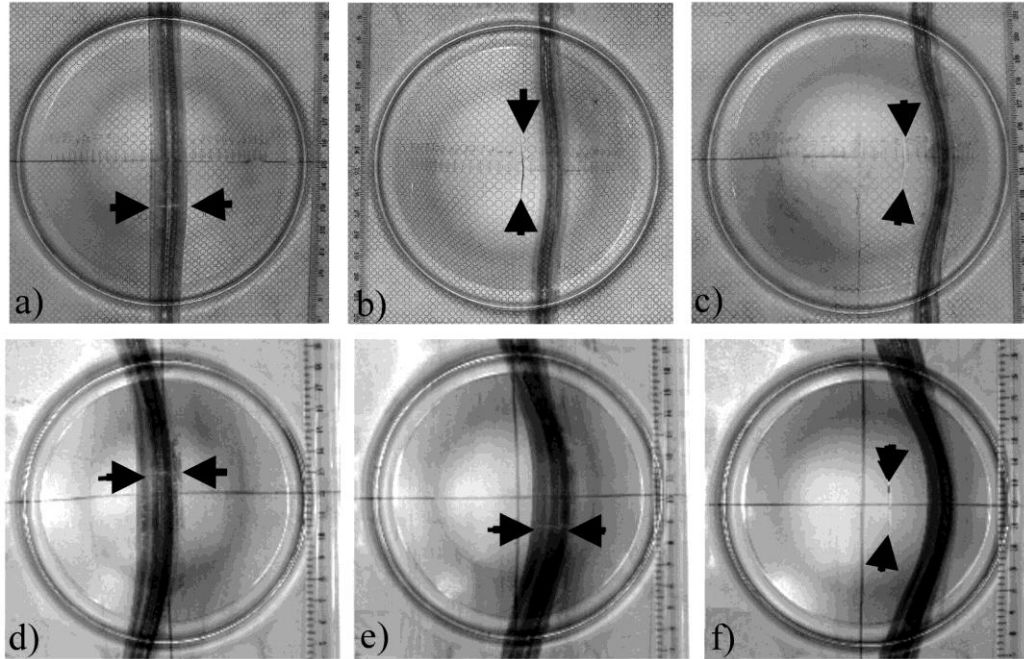


Figure 5.6 HSLA linear welded blanks a) to c); and curvilinear welded blanks d) to f) with weld locations at 0, 15, and 30 mm

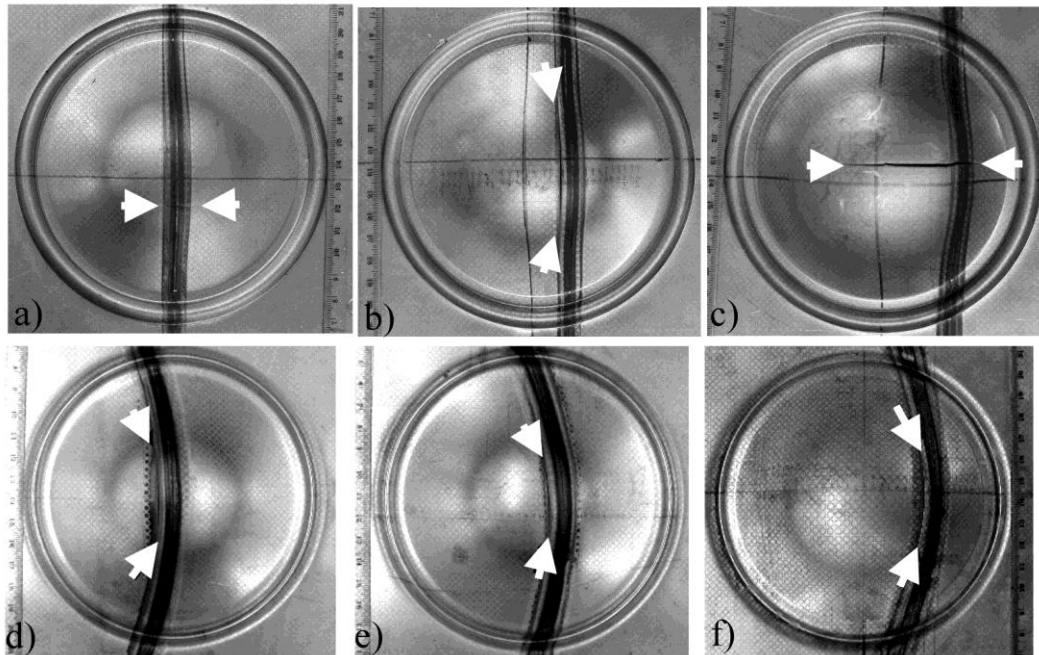


Figure 5.7 DP600 linear welded blanks a) to c); and curvilinear welded blanks d) to f) with weld locations at 0, 15, and 30 mm

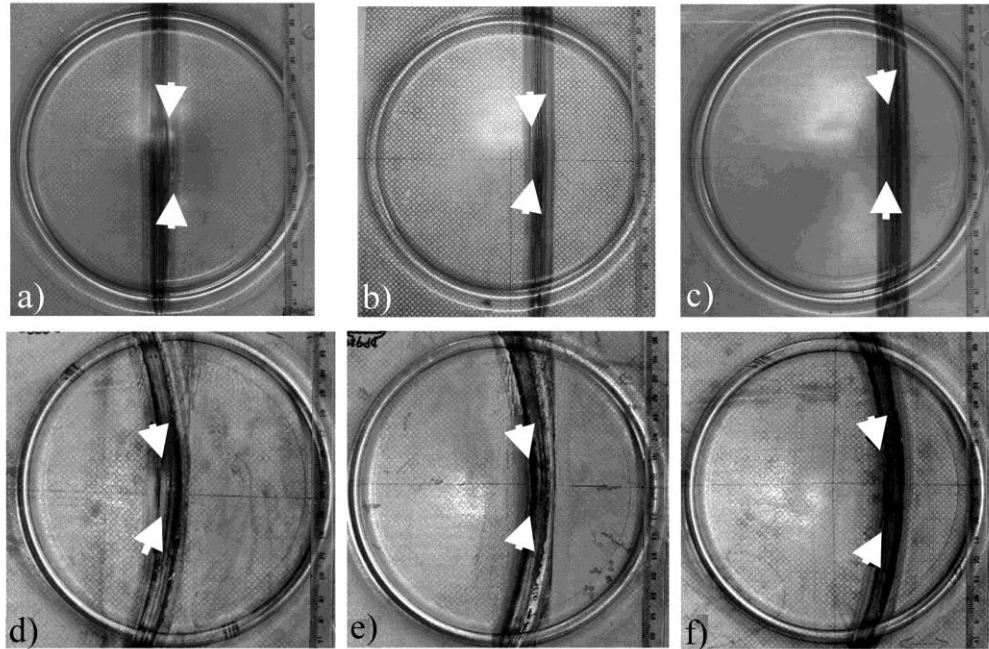


Figure 5.8 DP980 linear-welded blanks a) to c); and curvilinear welded blanks d) to f) with weld locations at 0, 15, and 30 mm

5.5 Limiting Dome Height

Similar to the strain distribution profiles, the LDH values of the curvilinear welded blanks were compared to the linear welded blanks at their respective weld locations. Figure 5.9 shows the LDH values of the HSLA, DP600, and DP980 steels in the unwelded, linear welded, and curvilinear welded conditions. This figure shows that shifting the weld line farthest away from the centre at 30 mm resulted in the highest LDH for all the laser welded blanks, with HSLA steel having the highest LDH of the three materials.

The LDH values for the linear welded HSLA blanks increased as the weld position shifted away from the centre. The same increase was seen in the curvilinear welded HSLA blanks. The similarity in the linear and curvilinear welded HSLA steels was seen in the strain distribution profiles in Figure 5.3. Thus, confirming that weld geometry did not affect the formability of the welded HSLA steel.

The linear welded DP600 steel showed an increase in the LDH values as the weld position shifted away from the pole. This change in formability was also observed in the strain distribution profiles of the DP600 steel in Figure 5.4. Comparatively, the LDH values in the curvilinear welded steel showed that placing the weld at 15 mm from the centre of the blank gave the lowest LDH. This

drop in LDH when the weld was placed 15 mm from the pole was observed in the dissimilar materials TWB (DP600-HSLA) in Figure 4.16. Overall, the LDH values of the curvilinear welded DP600 steel were lower than the linear welded blanks. The difference between the LDHs of the linear versus curvilinear welded blank for the DP600 steel specimens was ~22%, with the largest difference seen where the weld was 15 mm away from the centre at 22.2%. Thus, unlike the case with HSLA steel, weld geometry affected the formability of welded DP600 steel.

The welded DP980 steel showed the lowest LDH compared to the unwelded DP980 parent material and all the other welded blanks (HSLA and DP600 steels). The LDH values of the linear welded blanks were similar to those of the curvilinear welded blanks. Unlike the case of the welded HSLA steel, the similarity between the LDH of the linear and curvilinear welded DP980 steel was due to the premature failure in the softened region. In addition, the extent of the soft zone contributed to the significant decrease in the formability in curvilinear welded DP980 steel blanks. Therefore, the dominant effect in welded DP980 was the presence of the softened region [18,27,39,58].

Therefore, unlike the case with HSLA steel, weld geometry affected the formability of welded DP600 steel; and like DP980 steel, softening in the HAZ did play a role in the formability of DP600 since the failure locations in welded DP600 steel were in the softened region. This could be the reason why the LDH differed when the weld geometry changed from linear to curvilinear.

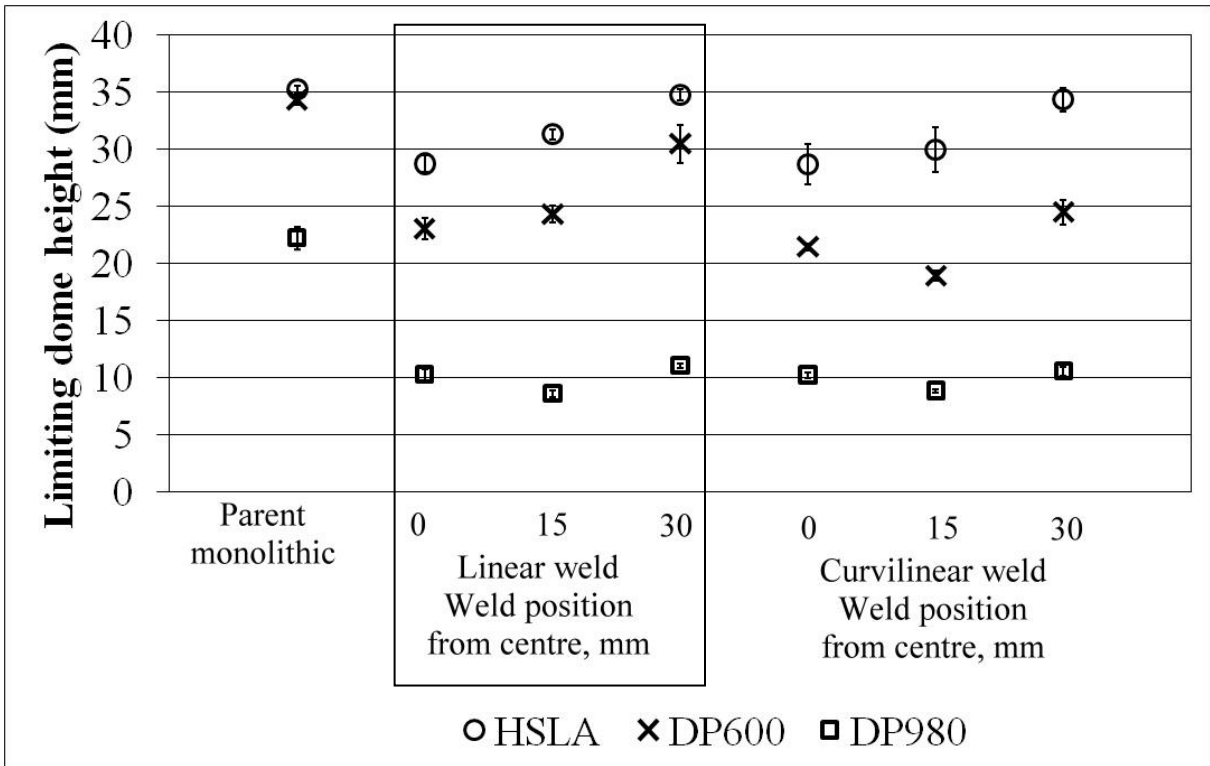


Figure 5.9 Comparison of limiting dome height of laser welded bead-on plate straight weld blanks and bead-on plate curvilinear blanks with different weld locations from the centre during biaxial stretch forming

5.6 *Summary*

The potential of using curvilinear welds in TWB applications lies in the absence of weld intersection defects such as an inflection point for complex shaped parts where typically manufacturers have relied on multiple angular welds to assemble blanks. This chapter has examined the effects on the formability of curvilinear welds versus linear welds at different weld locations for HSLA, DP600, and DP980 steels. The result showed that curving the weld affected the cross sectional hardness profiles of all the steels, but the DP steels were most affected. In the DP steels, the extent of the softened region on the left side (inner region) of the blank was 33-38% longer than the outer region; while the extent of the HAZ in the HSLA differed by 14%. Since, the hardness profile of HSLA steel was not significantly affected, the strain distribution profiles of the curvilinear welded blanks were well-developed and strains were high, and comparable to the linear welded blanks.

Although the softening in the DP600 steel was not severe, curving the welded changed the strain distribution profile. The strain distribution profiles of the curvilinear welded DP600 were inferior to the linear welded DP600 steel, which indicated a decrease in formability with the change in weld geometry. This change in strain profiles was also reflected in the LDH data, where the curvilinear welded blanks had a lower LDH than the linear welded blanks. In contrast, the severe softening in the welded DP980 steel dominated the formability of the welded blanks despite the weld geometry. The strain profiles are reflective of this, as limited strain magnitudes were seen in all the DP980 steel profiles.

CHAPTER 6

6 EFFECT OF TWBS WITH MULTIPLE WELDS ON FORMABILITY

In chapters 4 and 5, the formability of welded blanks increased when the weld was placed farthest from the centre *i.e.* 30 mm offset from the pole. Also, seen in chapter 4 was the effect of weld orientation for dissimilar material combinations on formability. In similar material TWBs, the effect of weld orientation in plane strain stretch forming was negligible; while in TWBs between materials of dissimilar properties, the weld orientation significantly affected the formability of the TWBs.

The tailored blanks studied so far involved a single weld; however, many TWB applications in practice may require multiple welds, such as the body sides and the floor pans of an automobile. Thus, the study of multiple-weld TWBs is important. However, research results in this area are not available in open literature. Therefore, this chapter examines the effect of multiple welds on the formability of laser welded TWBs consisting of AHSS-HSLA-AHSS. The placements of the welds for the multiple-weld TWBs was consistent at ± 30 mm away from the centre of the blank, as seen in the single weld TWBs since, this position gave the highest formability (in terms of strain profiles and LDHs as observed in chapters 4 and 5). In addition, three weld angles have been explored, two parallel vertical welds with no angles; two low angle welds (at 8°); and two high angle welds (at 17°).

6.1 *Limiting Dome Height Testing*

As in previous biaxial stretched samples, the TWBs had dimensions of 200 mm x 200 mm. The welds were placed 30 mm away from the centre of the blank with respect to the horizontal line as shown in Figure 6.1. Figure 6.1 a) shows multiple-weld TWB with parallel vertical welds with no angles, Figure 6.1 b) shows multiple-weld TWB with low angle welds (low angle welds were welds made with an angle of 8° from a straight line); and Figure 6.1 c) shows multiple-weld TWB with high angle welds (high angle welds referred to welds made with an angle of 17° from a straight line). By offsetting the weld angles the interaction of the welds on formability and the unbalanced amount of HSLA steel at the top and the bottom of the blank could be studied without changing the area of the materials used.

All multiple-weld TWBs had HSLA steel at the centre and DP steels at either side. These weld locations were chosen for the following reasons:

1. The welds are away from the major strain concentration area as shown in the strain distribution patterns for the base metal in biaxial stretch forming, shown in Figure 4.2.
2. In the single weld TWB, the formability with the weld line positions ± 30 mm away from the pole was the highest, especially in the DP600-HSLA combination seen in chapter 4.

Two material combinations were studied, DP600-HSLA-DP600 and DP980-HSLA-DP980. The materials in the former combination had similar material properties and the formabilities of DP600-HSLA TWBs were good, as seen in Figure 4.16; while the latter had dissimilar material properties and the formability of welded DP980-HSLA (depending on the amount of HSLA steel present) was poor.

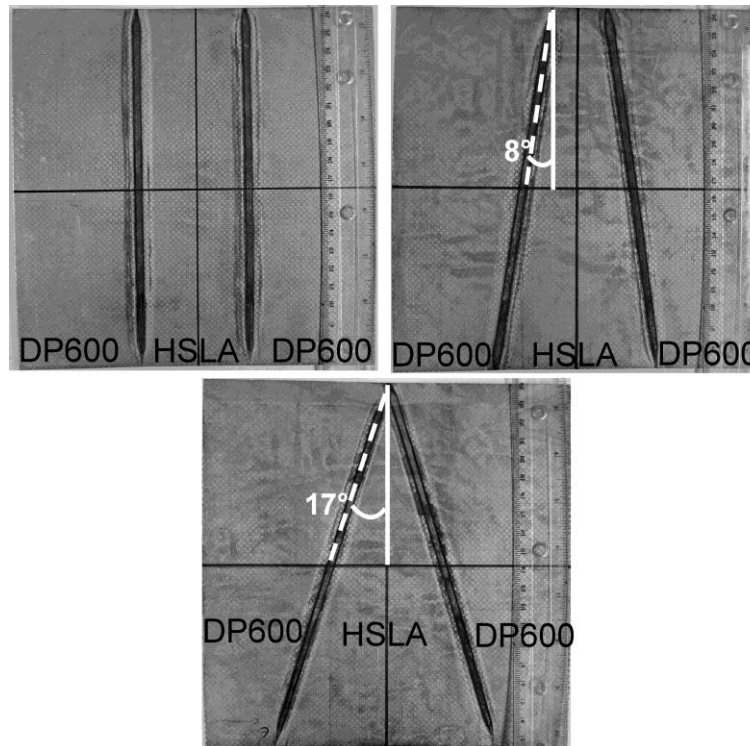


Figure 6.1 Multiple-weld TWBs with different weld slopes a) parallel welds, b) low angle welds, and c) high angle welds

6.2 *Strain Distribution Profiles*

The interaction of the multiple welds in these TWBs across the blank is shown in Figure 6.2. Figures 6.2 a) - c) show the strain distribution patterns of DP600-HSLA-DP600 parallel welds, low angle welds, and high angle welds TWBs, respectively. Figures 6.2 d) - f) show the strain distribution patterns of DP980-HSLA-DP980 parallel welds, low angle welds, and high angle welds TWBs, respectively.

The strain profiles of DP600-HSLA-DP600 were well-developed. The minor strains were close to the major strains except at the peaks, where failure is expected to occur. This closeness of strains indicates biaxial stretch forming. The strains at the pole were high, which is an indicator of good formability. The twin peaks were roughly 15-20 mm away from the pole, unlike the dissimilar TWB strain profiles seen in Figures 4.20 a) and e) at weld positions -30 mm and +30 mm, but similar to the parent unwelded HSLA steel's behaviour as seen in Figure 4.2. In the three strain profiles of DP600-HSLA-DP600, the true strains at the pole of the parallel welds and low angle welds conditions were high, at 0.28 and 0.26, respectively. The true strain at the pole of the high angle welds TWB was 0.22, which was ~21% lower than the parallel welds condition. This lower strain in the high angle welds condition resulted in the lower LDH value for the DP600-HSLA-DP600 TWBs in Figure 6.4. In addition, there was less strain experienced in the DP600 steel in the high angle welds case than in parallel welds and low angle welds. It is possibly that due to the weld angles that the strain in the DP600 steel was limited and restricted in this condition causing reduced overall strain and formability.

The strain profiles of DP980-HSLA-DP980 (Figures 6.2 d) - f)) were not as well-developed as DP600-HSLA-DP600, but better than most strain distributions in the single weld dissimilar (DP980-HSLA) TWBs at different weld positions (Figure 4.21). However, like the DP600-HSLA-DP600 TWBs, twin peaks were present and at ~20 mm away from the pole, but the distance between the peaks were different from the parent HSLA steel (Figure 4.2). These DP980-HSLA-DP980 peaks were narrower than the DP600-HSLA-DP600 and the true strains at the pole were ~0.1. This reduced strain could be caused by the large difference in material properties and with DP980 steel at the sides of the blank; it restricted the amount of deformation HSLA steel could experience before failure.

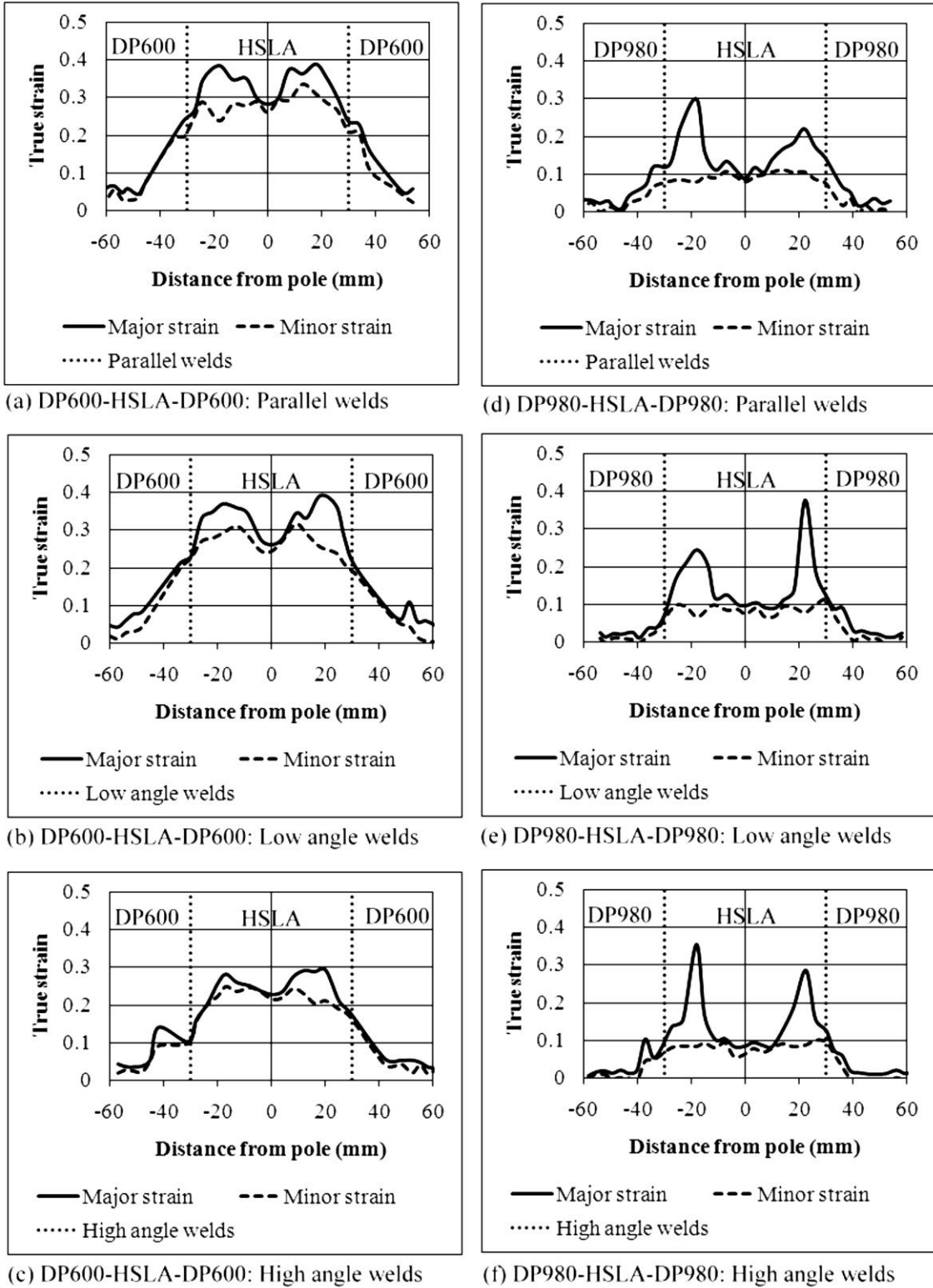


Figure 6.2 Strain distribution of the multiple welded TWBs

Another factor that evidently contributes to the low formability of the DP980-HSLA-DP980 TWBs was the negligible strain in the DP980 steel; whereas, in DP600-HSLA-DP600 TWBs, there was deformation seen in the DP600 steel as noted by the gradual increase in the strain curve. Observable in the DP980-HSLA-DP980 strain profiles was the strain at the pole for the major and minor strains were consistently 0.1. This consistent deformation at the pole could be a factor which resulted in similar LDHs, despite the weld angle and the uneven distribution of HSLA steel in the low angle welds and high angle welds TWBs.

6.3 Fracture Locations

The multiple-weld TWBs, DP600-HSLA-DP600 and DP980-HSLA-DP980 were stretched in the biaxial condition. According to the strain distribution profiles in Figure 6.2 failure occurred in the areas of peak strain *i.e.* ~20 mm from the pole in the HSLA steel. However, the fractured locations Figure 6.3 a) shows failure occurring across the weld line and in the HSLA steel; Figure 6.3 b) shows failure in the HSLA steel base metal; and Figure 6.3 c) shows failure across the weld. The failure modes and locations in the DP600-HSLA-DP600 TWBs varied with weld angles. Figures 6.3 d) to f) of the DP980-HSLA-DP980 TWBs show failure locations consistently on the HSLA steel ~20 mm from the pole, which conformed to the areas of peak strains in the strain profiles in Figure 6.2. It appeared that the weld angles in the DP980-HSLA-DP980 TWBs did not affect the failure locations.

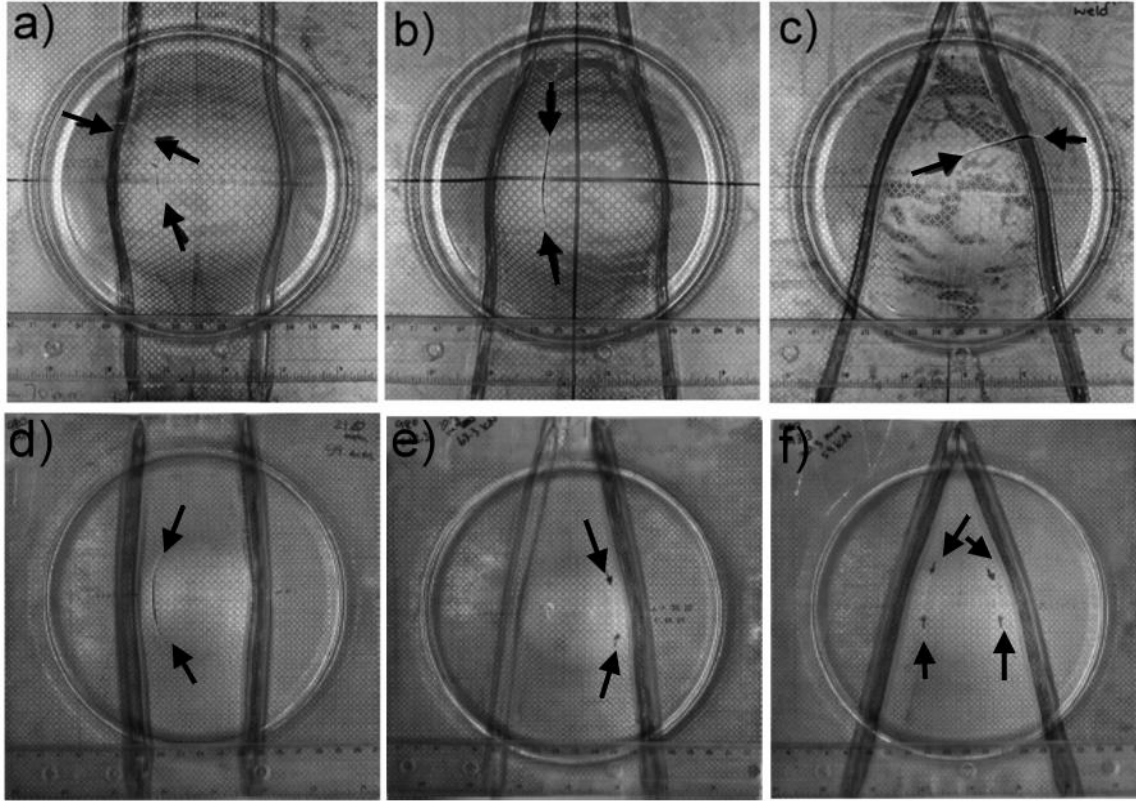


Figure 6.3 Multi weld TWB DP600-HSLA-DP600 a) parallel welds, b) low angle welds, and c) high angle welds; DP980-HSLA-DP980 d) parallel welds, e) low angle welds, and f) high angle welds

6.4 Limiting Dome Height

The comparison of LDH values of the multiple-weld TWBs is shown in Figure 6.4. These multiple-weld TWBs had lower LDH than the parent unwelded material (Figure 5.9). This lowering of the LDH was due to the presence of the weld zones and material properties within the blank similar to the single welded TWBs in chapter 4. The larger material properties differences (DP980-HSLA-DP980) led to lower values of LDH, similar to the results in chapter 4 (Figure 4.16). As seen in Figure 6.4, the LDH values of the DP600-HSLA-DP600 TWBs decreased as the weld angles increased. The LDH of the parallel weld blank was ~16% higher than the high angle blank. This indicated that high weld angles did affect the formability of the similar material TWBs. Interestingly, the LDH of the DP600-HSLA-DP600 TWBs were comparable to the DP600-HSLA TWBs with weld locations at -30 mm and +30 mm offset. The LDH of the single weld TWBs at weld positions -30 mm and +30 mm were 29.82 mm and 30.17 mm, respectively; while the LDHs of the DP600-HSLA-DP600 TWBs were 33.21 mm (parallel weld), 29.32 mm (low angle welds), and 27.89 mm (high angle welds).

This shows that multiple welds gave favourable results and that weld angles in TWBs made with similar materials do affected formability.

Unlike the DP600-HSLA-DP600 TWBs, the DP980-HSLA-DP980 TWBs showed consistent LDH values. The similarity in the LDH values of these TWBs with dissimilar material properties (DP980-HSLA-DP980) indicates that the weld angles did not significantly affect the formability of these TWBs. The LDH values of the DP980-HSLA-DP980 TWBs were comparable to the DP980-HSLA TWBs for all the weld positions except for the -30 mm offset TWB (Figure 4.16). It appears that the LDH of the DP980-HSLA TWBs depends on the amount of HSLA steel present, since the DP980 steel contributed negligible strain, as seen in Figure 4.21.

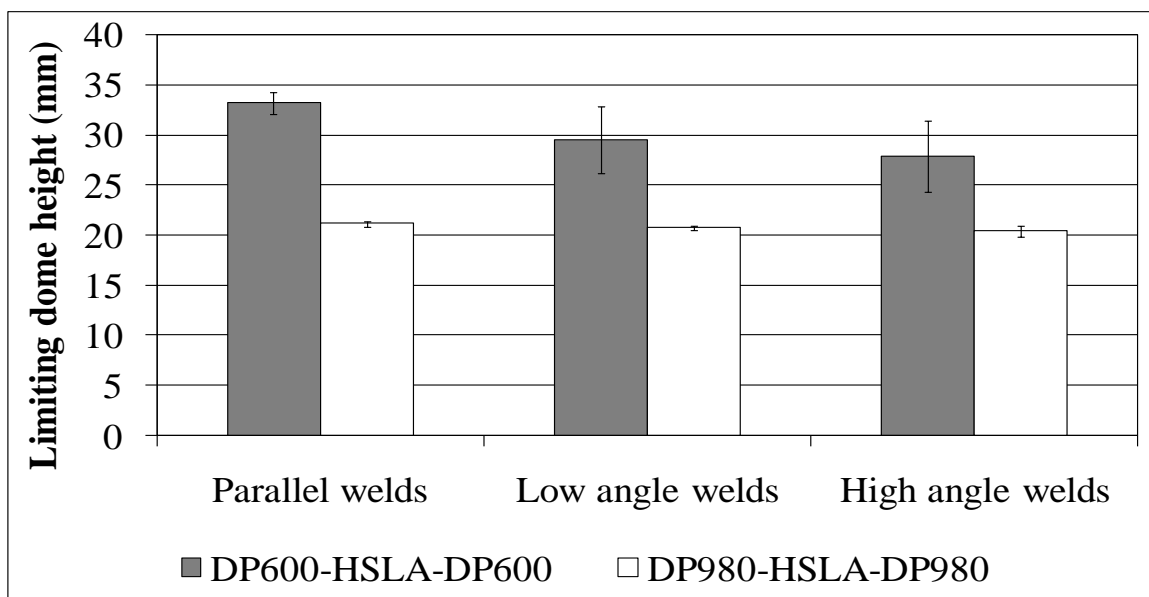


Figure 6.4 LDH graph of multiple weld TWBs

6.5 Summary

In this chapter the effect of multiple welds TWBs (DP600-HSLA-DP600 and DP980-HSLA-DP980) with different weld orientations has been examined. The three weld angles studied were: parallel vertical welds with no angles; low angle welds at 8° offset; and high angle welds at 17° offset. The results showed that the similar materials combination TWBs had different failure modes and the formability decreased as the weld angles changed from parallel welds to high angle welds. However, the dissimilar material combination TWBs showed similar formability despite the weld angles, since DP980 steel restricted the amount of strain experienced in the TWB during the deformation process. Therefore, when designing multiple-weld TWBs with materials having similar properties, it is necessary to keep the most formable material in the centre of the blank and the welds parallel. However, with dissimilar material properties, the effect of weld orientation is negligible in terms of formability.

CHAPTER 7

7 CONCLUSIONS AND RECOMMENDATIONS

7.1 *Conclusions*

This thesis has investigated methods to optimize formability of tailor welded blanks made with advanced high strength steels by measuring the response of blanks made with various designs and material combinations, using the limiting dome height test. This thesis was divided into three parts. In the first part, the effects of weld locations, weld orientation and strain path on formability were studied. In the second part, the effect of weld geometry (curvilinear welds) on formability was studied. In the last part, the effect of multiple-welded TWBs was studied.

7.1.1 The Effect Of Weld Location, Orientation And Strain Path

The major findings in the first part of this thesis are as follows:

1. **Placing the weld close to the centre of the blank (± 15 mm) resulted in the lowest formability**; however, placing the weld farthest from the centre resulted in increased formability. The increase in formability was dependent on the type of materials combination. Therefore, formability is dependent on both weld location and materials combination.
2. **Welding decreases the formability of the TWB compared with the parent material** and this was reflected in the forming behaviour, represented by the strain distribution profiles. The main characteristic of decreased formability was non-uniform strain distributions. On the other hand, the strain distribution on the dome surface could be manipulated by placing the weld line farthest from the centre, which increased formability.
3. **The lowest limiting dome height of the laser welded blanks occurred during plane strain stretch forming** compared to biaxial stretch forming when the weld was placed at the centre. It appeared that during plane strain stretch forming, the fracture morphology changed from dimple like (biaxial) to a combination of sheared surface with dimples or transgranular cleavage (in plane strain stretch forming) depending on weld orientation.

4. **In plane strain stretch forming, the weld orientations with respect to the major strain direction have little influence on the formability of TWBs with similar material properties** (e.g. DP600-HSLA). However, weld orientation significantly influences the formability of dissimilar TWBs with large difference in material properties (e.g. DP980-HSLA). These results could be seen in the strain distribution patterns. Therefore, under plane strain stretch forming, formability was influenced by weld orientation and material combinations.

Therefore, the formability of blanks using these laser-welded advanced high strength steels could be manipulated by changing the TWB designs by modifying the weld location and orientation. In addition, these changes led to the alteration of the strain path during stretch forming. However, the amount of increase in formability is dependent on the materials combination.

7.1.2 The Effect Of Curvilinear Welds

The major findings in the second part of this thesis are as follows

1. **Curvilinear welds increased the extent of the HAZ on the inner region of the welded blank.** An increase in the length of the HAZ was seen clearly in the DP steels, which caused peak softening to occur on the inner region of the blank. During deformation of the DP steel, failure occurred in the HAZ of the inner region.
2. **Formability of curvilinear seams is dependent on the position of the curved weld.** With the curvilinear seam farthest from the centre of the blank, the formability was the highest for all materials, which was similar to the linear welded blanks.
3. **Weld geometry affected DP600 steel the most.** DP600 steel showed that changing the weld path from a straight line to a curve reduced the formability of the welded blanks. The reason could be attributed to the combination of weld geometry and softened zone failure of the blank. In contrast, HSLA steel did not experience changes in formability with respect to weld geometry. The formability of welded DP980 steel was restricted by the presence of severe softening in the HAZ, which led to premature failure.

7.1.3 The Effect Of TWBs With Multiple Welds

1. **Formability of dissimilar materials in terms of the limiting dome height for laser welded blanks having multiple welds is dependent on the material combination.** In DP600-HSLA-DP600, the formability was comparable or improved when compared to the highest formability of the single weld TWB. However, with a large difference in properties of materials, the formability was good, but was not comparable to the highest formability results of the single weld TWBs. The limited deformation contributed by the DP980 steel restricted the formability of the multiple-weld TWBs.
2. **The strain distributions of the multiple-weld TWBs resemble the parent HSLA steel strain distribution pattern, since HSLA steel was placed in the middle of the TWB.** However, formability can be increased by placing material with properties similar to HSLA steel on either side. During forming this material may contribute to the deformation and further develop the strain pattern.

In conclusion, formability of dissimilar laser welded tailored blanks is dependent on weld location, weld orientation, and number of welds. Ultimately, the increase in formability with respect to these weld designs depends on the materials combination.

7.2 Recommendations

In the present study, the materials tested were limited in terms of supply and selection. To get a complete understanding of the effect of weld positions, orientations and strain path on formability, TWBs composed of only DP steels should be investigated. Welding dissimilar DP steels together may highlight the effect (and severity) of softening with respect to the weld positions and orientations.

As for the formability of TWBs having multiple welds, this study investigated one combination of multiple-weld TWBs, DP steel-HSLA-DP steel. However, changing the order, such as placing the HSLA on the sides could change the formability significantly. For example, placing DP600 in the middle of the blank with HSLA steel on the side may further increase the formability of the TWBs with multiple welds, as DP600 steel has better formability than HSLA steel. On the other hand, placing DP980 steel in the middle of the blank is not recommended because DP980 steel fails catastrophically at the high strain concentration region, around the pole.

REFERENCES

- [1] B Rooks, "Tailor-Welded Blanks Bring Multiple Benefits to Car Design," *Assembly Automation*, vol. 21, no. 4, pp. 323-328, 2001.
- [2] F I Saunders and R H Wagoner, "Forming of Tailor-Welded Blanks," *Metallurgical and Materials Transactions A*, vol. 27A, pp. 2605-2616.
- [3] Auto/Steel Partnership. (1995) Auto Steel Partnership - Tailor Welded Blank Design and Manufacturing Manual. [Online]. HYPERLINK "<http://www.a-sp.org/database/custom/twbmanual/>"
- [4] The Auto/Steel Partnership. (2001) Tailor Welded Blank Applications and Manufacturing: A State-of-the-Art Survey.
- [5] International Organization of Motor Vehicle Manufacturers. (2007) OICA Production Statistics. [Online]. HYPERLINK "<http://oica.net/category/production-statistics/>"
- [6] E Kubel, *Manufacturers Want More Tailored Blanks*, 1997, http://findarticles.com/p/articles/mi_qa3618/is_199711/ai_n8774982/.
- [7] M Pfestorf and D Copeland. (2008) Technological Innovations in Body in White Manufacturing of the BMW X6. [Online]. HYPERLINK "http://www.autosteel.org/AM/Template.cfm?Section=Great_Designs_in_Steel_2008_Presentations&TEMPLATE=/CM/ContentDisplay.cfm&CONTENTID=24685"
- [8] G T Kridli, P A Friedman, and A M Sherman, "Formability of Aluminum Tailor-Welded Blanks," *SAE 2000-01-0772*, pp. 1-9, 2000.
- [9] B Kinsey, V Viswanathan, and J Cao, "Forming of Aluminum Tailor Welded Blanks," *Journal of Materials & Manufacturing*, vol. 110, pp. 673-679, 2001.
- [10] S. Kou, *Welding Metallurgy*, 2nd ed. Hoboken, NJ: John Wiley & Sons, Inc., 2003.

- [11] E JM Powidajko, "Weldability of AZ31B Magnesium Sheet by Laser Welding Processes," Mechanical Engineering, University of Waterloo, Waterloo, M.A.Sc Thesis 2009.
- [12] K H Leong, G Kornecki, P G Sanders, and J S Keske, "Laser Beam Welding of AZ31B-H24 Magnesium Alloy," in *ICALEO: Laser Materials Processing Conference*, Orlando, FL, 1998, pp. 28-36.
- [13] D R Kumar, "Formability Analysis of Extra-Deep Drawing Steel," *Journal of Materials Processing Technology*, vol. 130-131, pp. 31-41, 2002.
- [14] S K Panda, D R Kumar, H Kumar, and A K Nath, "Characterization of Tensile Properties of Tailor Welded IF Steel Sheets and Their Formability in Stretch Forming," *Journal of Materials Processing Technology*, vol. 183, pp. 321-332, 2007.
- [15] S Chatterjee, R Saha, M Shome, and R H Ray, "Evaluation of Formability and Mechanical Behavior of Laser-Welded Tailored Blanks Made of Interstitial-Free and Dual-Phase Steels," *Metallurgical and Materials Transactions A*, vol. 40A, pp. 1142-1152, 2009.
- [16] L J Kilfoil, "In-Plane Plane Strain Testing to Evaluate Formability of Sheet Steels Used in Tubular Products," Mechanical and Materials Engineering, Queen's University, Kingston, Ontario, MasterThesis 2007.
- [17] N Sreenivasan, S Lawson, Y Zhou, and Z Tian, "A Comparative Study of Formability of Diode Laser Weldments in DP980 and HSLA Steels," *Journal of Engineering Materials and Technology*, vol. 129, pp. 446-452, 2007.
- [18] M F Shi, G H Thomas, M X Chen, and J R Fekete, "Formability Performance Comparison Between Dual Phase and HSLA Steels," *L&SM*, pp. 27-32, 2002.
- [19] F I Saunders and R H Wagoner, "The Use of Tailor-Welded Blanks in Automotive Applications," *Simulation of Materials Processing: Theory, Methods and Applications*, pp. 157-164, 1995.
- [20] WorldAutoSteel, "Advanced High Strength Steel (AHSS) Application Guidelines: Version 4.1," 2009.

- [21] W Bleck, "Cold-Rolled, High-Strength Sheet Steels for Auto Applications," *JOM*, pp. 26-30, 1996.
- [22] L Huang, "Application of Advanced High-Strength Steels in Roof Strength Design," in *Great Designs in Steel Seminar*, URL:
<http://members.steel.org/AM/Template.cfm?Section=PDFs&CONTENTFILEID=9298&TEMPLATE=/CM/ContentDisplay.cfm>. [Online]. HYPERLINK
 "http://members.steel.org/AM/Template.cfm?Section=PDFs&CONTENTFILEID=9298&TEMPLATE=/CM/ContentDisplay.cfm"
<http://members.steel.org/AM/Template.cfm?Section=PDFs&CONTENTFILEID=9298&TEMPLATE=/CM/ContentDisplay.cfm>
- [23] ArcelorMittal. (2008) Multi-Thickness Laser Welded Blanks: Tailored Blanks. Report.
- [24] HKDH Bhadeshia. (2007) University of Cambridge. [Online]. HYPERLINK
 "http://www.msm.cam.ac.uk/phase-trans/2007/LDH.html"
<http://www.msm.cam.ac.uk/phase-trans/2007/LDH.html>
- [25] W F Hosford and J L Duncan, "Sheet Metal Forming: A Review," *JOM*, vol. 51, no. 11, pp. 39-44, 1999.
- [26] S K Panda and D R Kumar, "Study of Formability of Tailor-Welded Blanks in Plane-Strain Stretch Forming," *Int J Adv Manuf Technol*, vol. 44, pp. 675-685, 2009.
- [27] S K Panda, V H Baltazar Hernandez, M L Kuntz, and Y Zhou, "Formability Analysis of Diode-Laser-Welded Tailored Blanks of Advanced High-Strength Steel Sheets," *Metallurgical and Materials Transactions A*, vol. 40A, pp. 1955-1967, 2009.
- [28] B Breakiron and J R Fekete, "Formability Analysis of High Strength Steel Laser-Welded Blanks," *SAE Technical Paper Series*, vol. 2005-01-1326, 2005.
- [29] T S Yang and T C Hsu, "Forming Limit Analysis of Hemispherical-Punch Stretch Forming," *Journal of Materials Processing Technology*, vol. 117, pp. 32-36, 2001.
- [30] J Datsko, *Material Properties and Manufacturing Processes*. New York: John Wiley & Sons, Inc, 1966.

- [31] A R Ragab and B Baudelet, "Forming Limit Curves: Out-of-Plane and In-Plane Stretching," *Journal of Mechanical Working Technology*, vol. 6, pp. 267-276, 1982.
- [32] W F Hosford and R M Caddel, *Metal Forming: Mechanics and Metallurgy*. Englewood Cliffs, N.J: Prentice-Hall, Inc, 1983.
- [33] American Iron and Steel Institute. (1989, January) Stamping and Formability: Automotive Sheet Metal Stamping and Formability. [Online]. HYPERLINK "http://www.a-sp.org/database/print.asp?doc=27" <http://www.a-sp.org/database/print.asp?doc=27>
- [34] S P Keeler and W G Brazier, *Micro Alloying 75.*: Union Carbide, 1977.
- [35] S Kalpakjian and S R Schmid, *Manufacturing Engineering and Technology*. India: Pearson Education, 2003.
- [36] R Padmanabhan, A J Baptista, M C Oliveira, and L F Menezes, "Effect of Anisotropy on the Deep-Drawing of Mild Steel and Dual-Phase Steel Tailor-Welded Blanks," *Journal of Materials Processing Technology*, vol. 184, pp. 288-293, 2007.
- [37] P K Ghosh, P C Gupta, R Avtar, and B K Jha, "Weldability of Intercritical Annealed Dual-Phase Steel with the Resistance Spot Welding Process," *Weld. J.*, vol. 70, no. 1, pp. 7s-14s, 1991.
- [38] M Xia, N Sreenivansan, S Lawson, Y Zhou, and Z Tian, "A Comparative Study of Formability of Diode Laser Welds in DP980 and HSLA Steels," *Transactions of the ASME*, vol. 129, pp. 446-452, 2007.
- [39] M S Xia, E Biro, Z Tian, and N Zhou, "Effect of Heat Input and Martensite on HAZ Softening in Laser Welding of Dual Phase Steels," *ISIJ International*, vol. 48, pp. 809-814, 2008.
- [40] Y Choi, Y Heo, H Y Kim, and D Seo, "Investigations of Weld-Line Movements for the Deep Drawing Process of Tailor Welded Blanks," *Journal of Materials Processing Technology*, vol. 108, pp. 1-7, 2000.

- [41] Auto Steel Partnership. Brief History and Purpose of Tailor-Welded Blanks. [Online].
HYPERLINK "http://www.a-sp.org/database/custom/twbmanual/printsection.asp?hid=9"
<http://www.a-sp.org/database/custom/twbmanual/printsection.asp?hid=9>
- [42] H M Jiang, S H Li, H Wu, and X P Chen, "Numerical Simulation and Experimental Verification in the Use of Tailor-Welded Blanks in the Multi-Stage Stamping Process," *Journal of Materials Processing Technology*, vol. 151, pp. 316-320, 2004.
- [43] L C Chan, S M Chan, C H Cheng, and T C Lee, "Formability and Weld Zone Analysis of Tailor-Welded Blanks for Various Thickness Ratio," *Journal of Engineering Materials and Technology*, vol. 127, pp. 179-185, 2005.
- [44] S M Chan, L C Chan, and T C Lee, "Tailor Welded Blanks of Different Thickness Ratios Effects on Forming Limit Diagrams," *Journal of Materials Processing Technology*, pp. 83-89, 2003.
- [45] L C Chan, C H Cheng, S M Chan, T C Lee, and C L Chow, "Formability Analysis of Tailor-Welded Blanks of Different Thickness Ratio," *Journal of Manufacturing Science and Engineering*, vol. 127, pp. 743-751, 2005.
- [46] MF Shi, KM Pickett, and KK Bhatt, "Formability Issues in the Application of Tailor Welded Blank Sheets," in *SAE Technical Paper*, 1993, pp. 27-35.
- [47] A P Lee, E Feltham, and J V Deventer, "Tailor Welded Blank Technology for Automotive Applications," *SAE Technical Paper Series 960817*, pp. 91-101, 1996.
- [48] P J Scriven, J A Brandon, and N T William, "Influence of Weld Orientation on Forming Limit Diagrams of Similar/Dissimilar Thickness Laser Welded Joints," *Ironmaking Steelmaking*, vol. 23, no. 2, pp. 177-182, 1996.
- [49] K Azuma, K Ikemoto, H Sugiura, K Arima, and T Takasago, "Press Formability of Laser Welded Blanks," *Presented in IDDRG Working Group I*, 1990.

- [50] Y M Heo, S H Wang, H Y Kim, and D G Seo, "The Effect of the Drawbead Dimensions on the Weld-Line Movements in the Deep Drawing of Tailor-Welded Blanks," *Journal of Materials Processing Technology*, vol. 113, pp. 686-691, 2001.
- [51] Y Adony and C C Chen, "Laser-Welded Steel Performance in Tailored Blank Applications," *29th International Symposium on Automotive Technology and Automation*, vol. 1, pp. 157-164, 1996.
- [52] J K Baysore, M S Williamson, Y Adonyi, and J L Milian, "Laser Beam Welding and Formability of Tailored Blanks," *Welding Research Supplement*, pp. 345s-352s, 1992.
- [53] H Shao, J Gould, and C Albright, "Laser Blank Welding High-Strength Steels," *Metallurgical and Materials Transaction B*, vol. 38B, pp. 321-331, 2007.
- [54] C H Cheng, M Jie, L C Chan, and C L Chow, "True Stress-Strain Analysis on Weldment of Heterogeneous Tailor-Welded Blanks - A Novel Approach for Forming Simulation," *International Journal of Mechanical Science*, vol. 49, pp. 217-229, 2007.
- [55] K J Larsson, "Supporting Welding Methods for Future Light Weight Steel Car Body Structures," *SAE Technical Paper Series No. 2002-01-2091*, 2002.
- [56] M Schaik and D Wenk, "The Future for Welding of AHSS Tailored Blanks," *SAE Technical Paper Series No. 2003-01-2770*, 2003.
- [57] M Uchihara and K Fukui, "Tailored Blanks of High Strength Steels-Comparison of Welding Processes," *JSAE 20037108*, pp. 29-34, 2003.
- [58] N Sreenivasan, M Xia, S Lawson, and Y Zhou, "Effect of Laser Welding on Formability of DP980 Steel," *Journal of Engineering Materials and Technology*, vol. 130, no. 4, 2008.
- [59] B Hartley and M Ono, "Laser Weldability of Dual Phase Steels in Tailored Blank Applications," *SAE Technical Paper Series: 2002-01-0150*, 2002.
- [60] S K Panda, N Sreenivasan, M L Kuntz, and Y Zhou, "Numerical Simulations and Experimental Results of Tensile Test Behaviour of Laser Butt Welded DP980 Steels,"

Journal of Engineering Materials and Technology, vol. 120, 2008.

- [61] M S Xia, M L Kuntz, L Tian, and Y Zhou, "Failure Study on Laser Welds of Dual Phase Steel in Formability Testing," *Science and Technology of Welding and Joining*, vol. 13, no. 4, pp. 378-387, 2008.
- [62] M P Miles, J Pew, T W Nelson, and Li M, "Comparison of Formability of Friction Stir Welded and Laser Welded Dual Phase 590 Steel Sheets," *Science and Technology of Welding and Joining*, vol. 11, no. 4, pp. 384-388, 2006.
- [63] I-CAR: Advantage Online. (2004) Tailor-Welded Blanks. [Online]. HYPERLINK "http://www.i-car.com.au/pdf/advantage/online/2004/120604.pdf" <http://www.i-car.com.au/pdf/advantage/online/2004/120604.pdf>
- [64] M Uchihara and K Fukui, "Formability of Tailor Welded Blanks Fabricated by Different Welding Processes. Study of Tailor Welded Blanks Using Automotive High-Strength Steel Sheets (1st Report)," *Welding International*, vol. 20, no. 8, pp. 612-621, 2006.
- [65] R Ganesh Narayanan and K Narasimhan, "Influence of the Weld Conditions on the Forming-Limit Strains of Tailor-Welded Blanks," vol. 43, pp. 217-227, 2008.
- [66] Y Heo, Y Choi, H Kim, and D Seo, "Characteristics of Weld Line Movements for the Deep Drawing with Drawbeads of Tailor-Welded Blanks," *J. Mater. Process. Technol.*, vol. 111, pp. 164-169, 2001.
- [67] C H Cheng, L C Chan, C L Chow, and T C Lee, "Experimental Investigation on the Weldability and Forming Behavior of Aluminum Alloy Tailor Welded," *J. Laser Appl.*, vol. 17, no. 2, pp. 81-88, 2005.
- [68] R G Narayanan and K Narasimhan, "Predicting the Forming Limit Strains of Tailor-Welded Blanks," *J. Strain Analysis*, vol. 43, pp. 551-563, 2008.
- [69] H Kusuda, T Takasago, and F Natsumi, "Formability of Tailored Blanks," *Journal of Materials Processing Technology*, vol. 71, pp. 134-140, 1997.
- [70] D Dry, D Hughes, and R Owen, "Methods of Assessing Influence of Weld Properties on Formability of Laser Welded Tailored Blanks," *Ironmaking and Steelmaking*, vol. 28, no. 2,

pp. 89-95, 2001.

- [71] B L Kinsey, "A Combined Approach to Improve and Assess the Formability of Tailor Welded Blanks," Dissertation for Doc Degree 2001.
- [72] H Tian, X Liu, and J Lin, "Investigation on the Formability of Tailor-Welded Blanks," *Advanced Materials Research*, vol. 97-101, pp. 260-263, 2010.
- [73] H Tian, X Liu, J Lin, and L M Smith, "Investigation on the Formability of Tailor Welded Blanks with Curved Seams," *Advanced Materials Research*, vol. 83-86, pp. 1160-1164, 2010.
- [74] ASTM Standards, *Metals Test Methods and Analytical Procedures.*, 1999, pp. 78-98, 501-508, Annual Book of ASTM Standards.
- [75] R Smerd, S Winkler, and M Worswick, "High Rate Tensile Testing of Automotive Aluminum Alloy Sheet," *International Journal of Impact Engineering*, vol. 32, pp. 541-560, 2005.
- [76] Nuvonyx, Nuvonyx ISL-4000L Industrial Laser: Owner's Manual, 2001.
- [77] K Howard, "Diode Laser Welding of Aluminum Sheet," Mechanical Engineering, University of Waterloo, Waterloo, Master Thesis 2005.
- [78] H Metcalf. (2002) Injection in Anti-Reflection Coated Diode Laser. [Online]. HYPERLINK "http://grad.physics.sunysb.edu/~campbell/optics/metcalf/metcalf.html" <http://grad.physics.sunysb.edu/~campbell/optics/metcalf/metcalf.html>
- [79] N Sreenivasan, "Effects of Laser Welding on Formability Aspects of Advanced High Strength Steel," Mechanical Engineering, University of Waterloo, Waterloo, Master Thesis 2007.
- [80] S S Hecker, "A Cup Test for Assessing Stretchability," *Metals Eng Quart*, vol. 14, pp. 30-36, 1974.
- [81] A K Ghosh and S S Hecker, "Failure in Thin Sheets Stretched Over Rigid Punches," *Metals*

Eng. Quart., pp. 30-36, 1975.

- [82] G E Dieter, *Mechanical Metallurgy*, 3rd ed.: McGraw Hill Book Company, 1996.
- [83] R W Hertzberg, *Deformation and Fracture Mechanics of Engineering Materials*. Toronto: John Wiley & Sons, Inc, 1976.
- [84] ASM. (2010) ASM Handbook Online. [Online]. HYPERLINK
"http://products.asminternational.org/hbk/index.jsp"
<http://products.asminternational.org/hbk/index.jsp>
- [85] S S Hecker, "Simple Technique for Determining Forming Limit Curves," *Steel Metal Industries*, vol. 52, pp. 671-675, 1975.
- [86] F P Incropera, D P Dewitt, T L Bergman, and A S Lavine, *Fundamentals of Heat and Mass Transfer*, Sixth Edition ed.: John Wiley & Sons, Inc, 2007.
- [87] W W Duley, *Laser Welding*. New York: John Wiley & Sons, Inc, 1999.
- [88] D Sands, *Diode Lasers*. London: IOP Publishing Ltd., 2004.
- [89] Mario Bertolotti, *The history of the laser*. London: Institute of Physics Publishing, 2005.
- [90] JL Bocos et al., "Application of the diode laser to welding on tailored blanks," vol. 19, no. 7, pp. 539-543, 2005.
- [91] Engineers Edge LLC. (2000-2010) Laser Welding Review. [Online]. HYPERLINK
"http://www.engineersedge.com/manufacturing/laser_welding.htm"
http://www.engineersedge.com/manufacturing/laser_welding.htm

APPENDICES

A LASER

Since, the first laser was developed in 1960, many laser applications were developed. For example, materials processing, such as laser welding is one of the laser applications, which began in 1962 [87]. LASER, light amplification by simulated emission of radiation, has three essential characteristics that define it. The three characteristics [88] are as follow:

1. The ability to produce a monochromatic light energy at a specific wavelength depending on the lasing medium;
2. The light produce is coherent and
3. The light is directional *i.e.* the light is in the form of a tight concentrated beam.

The laser works by exciting in the atoms of the lasing medium, such as a ruby. An effective lasing medium must have a specific population inversion, where there are more excited atoms than ones in the fundamental state. The population inversion allows the energy to release when simulated in the lasing medium [89]. When the excited atoms return to its ground state photons are emitted at a specific wavelength depending on the lasing medium. The photons reflect by the two mirrors in either end of the laser cavity and travel within the cavity simulating the lasing medium; thus, releasing more photons. One of the two mirrors in the laser system is half reflective, *i.e.* half the photons are reflected and the other half of the photons emitted in the correct direction are release to form the laser beam which is focused by optics and delivered to the application [77,87,89] .

A.1 Laser Welding

Laser welding is used extensively in the automotive industry because of its ability to focus the intense beam (heat source) and reduce the weld bead width and the heat affected zone (HAZ) regions [90]. In laser welding there are two modes of welding, conduction mode and keyhole mode.

Conduction welding is dependent on the conductivity of the metal. This type of welding occurs when the heat source melts the metal and creates a pool of molten metal, but the surface of the weld pool is unbroken. In contrast, keyhole welding occurs when the laser beam is concentrated in an

area until the metal is melted through where some of the metal is vaporized to create a keyhole the same thickness as the metal sheet. The laser beam reflects within the keyhole and continues to melt the metal as the laser travels across the joint. The weld finishes when the liquid metal cools and solidifies, creating a joint seam [91]. Generally, welding in conduction mode creates a weld pool that is wider than keyhole. These two modes of laser welding are shown in Figure A.1. Not all laser systems can create keyhole welding.

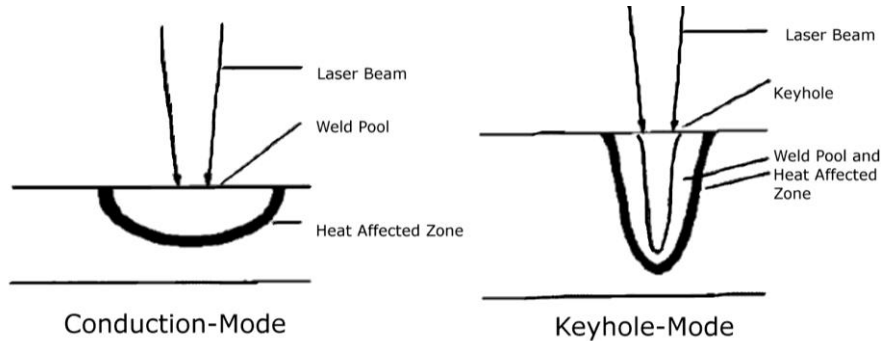


Figure A.1 Modes of welding, conduction mode (left) and keyhole mode (right)

A.2 Laser Systems

Many different types of lasers are used, two common ones are the Nd:YAG and the CO₂ lasers. These lasers are capable of conduction and keyhole welding; whereas, the diode laser (a solid state laser) is capable of conduction mode welding, but the array diode laser has the potential to challenge Nd:YAG and CO₂ lasers. Table A-1 shows the laser system characteristics. As seen in this table, the advantage of the diode laser over traditional lasers lies in its specifications. The diode laser can have a maximum power of up to 6 kW, generate a near infrared light beam with a wavelength of 800-900nm and is suitable for processing material without the use of beam transporting optics like the other lasers [88,90]. Also, diode lasers can be mounted on coolers that do not interfere with the beam, which increases the efficiency to 25% whereas lamp pumped lasers are typically 2-3% efficient [88].

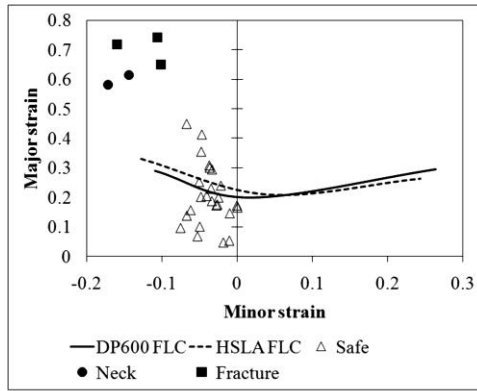
Table A-1 Summary of laser system characteristics

Laser systems	Lasing medium	Average output power	Wavelength	Welding mode
Nd:YAG laser	neodymium-doped yttrium aluminum garnet	Up to 4kW	1.06 μ m	Conduction and keyhole
CO₂ laser	carbon dioxide gas mixed with helium and nitrogen	Up to 50kW	10.6 μ m	Conduction and keyhole
Diode laser	semiconductors	6kW	800-900nm	Conduction

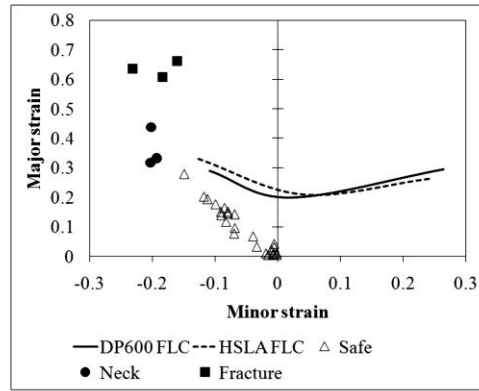
B. STRAIN PATHS WITH RESPECT TO EXPERIMENTAL FLD

The following figures show the different strain paths with respect to the FLCs of the parent material, which were discussed in Chapter 4 in terms of the strain distribution profiles. The disadvantages of the strain distribution profiles are it does not show the forming limit strain and the change in the strain path due to the change in the weld line position and weld orientation. The two experimental parent FLCs (DP600-HSLA and DP980-HSLA) were plotted for their respective TWBs, since the TWBs were made of dissimilar materials. Although, the following figures show some necking and fractured points, both are taken as failure according to Chan *et al.* [44] since stopping the formability test at necking was very difficult. Figure B.1 and Figure B.2 show the strain paths of the uniaxial tensile specimens with different weld positions. Figure B.3 and Figure B.4 show the strain paths of the biaxial stretched specimens with different weld positions. Figure B.5 and Figure B.6 show the strain paths of the plane strain stretch TWBs with different weld orientations.

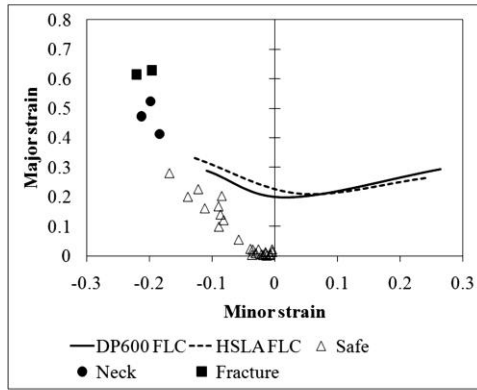
B.1 Uniaxial Tensile Strain Paths For Different Weld Position



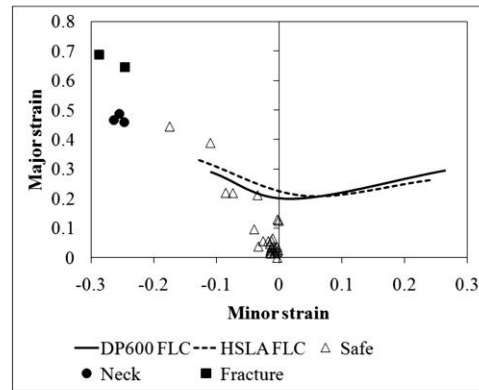
(a) DP600-HSLA and weld position: -30 mm



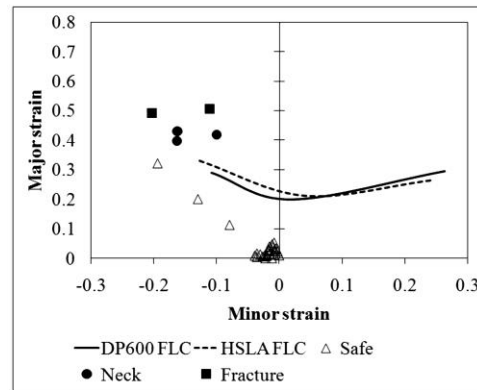
(b) DP600-HSLA and weld position: -15 mm



(c) DP600-HSLA and weld position: 0 mm

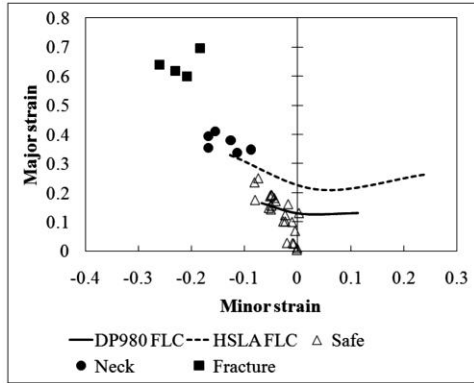


(d) DP600-HSLA and weld position: +15 mm

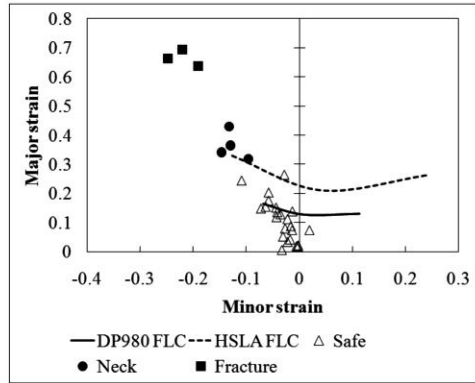


(e) DP600-HSLA and weld position: +30 mm

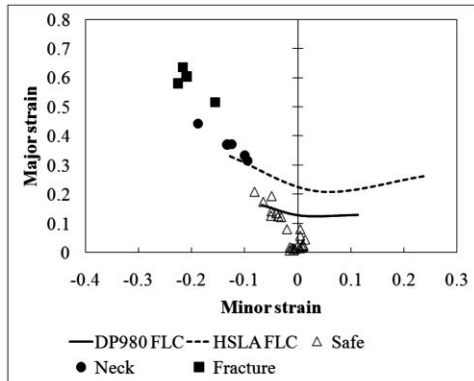
Figure B.1 Strain paths of the DP600-HSLA uniaxial tensile specimens with different weld positions



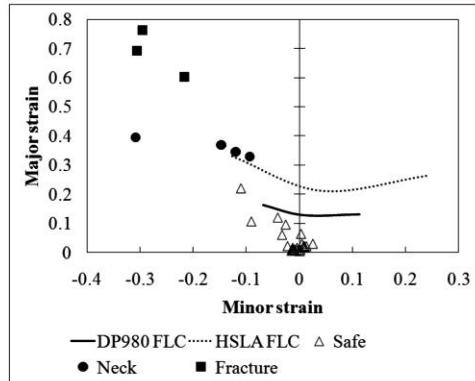
(a) DP980-HSLA and weld position: -30 mm



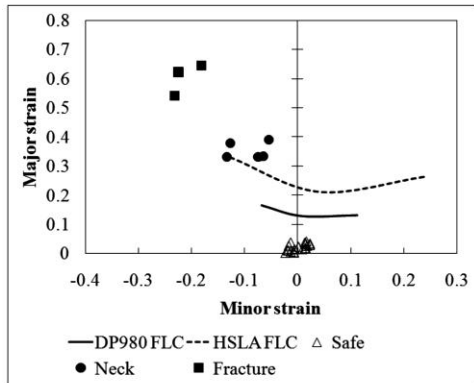
(b) DP980-HSLA and weld position: -15 mm



(c) DP980-HSLA and weld position: 0 mm



(d) DP980-HSLA and weld position: +15 mm



(e) DP980-HSLA and weld position: +30 mm

Figure B.2 Strain paths of the DP980-HSLA uniaxial tensile specimens with different weld positions

B.2 Biaxial Stretching Strain Paths For Different Weld Positions

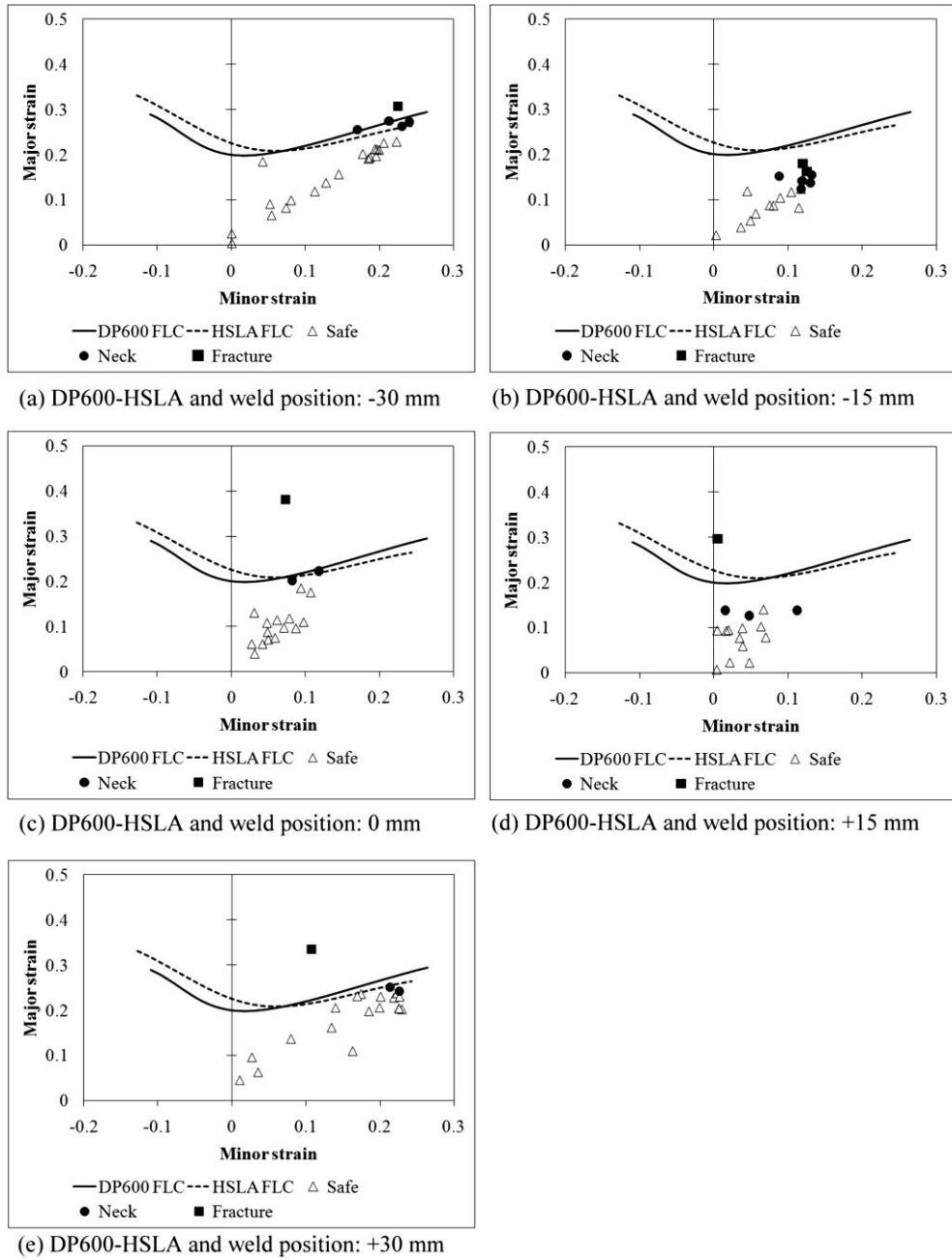
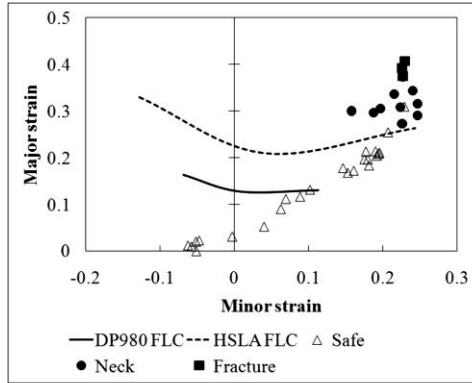
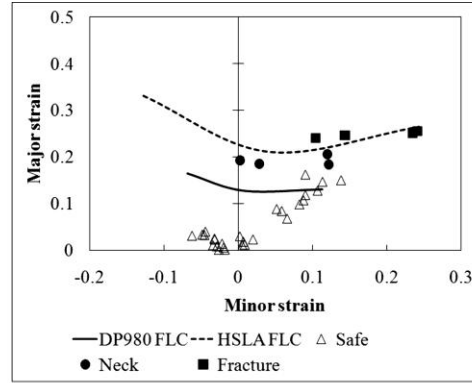


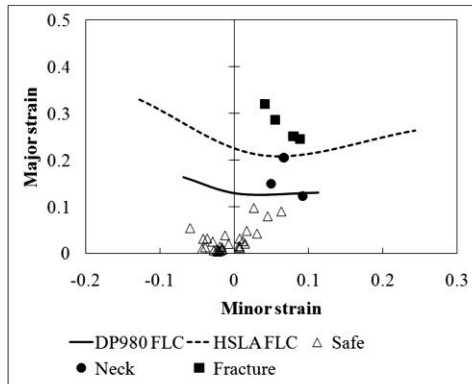
Figure B.3 Strain paths for DP600-HSLA biaxial stretched TWBs with different weld positions



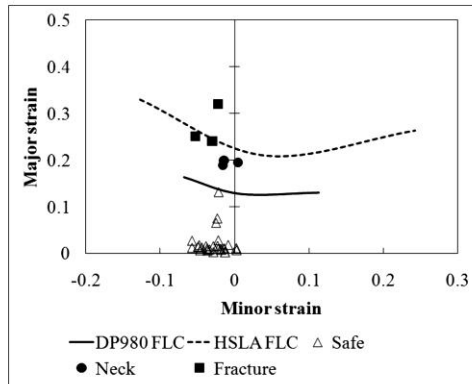
(a) DP980-HSLA and weld position: -30 mm



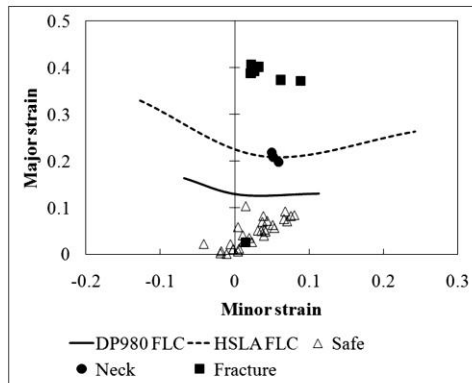
(b) DP980-HSLA and weld position: -15 mm



(c) DP980-HSLA and weld position: 0 mm



(d) DP980-HSLA and weld position: +15 mm



(e) DP980-HSLA and weld position: +30 mm

Figure B.4 Strain paths for DP980-HSLA biaxial stretched TWBs with different weld positions

B.3 Near Plane-Strain Stretching Strain Paths For Different Weld Orientations

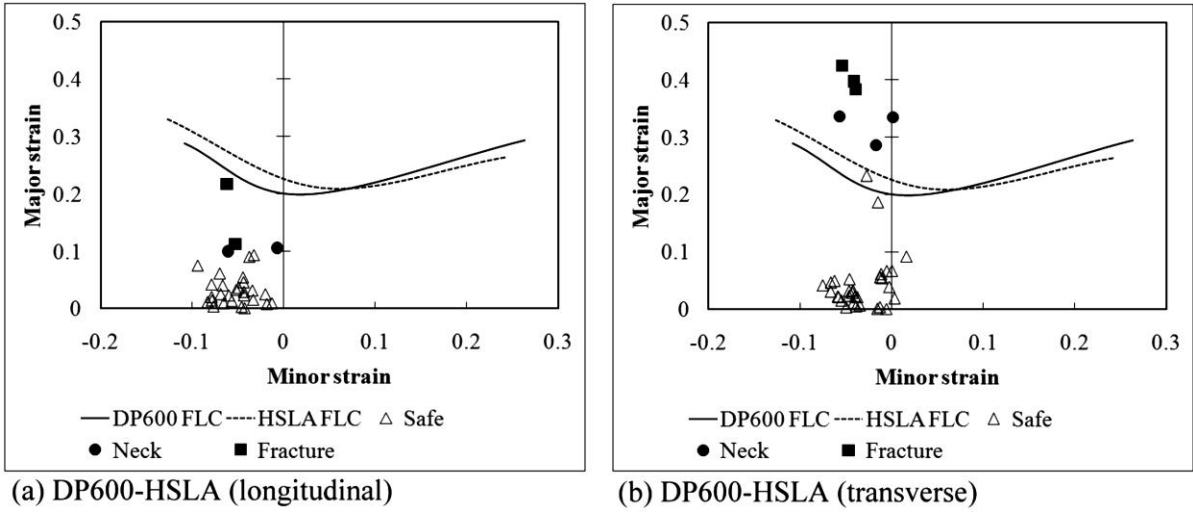


Figure B.5 Strain paths for DP600-HSLA plane strain TWBs with different weld orientations

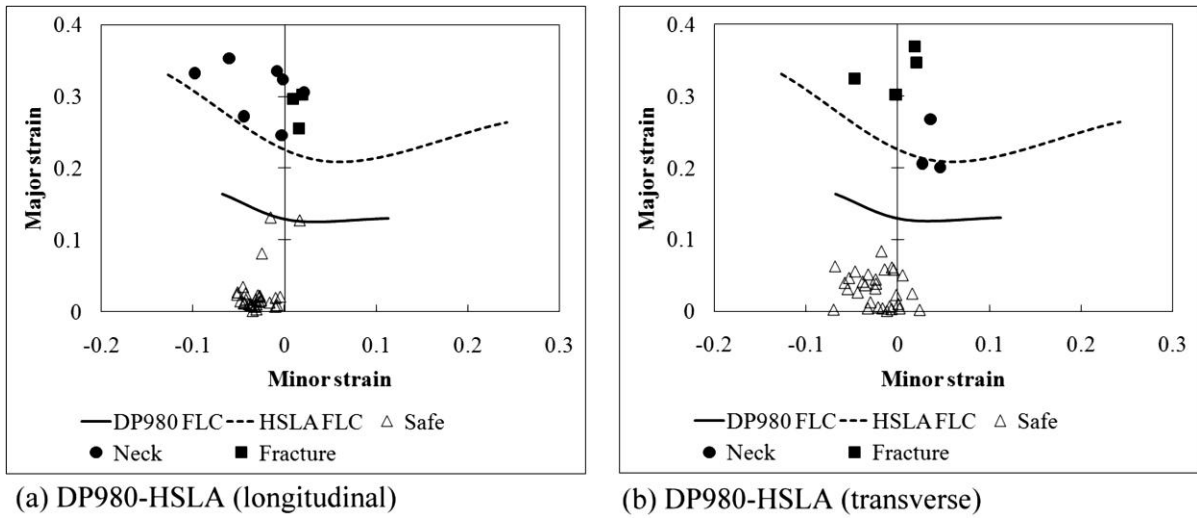


Figure B.6 Strain paths for DP980-HSLA plane strain TWBs with different weld orientations